Impact of Cell Surface Glycosylation on Tumor Cell Migration:

The glycocalyx as multivalent and universal adhesion scaffold

Samuel Schmidt

Cover design: Robin Kohze, Samuel Schmidt
Layout and printing: Gildeprint – the Netherlands
ISBN: 978-94-6233-522-6

The research presented in this thesis was performed at the Department of Cell Biology, Radboud Institute for Molecular Life Sciences (RIMLS), Radboud University Medical Center, Nijmegen, the Netherlands.

Promotor:
Prof. dr. Peter H.A. Friedl

Copromotoren:
Dr. Dirk J. Lefeber
Dr. Katarina A. Wolf

Manuscriptcommissie:
Prof. dr. Gosse J. Adema
Dr. Johan van der Vlag
Prof. dr. Robert Grosse (Philipps-Universität Marburg, Duitsland)

Impact of Cell Surface Glycosylation on Tumor Cell Migration:

The glycocalyx as multivalent and universal adhesion scaffold

Proefschrift
ter verkrijging van de graad van doctor
aan de Radboud Universiteit Nijmegen
op gezag van de rector magnificus prof. dr. J.H.J.M. van Krieken,
volgens besluit van het college van decanen
in het openbaar te verdedigen op dinsdag 21 februari 2017
om 14.30 uur precies

door
Samuel Schmidt
geboren op 23 oktober 1978
te Magdeburg, Duitsland

MB

Supervisor:
Prof. dr. Peter H.A. Friedl

Co-supervisors:
Dr. Dirk J. Lefeber
Dr. Katarina A. Wolf

Doctoral Thesis Committee:
Prof. dr. Gosse J. Adema
Dr. Johan van der Vlag
Prof. dr. Robert Grosse (Philipps-Universität Marburg, Germany)

Impact of Cell Surface Glycosylation on Tumor Cell Migration:

The glycocalyx as multivalent and universal adhesion scaffold

Doctoral thesis
to obtain the degree of doctor
from Radboud University Nijmegen
on the authority of the Rector Magnificus prof. dr. J.H.J.M. van Krieken,
according to the decision of the Council of Deans
to be defended in public on Tuesday, February 21, 2017
at 14.30 hours

by
Samuel Schmidt
born on October 23, 1978
in Magdeburg, Germany

Table of Contents

"There exists a passion for comprehension, just as there exists a passion for music. That passion is rather common in children but gets lost in most people later on. Without this passion, there would be neither mathematics nor natural science."

Albert Einstein

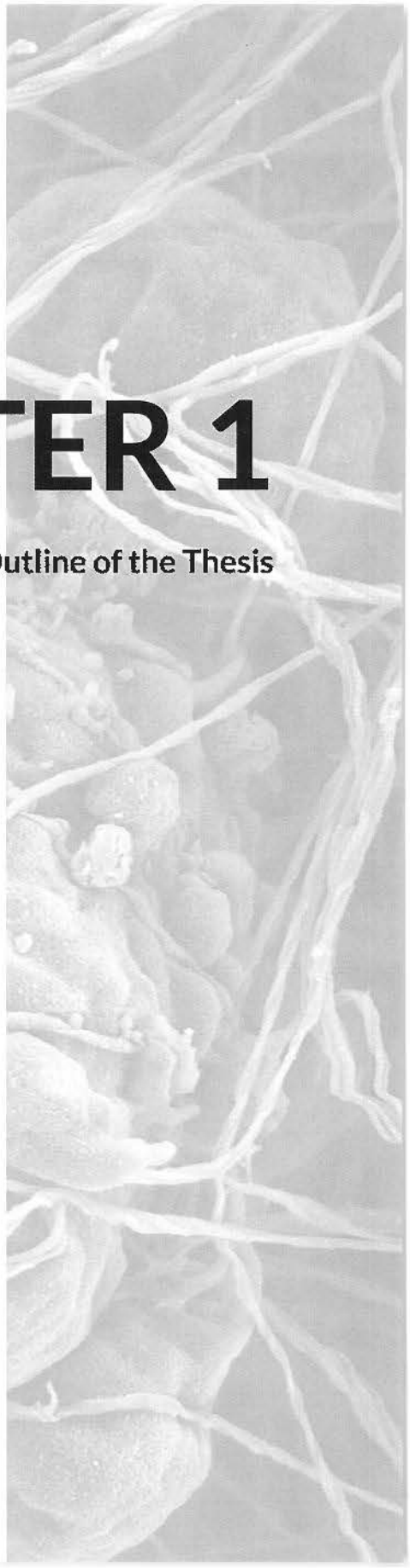

CHAPTER 1

Introduction and Outline of the Thesis

Glycosylation in tumor cell migration and invasion

The ability of cells to adhere to and migrate through the extracellular matrix (ECM) of tissues and organs is essential to maintain fundamental processes such as morphogenesis and tissue repair. In addition, deregulated cellular adherence can result in cancer invasion and metastasis. Adhesion receptors, particularly members of the integrin superfamily, are required to mediate and regulate cell adhesion to structural proteins of tissues, including fibrillar collagens, laminins, and fibronectin. However, due to the dominant contribution of integrins to mechanotransduction and migration in most experimental models, additional low-affinity interactions that might contribute to cell adhesion and migration in three-dimensional (3D) environments are still poorly understood. Typical examples of molecules mediating low-affinity interactions include alternative adhesion receptors carrying compensatory functions such as syndecans (SDCs)[1] or CD44[2], but their contribution to migration is controversially discussed. Among all potential candidates, cell surface carbohydrates that surround cells as a polar outer layer, raised increasing attention. The nature of this so-called glycocalyx is dominated by carbohydrate chains carrying high content of sulfation, carboxylation and acetylation in their backbone providing the negative charge to this layer.[3] These carbohydrate chains are covalently bound to protein or lipid cores, classified as glycoproteins, glycolipids and proteoglycans that are anchored in the cellular membrane or non-covalently linked to binding regions of other proteins at the cell surface.[4] The thickness of the glycocalyx can vary from 7 nm for red blood cells to several 100 nm and even up to several µm[5] for some epithelial and endothelial cells.[6] In contrast, integrin adhesion receptors reach only 20 nm from the plasma membrane in their extended active conformation[7], with the consequence that the first encounter of molecules or ligands with the cell surface during attachment will constitutively occur through the glycocalyx.[8] An increasing number of studies, focusing on the role of carbohydrates and carbohydrate-containing biomolecules in biological systems, indicates the role of cell surface glycans in many physiologically important processes such as embryonic development, differentiation, growth, immune response[9], adhesion, migration and metastasis.[3b, 10] Cells embedded in the extracellular matrix (ECM) with proteoglycans and glycosaminoglycans as major constituents next to growth factors and cytokines[11], will in all likelihood face repelling events based on electrostatic forces between the negative charges of the cell surface glycocalyx and the immediate environment, consistent with local repulsion. Consequently, displacement or reduction of glycocalyx thickness has been associated with sites of adhesion and increases in adhesion to the substrate.[12] A recent model suggests that the glycocalyx provides an essential anti-adhesive role in the regulation of cell adhesion and is essential for the generation of integrin clusters.[8a] Other studies in turn revealed highly basic triple helical domains including disaccharide acceptor sites[13] within collagen I[14] and fibronectin[15] as specific binding sites for negatively charged glycosaminoglycans, indicating a pro-

adhesive function of glycans. Thus, due to these putatively very divergent functions of the glycocalyx, mechanisms through which glycans mediate migratory and invasive potential of malignant cells directly remain unclear.

In this thesis, the potential role of the glycan component in cell migration and invasion independently of the protein cores was investigated. First, a non-cytotoxic approach to transiently remove a major portion of the glycocalyx in live cells was developed, which allows to: (i) probe and quantify surface-glycan-mediated binding forces to fibrillar collagen; (ii) show the dependence of integrin-independent cell migration in three dimensional environments *in vitro* and in mouse models *in vivo* on the availability of surface glycans; and (iii) reveal novel types of glycan-mediated filopodial and bleb-like cell-matrix interactions. Consequently, a conceptually and mechanistically novel model of glycan-based cell migration was developed, which recognizes the surface glycocalyx as generic low-affinity but high-avidity adhesion scaffold to the ECM. Next to tumor cells, glycan-mediated cell adhesion and migration was confirmed for fibroblasts and leukocytes, thus combining glycan biology and matrix research to provide new insights into cell-tissue interactions, migration and invasion.

In addition to integrins a selection of alternative adhesion-systems involved in two- as well as three-dimensional (3D) cell adhesion and migration ***in vitro*** and ***in vivo*** are summarized in **Chapter 2.** The aim is to present the complexity in terms of molecular structures and associated signaling as well as concerning the cellular processes of adaptation to existing requirements of the environment, which cells encounter during cell migration and invasion. In conclusion, integrins cooperate with alternative adhesion mechanisms to mediate interstitial cell migration.

Although glycans as biopolymers play a key role in numerous biological processes[16], the analysis of glycans in live cell models was hampered by the lack of technical tools for appropriate staining and visualization. Only more recently, glycan detection in living cells has received increased attention due to employment of cationic dyes[17], advanced spectroscopic methods and introduction of sensitive live-cell microscopy in the expanding field of glycobiology.[3b, 10c, 10e, 10f] Glycans are not directly encoded in the genome and are thus not amenable to imaging techniques that rely on genetic reporters, e.g. GFP fluorescent fusion proteins.[18] A widely used method for the visualization of glycoconjugates[19] is the staining with naturally occurring glycan-binding proteins, known as lectins[20]. However, lectins typically have low affinity for their glycan epitope, require multivalency for high-avidity binding[21], alter cell function by crosslinking surface receptors and are partly even toxic.[22] For these reasons lectins cannot be used as neutral reporters in live cell studies. Well characterized antibodies recognize, e.g. distinct epitopes within glycosaminoglycans (GAGs)[23] for imaging of live or fixed cells,[24]

but the availability of antibodies is rare due to technical limitations in antibody synthesis recognizing especially small glycan structures.[25] Hence, in recent years efforts to image glycans in living systems have focused on the use of affinity reagents and chemical tools.[18, 26] As strategy, bioorthogonal labeling was developed for tagging cell surface glycans, by combining the simplicity of genetically encoded tags with the specificity of antibody labeling and the versatility of small-molecule probes. In recent years a number of biorthogonal chemical reporters, probes and related bioorthogonal reactions has been developed.[26-27] In **Chapter 3** we introduce Bicyclo [6.1.0] nonyne (BCN) as a novel probe, which combines its exceptionally easy preparation with high reactivity to visualize cell surface sialic acid residues in living cells during cell adhesion and migration. Figure 1 summarizes the experimental procedure and underlying reactions.

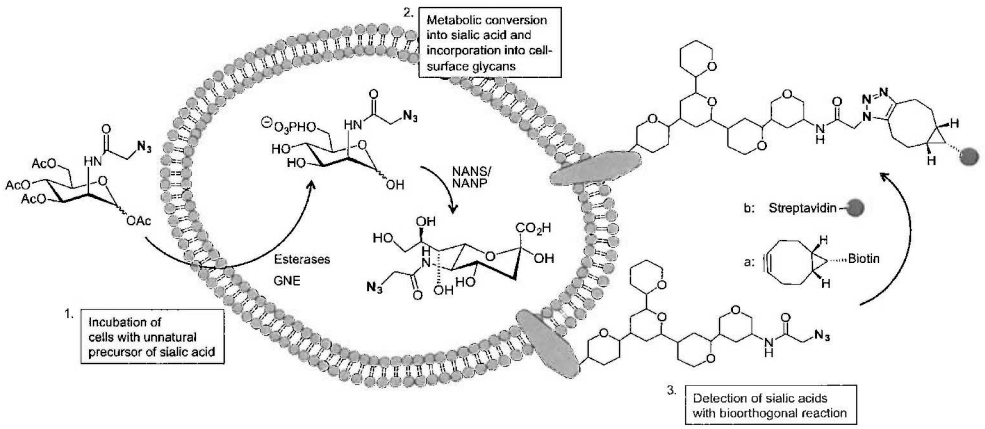

Fig. 1:

Scheme of metabolic labeling. Exogenously added non-native and non-perturbing bioorthogonal chemical reporter peracetylated N-azidoacetyl-D-mannosamine (Ac4ManNAz)[28], bearing azide as a reactive tag[29], can be taken up by cells and is deacetylated by intracellular esterases. Subsequently it enters into the salvage pathway, including UDP-GlcNAc 2-epimerase/ManNAc-6-kinase (GNE)-mediated phosphorylation of ManNAz, the generation of phosphorylated Neu5Ac (Neu5Ac-9-phosphate) by N-acetylneuraminic acid synthase (Neu5Ac-9-P synthetase/NANS) and dephosphorylation of Neu5Ac by N-acetylneuraminic-acid Phosphatase (Neu5Ac-9-P Phosphatase/NANP). After further modifications in the nucleus and the Golgi apparatus, the azido-sialic acids appear as a part of glycan moities of glycoproteins at the cell surface.[30] The detection of cell surface azido-sialic acids (SiaNAz) can be performed by using e.g. Bicyclo [6.1.0] nonyne (BCN) (a) in a metal-free strain promoted alkyne-azide cycloaddition (SPAAC) reaction, giving stable 1,2,3-triazoles. Finally, a fluorophore-conjugated streptavidin (b) can be used to visualize bioorthogonally labeled sialic acids using, e.g. confocal microscopy. Figure taken from Schmidt et al.[32]

The composition of the glycocalyx in different cell types varies greatly, and is further modified in response to environmental conditions, activation, differentiation signals and during cell death.[3b, 16a, 33] To experimentally manipulate a broad range of cell surface glycan types, a novel and stringent two-step multi-enzyme digestion protocol in live cells for the removal of a maximum of surface glycan was developed (**Chapter 4**). Multi-glycan

removal included glycosaminoglycans (GAGs) hyaluronic acid (HA), heparan sulfate (HS), chondroitin sulfate (CS) and dermatan sulfate (DS) and glycan residues of glycoproteins and glycolipids, sialic acids and β-1,4 coupled galactose quantitatively and transiently in a non-toxic manner. Using this approach, digestion efficiencies of more than 95 percent could be achieved. The proof for quantitative multi-glycan removal together with intact cell viability after treatment with glycosidases is essential for subsequent functional studies of glycans in cellular processes, such as adhesion and migration.

The contribution of the surface glycocalyx to cell adhesion and migration was tested in live-cell models after integrin inhibition. The results are summarized in **Chapter 5**. Interference with expression and function of integrins results in morphological transition from a spindle shaped to an amoeboid blebbing phenotype with the consequence that cells maintain the ability to migrate within collagen-based 3D tissue by using an amoeboid migration phenotype of lower speed. Migrating cells with intact glycocalyx maintain adhesion, direct engagement with fibrillar collagen via novel "grip-like" contact structures of membrane blebs grasping a collagen fiber and preserve polarized cell-matrix contacts. However, adhesion on a 2D substrate was abrogated after integrin blockage,[34] which makes surface anchoring a prerequisite for migration in 2D and points to only low adhesive forces involved in this residual adhesion mechanism, which requires an additional physical confinement provided by a three dimensional environment.[35] Using glycan targeted approaches for partial and complete digestion of cell surface glycans in living cells, β-1,4 coupled galactose residues were identified as non-redundant mediators of integrin-independent amoeboid migration, as cells lost the ability to form contact structures to collagen fibers and to migrate. The here established novel enzyme-based glycan targeted approach promotes the concept that the glycocalyx provides a generic low-affinity but high-avidity scaffold and thereby mediates adhesion through adaptive interfaces to mediate integrin-independent mechanocoupling and cell migration in 3D tissue environments.

Aim and content of the thesis

The aim of this thesis was to study the contribution of the glycocalyx to cell adhesion and migration and to identify this polar glycan layer as an alternative mechanism used by cells to compensate for their loss of integrin-mediated adhesion and migration.

In **Chapter 2** integrin-dependend and alternative adhesion mechanisms that potentially contribute to cell anchoring and migration *in vitro* and *in vivo* are critically reviewed.

In **Chapter 3** a novel bioorthogonal approach for the visualization of cell surface sialic acids in living cells without influencing cell function is introduced.

In **Chapter 4** an enzyme-based protocol that allows a gradual enzymatic degradation of carbohydrate chains while maintaining optimal viability is introduced.

In **Chapter 5** the glycan digestion strategy was applied to probe cell functions, including adhesion, migration and formation of cellular contact structures to the surrounding collagenous ECM or tissue in an integrin-independent manner.

In **Chapter 6**, the findings and concepts of this thesis are summarized and discussed. Furthermore, future directions are provided.

Refrences

[1] aJ. R. Couchman, *Nat.Rev.Mol.Cell Biol.* **2003**, *4*, 926-937; bR. L. Longley, A. Woods, A. Fleetwood, G. J. Cowling, J. T. Gallagher, J. R. Couchman, *J.Cell Sci.* **1999**, *112*, 3421-3431; cG. Chalkiadaki, D. Nikitovic, A. Berdiaki, M. Sifaki, K. Krasagakis, P. Katonis, N. K. Karamanos, G. N. Tzanakakis, *Int.J.Biochem.Cell Biol.* **2009**, *41*, 1323-1331; dK. S. Midwood, Y. Mao, H. C. Hsia, L. V. Valenick, J. E. Schwarzbauer, *J.Investig.Dermatol.Symp.Proc.* **2006**, *11*, 73-78; eK. S. Midwood, L. V. Valenick, H. C. Hsia, J. E. Schwarzbauer, *Mol.Biol.Cell.* **2004**, *15*, 5670-5677.

[2] aD. Naor, S. Nedvetzki, I. Golan, L. Melnik, Y. Faitelson, *Crit Rev.Clin.Lab Sci.* **2002**, *39*, 527-579; bL. M. Negi, S. Talegaonkar, M. Jaggi, F. J. Ahmad, Z. Iqbal, R. K. Khar, *J Drug Target* **2012**, *20*, 561-573.

[3] aS. R. Stowell, T. Ju, R. D. Cummings, *Annu Rev Pathol* **2015**, *10*, 473-510; bS. S. Pinho, C. A. Reis, *Nat Rev Cancer* **2015**, *15*, 540-555.

[4] N. CHAFFEY, *Ann Bot* **2003**, *91*, 401.

[5] aE. E. Ebong, F. P. Macaluso, D. C. Spray, J. M. Tarbell, *Arterioscler Thromb Vasc Biol* **2011**, *31*, 1908-1915; bR. T. Megens, S. Reitsma, P. H. Schiffers, R. H. Hilgers, J. G. De Mey, D. W. Slaaf, M. G. oude Egbrink, M. A. van Zandvoort, *J Vasc Res* **2007**, *44*, 87-98; cP. M. van Haaren, E. VanBavel, H. Vink, J. A. Spaan, *Am J Physiol Heart Circ Physiol* **2003**, *285*, H2848-2856.

[6] aS. Ito, *Federation proceedings* **1969**, *28*, 12-25; bF. Martins Mde, V. A. Bairos, *International review of cytology* **2002**, *216*, 131-173.

[7] J. P. Xiong, T. Stehle, R. Zhang, A. Joachimiak, M. Frech, S. L. Goodman, M. A. Arnaout, *Science* **2002**, *296*, 151-155.

[8] aM. J. Paszek, D. Boettiger, V. M. Weaver, D. A. Hammer, *PLoS computational biology* **2009**, *5*, e1000604; bA. R. Pries, T. W. Secomb, P. Gaehtgens, *Pflugers Arch* **2000**, *440*, 653-666; cS. Weinbaum, J. M. Tarbell, E. R. Damiano, *Annu Rev Biomed Eng* **2007**, *9*, 121-167.

[9] R. E. Schweppe, C. E. Haydon, T. S. Lewis, K. A. Resing, N. G. Ahn, ***Acc Chem Res*** **2003**, *36*, 453-461.

[10] aR. S. Haltiwanger, J. B. Lowe, *Annual review of biochemistry* **2004**, *73*, 491-537; bS. D. Rosen, *Annual review of immunology* **2004**, *22*, 129-156; cM. M. Fuster, J. D. Esko, *Nat Rev Cancer* **2005**, *5*, 526-542; dJ. W. Dennis, M. Granovsky, C. E. Warren, *Biochim Biophys Acta* **1999**, *1473*, 21-34; eH. Ghazarian, B. Idoni, S. B. Oppenheimer, *Acta Histochem* **2011**, *113*, 236-247; fN. Taniguchi, Y. Kizuka, *Adv Cancer Res* **2015**, *126*, 11-51; gC. Boscher, J. W. Dennis, I. R. Nabi, *Curr Opin Cell Biol* **2011**; hJ. C. de-Freitas-Junior, S. Carvalho, A. M. Dias, P. Oliveira, J. Cabral, R. Seruca, C. Oliveira, J. A. Morgado-Diaz, C. A. Reis, S. S. Pinho, ***PLoS One*** **2013**, *8*, e81579; iC. Gomes, H. Osorio, M. T. Pinto, D. Campos, M. J. Oliveira, C. A. Reis, ***PLoS One*** **2013**, *8*, e66737; jE. Gorelik, U. Galili, A. Raz, *Cancer and Metastasis Reviews* **2001**, *20*, 245-277.

[11] aT. D. Tlsty, L. M. Coussens, *Annu Rev Pathol* **2006**, *1*, 119-150; bM. Aumailley, B. Gayraud, *J Mol Med (Berl)* **1998**, *76*, 253-265.

[12] aM. Soler, S. Desplat-Jego, B. Vacher, L. Ponsonnet, M. Fraterno, P. Bongrand, J. M. Martin, C. Foa, *FEBS Lett* **1998**, *429*, 89-94; bS. Sabri, M. Soler, C. Foa, A. Pierres, A. Benoliel, P. Bongrand, *J Cell Sci* **2000**, *113 (Pt 9)*, 1589-1600; cA. Datta, Q. Shi, D. E. Boettiger, *Mol Cell Biol* **2001**, *21*, 7295-7306.

[13] aW. T. Butler, L. W. Cunningham, *J Biol Chem* **1966**, *241*, 3882-3888; bW. T. Butler, L. W. Cunningham, *J Biol Chem* **1965**, *240*, Pc3449-3450.

[14] J. D. San Antonio, A. D. Lander, M. J. Karnovsky, H. S. Slayter, *J Cell Biol* **1994**, *125*, 1179-1188.

[15] A. Sharma, J. A. Askari, M. J. Humphries, E. Y. Jones, D. I. Stuart, *Embo J* **1999**, *18*, 1468-1479.

[16] aK. Ohtsubo, J. D. Marth, *Cell* **2006**, *126*, 855-867; bJ. R. Bishop, M. Schuksz, J. D. Esko, *Nature* **2007**, *446*, 1030-1037.

[17] J. H. Luft, *Federation proceedings* **1966**, *25*, 1773-1783.

[18] J. A. Prescher, C. R. Bertozzi, *Cell* **2006**, *126*, 851-854.

[19] aK. T. Pilobello, L. K. Mahal, *Methods Mol Biol* **2007**, *385*, 193-203; bJ. Hirabayashi, *Glycoconj J* **2004**, *21*, 35-40.

[20] aN. Sharon, *J Biol Chem* **2007**, *282*, 2753-2764; bF. Lehmann, E. Tiralongo, J. Tiralongo, *Cell Mol Life Sci* **2006**, *63*, 1331-1354.

[21] L. L. Kiessling, N. L. Pohl, *Chem Biol* **1996**, *3*, 71-77.

[22] aH. Ohba, R. Bakalova, *Cancer chemotherapy and pharmacology* **2003**, *51*, 451-458; bR. E. Schwarz, D. C. Wojciechowicz, A. I. Picon, M. A. Schwarz, P. B. Paty, *Br J Cancer* **1999**, *80*, 1754-1762.

[23] aT. H. van Kuppevelt, M. A. Dennissen, W. J. van Venrooij, R. M. Hoet, J. H. Veerkamp, *The Journal of biological chemistry* **1998**, *273*, 12960-12966; bG. J. Jenniskens, A. Oosterhof, R. Brandwijk, J. H. Veerkamp, T. H. van Kuppevelt, *J Neurosci* **2000**, *20*, 4099-4111; cN. C. Smits, S. Kurup, A. L. Rops, G. B. ten Dam, L. F. Massuger, T. Hafmans, J. E. Turnbull, D. Spillmann, J. P. Li, S. J. Kennel, J. S. Wall, N. W. Shworak, P. N. Dekhuijzen, J. van der Vlag, T. H. van Kuppevelt, *J Biol Chem* **2010**, *285*, 41143-41151; dG. David, X. M. Bai, B. Van der Schueren, J. J. Cassiman, H. Van den Berghe, *J Cell Biol* **1992**, *119*, 961-975; eJ. F. Lensen, T. J. Wijnhoven, L. H. Kuik, E. M. Versteeg, T. Hafmans, A. L. Rops, M. S. Pavao, J. van der Vlag, L. P. van den Heuvel, J. H. Berden, T. H. van Kuppevelt, *Matrix Biol* **2006**, *25*, 457-461; fG. B. Ten Dam, S. Yamada, F. Kobayashi, A. Purushothaman, E. M. van de Westerlo, J. Bulten, A. Malmstrom, K. Sugahara, L. F. Massuger, T. H. van Kuppevelt, *Histochem Cell Biol* **2009**, *132*, 117-127; gT. F. Smetsers, E. M. van de Westerlo, G. B. ten Dam, I. M. Overes, J. Schalkwijk, G. N. van Muijen, T. H. van Kuppevelt, *J Invest Dermatol* **2004**, *122*, 707-716; hZ. Avnur, B. Geiger, *Cell* **1984**, *38*, 811-822.

[24] C. L. de Graffenried, S. T. Laughlin, J. J. Kohler, C. R. Bertozzi, *Proc Natl Acad Sci U S A* **2004**, *101*, 16715-16720.

[25] H. C. Hang, C. R. Bertozzi, *Acc Chem Res* **2001**, *34*, 727-736.

[26] J. A. Prescher, C. R. Bertozzi, *Nat Chem Biol* **2005**, *1*, 13-21.

[27] aB. W. Zaro, Y. Y. Yang, H. C. Hang, M. R. Pratt, *Proc Natl Acad Sci U S A* **2011**, *108*, 8146-8151; bM. Grammel, H. C. Hang, *Nat Chem Biol* **2013**, *9*, 475-484; cP. Thirumurugan, D. Matosiuk, K. Jozwiak, *Chem Rev* **2013**, *113*, 4905-4979; dM. D. Best, *Biochemistry* **2009**, *48*, 6571-6584; eG. de Almeida, E. M. Sletten, H. Nakamura, K. K. Palaniappan, C. R. Bertozzi, *Angew Chem Int Ed Engl* **2012**, *51*, 2443-2447; fM. Zheng, L. Zheng, P. Zhang, J. Li, Y. Zhang, *Molecules* **2015**, *20*, 3190-3205.

[28] aS. J. Luchansky, H. C. Hang, E. Saxon, J. R. Grunwell, C. Yu, D. H. Dube, C. R. Bertozzi, *Methods Enzymol* **2003**, *362*, 249-272; bE. Saxon, C. R. Bertozzi, *Science* **2000**, *287*, 2007-2010; cD. M. Patterson, L. A. Nazarova, J. A. Prescher, *Acs Chem Biol* **2014**, *9*, 592-605; dC. P. Ramil, Q. Lin, *Chem Commun (Camb)* **2013**, *49*, 11007-11022.

[29] M. F. Debets, C. W. van der Doelen, F. P. Rutjes, F. L. van Delft, *Chembiochem* **2010**, *11*, 1168-1184.

[30] A. K. Munster-Kuhnel, J. Tiralongo, S. Krapp, B. Weinhold, V. Ritz-Sedlacek, U. Jacob, R. Gerardy-Schahn, *Glycobiology* **2004**, *14*, 43R-51R.

[31] J. Dommerholt, S. Schmidt, R. Temming, L. J. A. Hendriks, F. P. J. T. Rutjes, J. C. M. van Hest, D. J. Lefeber, P. Friedl, F. L. van Delft, *Angewandte Chemie-International Edition* **2010**, *49*, 9422-9425.

[32] S. Schmidt, R. Wallbrecher, T. H. van Kuppevelt, R. Brock, *Methods Mol Biol* **2015**, *1324*, 123-131.

[33] S. Hakomori, *Proc Natl Acad Sci U S A* **2002**, *99*, 10231-10233.

[34] aN. O. Carragher, S. M. Walker, L. A. Scott Carragher, F. Harris, T. K. Sawyer, V. G. Brunton, B. W. Ozanne, M. C. Frame, *Oncogene.* **2006**, *25*, 5726-5740; bM. H. Zaman, L. M. Trapani, A. L. Sieminski, D. Mackellar, H. Gong, R. D. Kamm, A. Wells, D. A. Lauffenburger, P. Matsudaira, *Proc.Natl.Acad.Sci.U.S.A.* **2006**, *103*, 10889-10894.

[35] T. Lammermann, M. Sixt, *Curr.Opin.Cell Biol.* **2009**.

I do not think there is any thrill that can go through the human heart like that felt by the inventor as he sees some creation of the brain unfolding to success... such emotions make a man forget food, sleep, friends, love, everything.

Nicola Tesla

CHAPTER 2

Interstitial Cell Migration: Integrin-dependent and Alternative Adhesion Mechanisms.

Cell Tissue Res. (2010) 339:83-92

Samuel Schmidt[1,2] *& Peter Friedl*[2,3,4]

[1] Radboud University Medical Centre, Department of Biochemistry, Nijmegen, (Netherlands); [2] Radboud University Medical Centre, Department of Cell Biology (Nijmegen, (Netherlands); [3] Cancer Genomics Center, (Netherlands); [4] The University of Texas MD Anderson Cancer Center, Department of Genitourinary Medical Oncology, Houston, Texas, (United States)

Abstract

Adhesion and migration are integrated cell functions that build, maintain and remodel the multicellular organism. In migrating cells, integrins are the main transmembrane receptors that provide dynamic interactions between extracellular ligands and actin cytoskeleton and signalling machineries. In parallel to integrins, other adhesion systems mediate adhesion and cytoskeletal coupling to the extracellular matrix (ECM). These include multifunctional cell surface receptors (syndecans and CD44) and discoidin domain receptors, which together coordinate ligand binding with direct or indirect cytoskeletal coupling and intracellular signalling. We review the way that the different adhesion systems for ECM components impact cell migration in two- and three-dimensional migration models. We further discuss the hierarchy of these concurrent adhesion systems, their specific tasks in cell migration and their contribution to migration in three- dimensional multi-ligand tissue environments.

Cell adhesion and migration are fundamental to the formation and maintenance of multicellular organisms. Cell adhesion is provided by adhesion molecules, which are expressed at the cell surface of all nucleated cells, mediate extracellular binding to cell and tissue substrates and transmit mechanical docking to the intracellular actomyosin or intermediate filament cytoskeleton. Cell adhesion underlies many important physiological processes, including cell spreading, polarity, anchoring and differentiation. When cell-tissue interactions undergo dynamic turnover, adhesion molecules further mediate cell migration and positioning during dynamic phases of the body, including morphogenesis, wound healing and, in a de-regulated form, during cancer invasion and metastasis (Hood and Cheresh 2002; Hynes 2002). Likewise, cell adhesion and migration underlie many functions of the immune system, including leukocyte recirculation, pathogen recognition and effector function (Friedl and Weigelin 2008).

To fulfill these various tasks in the different cell types and tissue contexts, diverse sets of adhesion receptors contribute to cell interaction with tissue components and to migration. Adhesion receptor ligands are another cell, a multimeric particle or macromolecules that are immobilized in the tissue, such as extracellular matrix (ECM) ligands. Important ECM proteins recognized by adhesion receptors are collagens, fibronectin, vitronectin, fibrinogen and laminin (van der Flier and Sonnenberg 2001). Non-protein ECM ligands comprise proteoglycan polysaccharides, such as heparan sulphate, chondroitin sulphate and keratin sulphate, and the non-proteoglycan polysaccharide hyaluronan (Iozzo 1998; Heino and Kapyla 2009).

Several classes of cell surface receptors fulfill adhesion and cytoskeletal coupling functions and provide a range of adhesion strength, specificity and turnover rates during cell migration (Fig. 1). High affinity adhesion to ECM ligands is predominantly provided by receptors of the integrin family (Hynes 2002) and CD44 (Goodison et al. 1999). Whereas integrins predominantly recognize extracellular protein scaffolds, such as interstitial collagen (Takada et al. 2007), CD44 preferentially binds to extracellular carbohydrate polymers, such as glycoproteins, glycosaminoglycans and hyaluronic acid (HA; Ponta et al. 2003). In addition to these "classical" adhesion receptors, other surface receptors can bind ECM components and induce signalling, including the syndecans (Bernfield et al. 1999) and the receptor tyrosine kinases discoidin domain receptors (DDRs; Yoshimura et al. 2005). Whereas integrin- and CD44-mediated adhesions have previously received substantial attention (Humphries et al. 2003), alternative adhesion mechanisms and their contribution to cell anchoring and migration have been less well studied. We summarize here the way that integrin- and non-integrin- mediated cell-substrate interactions contribute to different types of cell migration.

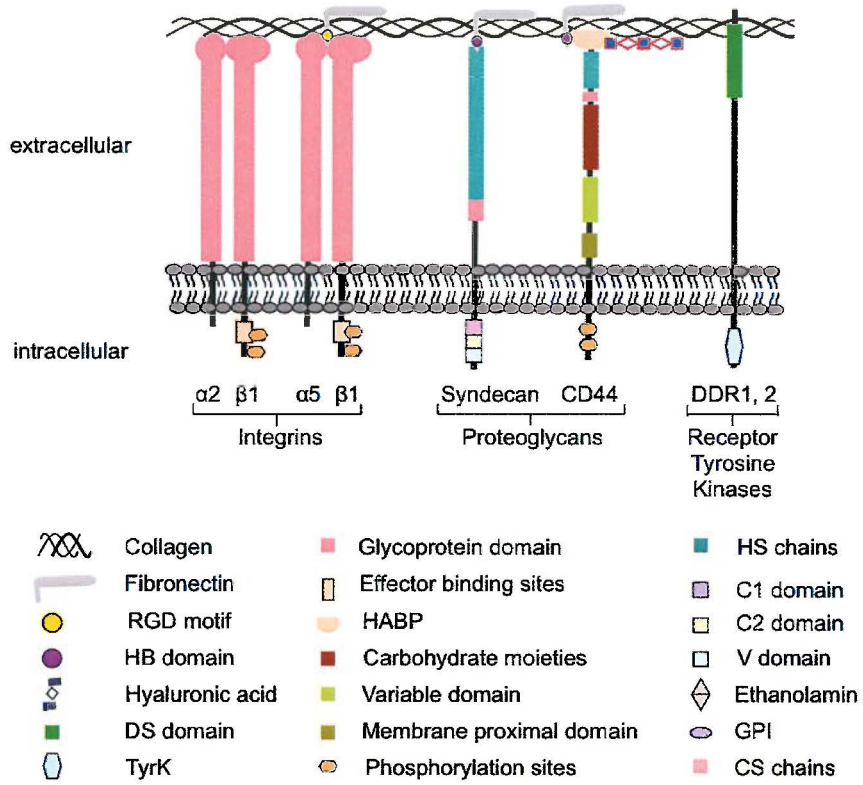

Fig. 1

Classes of adhesion receptors involved in cell adhesion and migration. Important domains of adhesion receptors and interstitial ECM ligands collagen, fibronectin and hyaluronan are shown.

Modes of cell migration and adhesion requirements

Cell migration is not a uniform event but comprises distinct modes of cell migration that are executed by different cell types and contexts. These migration types vary in cell shape, adhesion strength and migration speed and also in whether cell-cell junctions are retained (Fig. 2).

Arguably, the most "simple" migration mode is amoeboid migration (Friedl et al. 2001). Cells that move in an amoeboid manner include primordial germ cells, lymphocytes, dendritic cells, lymphoma cells and neutrophils, all of which exhibit low or no integrin-mediated traction force generation (Entschladen et al. 1997; Friedl et al. 1998; Blaser et al. 2006; Lammermann et al. 2008). These cells form relatively instable adhesion sites to a substrate; such sites rapidly turnover and, depending on extracellular context and signalling, allow for rapidly adaptive migration (Friedl et al. 2001). Amoeboid movement is driven by a roundish to ellipsoid cell shape, non-focalized but rather diffusely organized

adhesion sites to the substrate and a strictly cortical actin cytoskeleton that lacks stress fibres (Friedl and Wolf 2003). Two types of force generation contribute to amoeboid movement.

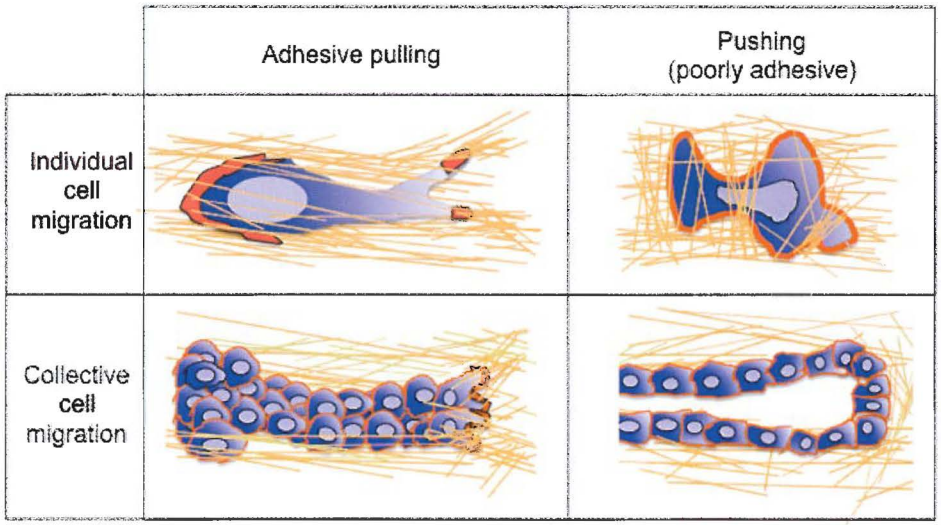

Fig. 2

Various migration strategies. Dependent on cell-matrix adhesion strengths and cell contractility, force generation occurs either via attachment to the ECM substrate and pulling or by cell propulsion. Dependent on the stability of cell-cell adhesion, cells mi- grate either individually or within multicellular strands (red actin cytoskeleton).

Based on relatively weak attachment and spreading on the substrate, a fast "gliding" type of movement is enabled that supports a weakly adhesive pulling-type migration across two-dimensional (2D) and in three-dimensional (3D) environments (Friedl and Wolf 2009). Alternatively, in non-adhesive cells, polarized dendrite or bleb formation coupled to rear-retraction fail to attach to 2D substrate and lack adhesion sites and, thus, provide an intercalating propulsive type of migration in 3D tissues (Fackler and Grosse 2008). The biophysical basis of this blebbing-type migration is incompletely understood as it shows signs of adhesion-independent migration. Instead of focalized adhesion complexes, a predominantly cortical actin cytoskeleton drives cell polarization and physical translocation by shape change and cytoskeletal stiffness in complex tissue environments (Paluch et al. 2006; Friedl and Wolf 2009). In cells with increased adhesion and cytoskeletal contractility, cell-matrix interactions become focalized and the cell adopts an elongated spindle-shaped morphology; this mode of migration is termed mesenchymal migration and is used by fibroblasts, myoblasts and many cancer cells (Friedl et al. 1998; Friedl 2004), generates substantial adhesion and traction force towards the surrounding tissue and further mediates proteolytic tissue remodelling

by the function of cell-produced proteases (Wolf and Friedl 2009). Both ligand binding and intracellular coupling of cell adhesions are turned over in the range of minutes to hours thereby regulating both local adhesion strength and the dynamics of the cell (Zamir and Geiger 2001; Ballestrem et al. 2001). During morphogenesis, regeneration and cancer invasion, cells that retain cell-cell junctions by means of cadherins and other cell-cell adhesion mechanisms migrate collectively either as monolayer sheets or as 3D strands, sprouts or isolated clusters (Friedl et al. 2004). Two types of force generation in collective migration are under discussion at present, depending on the amount of anterior adhesion and traction force generation. If one or several front- and mid-row cells generate adhesion and traction force towards the substrate, collective migration results from adhesive "pulling" mediated by adhesion-complexes that connect to the actin cytoskeleton, similar to mesenchymal movement (Hegerfeldt et al. 2002; Trepat and Wasserman 2009). This type of migration is commonly detected in sprouting vessels, epithelial sheets during wound healing and cancer invasion (Hegerfeldt et al. 2002; Friedl and Gilmour 2009). A second, less well understood mode of collective force generation is multicellular pushing, which is produced by a stable stick-like stalk and a relatively roundish terminal bud that protrudes into soft tissue in the absence of apparent force-generating adhesion complexes (Ewald et al. 2008). Thus, different cellular and molecular requirements for adhesion and force generation govern the different types of cell migration. Whereas, until recently, integrins have received ample attention and are considered as the main mediators of adhesion force generation during cell migration, the promigratory functions of non-integrin adhesion systems remain to be integrated into these concepts of cell movement.

Integrins

Integrins are heterophilic cell adhesion molecules consisting of non-covalently connected α and β chains that together determine ligand-binding specificity and intracel- lular coupling (Humphries 2000; Hynes 2002). Based on ECM/ligand recognition, integrins mediate binding to laminins (α2β1, α3β1, α6β1, α7β1), fibrillar collagens (α1β1, α2β1, α3β1, α10β1, α11β1) and Arg-Gly-Asp (RGD) motifs contained in many ECM proteins (α5β1, αvβ3, αvβ5, αIIbβ3; Takada et al. 2007). Thereby, integrins are the most important cell surface receptors for cell interactions with ECM structures.

Integrins control the strength and turnover of cell interactions with ECM scaffolds (Hynes 1992). After ligand binding, integrins multimerize in the plasma membrane in a focalized manner and connect, via intracellular signalling and adaptor proteins, to the actin cytoskeleton, termed focal contact or focal adhesion (Burridge and Chrzanowska-Wodnicka 1996; Zaidel-Bar et al. 2007; Moser et al. 2009). Alternatively, diffuse integrin

distribution devoid of microscopically detectable clustering and focalization of adhesion site mediates substrate binding and intracellular signalling (Friedl et al. 1998).
To mediate cell movement, the integrin-mediated cell- substrate interactions and linkages to the actin cytoskeleton form and turnover, the dynamics and polarity of which determine cell speed and directional persistence. The way that integrins govern migration type and rates depends upon net adhesion strength per cell, type of cell-matrix interactions and type of substrate. On 2D ECM substrates, including collagen, fibronection or vitronectin, integrin-mediated adhesions are preferentially mediated by α5β1, αvβ3 and α2β1, respectively (Takada et al. 2007). In integrin-dependent migration models, the highest velocities result from an intermediate level of net adhesion strength allowing both rapid focal contact formation and the generation of traction forces, which are regulated by the small GTPase Rho (DiMilla et al. 1991; Beningo et al. 2006). Accordingly, increasing adhesion to the substrate slows cells down and favours cell immobilization and anchoring attributable to delayed rear-retraction. Likewise, at low net adhesion, migration rates are impaired because of reduced binding strength and force generation at the leading edge, resulting in partial or complete loss of migration (Palecek et al. 1997). The impact of adhesion- and traction force-dependent integrin functions are commonly established in haptokinetic migration across a 2D ligand-coated substrate, so that some degree of attachment is indispensible for migration (Huttenlocher et al. 1995). This principle of adhesion-driven migration applies to many, if not all, actin-associated integrins, notably β1, β2, β3, and β4 integrins (Rabinovitz and Mercurio 1997; Maaser et al. 1999; Vicente-Manzanares et al. 2009). Consequently, both cell adhesion and migration are impaired by adhesion-perturbing anti-integrin antibodies or genetic deletion of integrins so that the cells either round up and partly detach or completely lose contact to the substrate (Friedl and Wolf 2003). If, however, cells move through a 3D ECM, distinct physical principles apply because cells are entirely surrounded by ECM and, even after loss of adhesion, continue to interact passively with the substrate (Friedl and Brocker 2000).
For cells of high integrin availability moving through a 3D ECM, including fibroblasts and certain cancer cells, integrins mediate adhesive pulling at the leading edge so that traction force towards the substrate is continually being generated (Fig. 2; Maaser et al. 1999; Petrie et al. 2009). Consequently, cell elongation and mesenchymal migration are dependent on integrin-mediated adhesion and focalization of the actin cytoskeleton to matrix contacts. The integrin engagement leads to the activation of focal adhesion kinase, Rho/Rac guanine nucleotide exchange factors and Rho kinase (ROCK), which together drive the formation and turnover of adhesions (Iwanicki et al. 2008). Following interference with integrin-mediated adhesion, mesenchymal migration is abrogated and no alternative adhesion receptors compensate for ablated integrin-dependent force generation and mesenchymal migration (Maaser et al. 1999; Grinnell 2008, 2009). In mesenchymal migration, integrin β1 or αvβ3 integrins cooperate with cell surface proteases, notably matrix metalloproteinases (MMPs) leading to the generation of

small microtracks bordered by remodelled collagen fibres (Deryugina et al. 1998; Wolf et al. 2007). Secondary to traction force generation, mesenchymal migration leads to contraction and remodelling of the ECM *in vitro* and to wound healing (Cooke et al. 2000; Larsen et al. 2006).

If integrin-mediated traction force is low or negligible, moving cells utilize the amoeboid migration mode (Fig. 2; Friedl et al. 2001). Whereas, on 2D surfaces, amoeboid migration is still dependent on low adhesion mediated by integrins (Lammermann et al. 2008), amoeboid migration in 3D fibrillar collagen or interstitial tissue *in vivo* persists either partly or fully after integrins are blocked by antibody or are genetically ablated (Friedl et al. 1998; Lammermann et al. 2008). In integrin-independent amoeboid migration, the leading edge produces pseudopodia, dendrites or roundish-shaped blebs, all of which are dependent on cortical actin networks but do not form focalized adhesion complexes with the ECM substrate (Friedl et al. 1998; Lammermann and Sixt 2009). The mechanisms underlying integrin-independent migration are incompletely understood, but are best explained by actin forward flow followed by cell intercalation between matrix pores and gaps and cell contraction mediated by myosin II to move both the cell rear and the nucleus forward (Lammermann et al. 2008). Thus, grossly different magnitudes of integrin-mediated adhesion and force generation are associated with the diverse migration modes.

Accordingly, in 3D ECM-based models, cells can switch between high and low integrin-dependence of migration. The lowering of integrin-mediated adhesion by blocking with antibodies or by interfering with the integrin-effector c-src does not abrogate migration of cancer cells in 3D ECM-based models, but is followed by persistent robust cell movement (Carragher et al. 2006; Zaman et al. 2006). Whether such plasticity is restricted to cancer cells and which alternative adhesion mechanisms compensate for impaired integrin function remain unclear.

Because of their multifunctional nature and ubiquitous expression, integrins contribute to most cell-tissue interaction models substantially and impact other adhesion path-ways in response to ECM. Thus, as we will discuss below, the study of adhesion mechanisms other than integrins is often compromised by an overlap with integrin-mediated substrate recognition and function.

Syndecans

Syndecans are a family of transmembrane cell surface heparan sulphate proteoglycans (HSPGs) with four members, syndecan 1–4. All vertebrate cells express at least one syndecan family member in a cell-type and tissue-specific manner, which is further modified during cell activation (Tkachenko et al. 2005). Syndecans bind to ECM ligands and further cooperate with other cell surface receptors for ligand-binding and signalling. Via their heparin-binding ectodomain, syndecans bind to extracellular glycosaminoglycans, including heparan sulphate and chondroitin sulphate, and to other ECM molecules, including collagen types I, III and IV, fibronectin and vitronectin (Beauvais et al. 2004). By distinct mechanisms, syndecans further bind via residues within the HSPG side chains to cytokines and growth factors, including fibroblast growth factor-2 and epidermal growth factor and "present" them laterally to their specific receptors (Wu et al. 2003; Tkachenko et al. 2005).

Syndecans mediate both cell adhesion and co-signalling, often in the same context, which renders the distinction between adhesion and co-signalling function difficult, if not impossible. In most cell models, overexpression of syndecans enhances cell adhesion and haptokinetic migration in normal and neoplastic cells, whereas interference with syndecan function decreases cell migration (Table 1). As an example, in endothelial cells, binding of syndecan-4 to fibronectin-coated substrate results in syndecan-4 co-clustering with integrin $\alpha5\beta1$ and the activation of Rac-1 through the intracellular scaffold protein synectin (Tkachenko et al. 2006; Morgan et al. 2007). Consequently, syndecans enhance cell spreading, polarization and migration *in vitro* and cell migration and tissue remodelling during wound healing and angiogenesis *in vivo* (Table 1; Echtermeyer et al. 2001; Stepp et al. 2002; Morgan et al. 2007).

Syndecans interact with a large number of ligands, which in parallel also bind to other cell surface receptors. Thus, a functional synergy between syndecans and integrins leads to an overlap in adhesion-dependent signalling pathways (Morgan et al. 2007). Given that syndecans functionally synergize with integrins, the extent to which syndecans can be understood as true adhesion receptors awaits further clarification by using models that isolate the direct contribution of syndecans to adhesion from its co-receptor and signalling activities.

Discoidin domain receptors (DDR)

Discoidin domain receptors (DDRs) belong to the discoidin-like domain-containing subfamily of receptor tyrosine kinases, with two members in mammalian cells: DDR1, expressed as five isoforms (DDR1a-e), and DDR2 with no known isoforms (Alves et al. 2001; Vogel et al. 1997). As main ligands, DDRs bind to all triple-helical fibrillar collagens, and DDR1 additionally binds to collagens type IV, VI and VIII (Curat et al. 2001). DDR1 is expressed in many epithelia (Vogel et al. 1997), and in tissue-infiltrating leukocytes (Kamohara et al. 2001), whereas DDR2 is expressed in muscle cells, kidney, lung, brain and connective tissue (Vogel 1999); both DDRs are upregulated in many cancer cell types (Vogel et al. 2006). After ligand binding, DDRs induce various intracellular signalling pathways, including the activation of Wiskott-Aldrich syndrome protein and Pyk-2s, the SH2-domain-containing-transforming protein and SH2-domain-containing phosphatase 2, all of which indirectly promote actin dynamics (Buday et al. 2002; Koo et al. 2006; Vogel et al. 2006). Accordingly, DDRs enhance cell migration, proliferation, and survival (Vogel 1999). In contrast to other receptor tyrosine kinases, initial signalling through DDRs occurs within minutes but peaks only several hours later, implicating DDRs in sustained and slow rather than acute responses to the ECM (Vogel et al. 1997, 2006).
Despite their collagen-binding capability, whether DDRs can be considered as classical adhesion receptors is unclear. DDR signalling typically co-engages with integrins (Shintani et al. 2008). DDRs enhance integrin-mediated cell adhesion to collagen (Kamohara et al. 2001) and enhance integrin- mediated signalling (Shintani et al. 2008). In addition, in some models, DDR1 overexpression enhances cell attachment to collagen that cannot be directly attributed to integrin function, suggesting either a direct adhesion function of DDR1 or the co-engagement of yet another adhesion system (Kamohara et al. 2001).
DDRs regulate cell migration in an isoform-specific manner. DDR1a-overexpressing leukemia and glioma cells show enhanced migration into 3D collagen lattices, whereas overexpression of DDR1b reduces migration in both cell types (Kamohara et al. 2001; Ram et al. 2006). On the basis that all DDRs bind to collagen by a similar mechanism, the signalling pathways that underlie such different fine-tuning of migration are unknown.

Syndecan type	Cell type	Experimental model	Function	Ref.
Syndecan-1	Breast cancer cells	2D spreading and migration assay; migration through 3D matrigel after overexpression	Increased spreading, adhesion and migration on 2D collagen I;increased cell invasion in 3D-Matrigel	(Burbach et al. 2004)
	Myeloma cells	*In vivo* model of experimental metastasis in mice	Increased metastasis and tumor growth	(Khotskaya et al. 2009)
Syndecan-2	Intestinal epithelial cells	2D adhesion and migration after overexpression	Increase of adhesion, spreading on collagen type I (in cooperation with α2β1 integrin)	(Choi et al. 2009)
	Colon carcinoma cells	Migration across type I collagen-coated surface after overexpression	Increased migration speed	(Park et al. 2002), (Contreras et al. 2001)
	Melanoma cells	Migration through polycarbonate filter (transwell) after overexpression	Increased migration and invasion	(Lee et al. 2009)
Syndecan-3	Neuronal cells	Migration through polycarbonate filter (transwell)	Increased migration	(Hienola et al. 2006)
Syndecan-4	Melanoma cells	Adhesion and migration across fibronectin-coated 2D surface	Increased adhesion and migration	(Chalkiadaki et al. 2009)
	Fibroblasts	Adhesion and migration in 3D fibrin-fibronectin-matrix	Increased adhesion and migration	(Midwood et al. 2004; Midwood et al. 2006)

Table 1

Regulation of cell migration by syndecans (2D two-dimensional, 3D three dimensional)

DDRs not only enhance cytoskeletal dynamics, but further induce a more complex "invasion program". DDR signalling upregulates pro-invasive MMPs 2 and 9, which leads to enhanced proteolytic degradation of ECM (Hou et al. 2002) and invasion and metastasis of tumour cells *in vivo* (Vogel et al. 1997). Although experimental over- expression of DDR1 acts in a promigratory manner (Ram et al. 2006), whether lower endogenous levels mediate the same effect remains unclear. To improve the discrimination between adhesive and signalling functions of DDRs, future studies should address DDR adhesion and other functions in integrin-independent models.

CD44

CD44 is a highly glycosylated member of the hyaladherin or link protein superfamily of adhesion molecules and is either expressed as the standard form (CD44s) or as one of 12 distinct isoforms (CD44v1-v12; Ponta et al. 2003; Naor et al. 2008). CD44 binds its main ligand, HA, via the hyaluronan-binding domain (Banerji et al. 2007). Other ligands, which instead interact with variable membrane- proximal domains of CD44, include heparan sulphate (exon v3), chondroitin sulphate (exon 5) and, via unmapped sites with probably weaker binding strength, collagen types I and VI, fibronectin and laminin and cell surface receptors, such as E- and L-selectin (Ponta et al. 2003; Bendall et al. 2004; Naor et al. 2007). The cytoplasmic domain of CD44 recruits the actin-binding proteins ezrin, radixin and moesin (ERM; Legg et al. 2002) and ankyrin and thereby physically bridges extracellular ligands to the actin cytoskeleton and induces intracellular signalling (Bourguignon 2008; Singleton et al. 2004). In addition to its adhesion function, CD44 serves as a co-receptor for other signalling receptors, such as the receptor tyrosine kinase mesenchymal-epithelial transition factor (c-Met), epidermal growth factor receptor and tumour growth factor-β (Orian-Rousseau et al. 2002).

CD44s is expressed by all nucleated vertebrate cells, including most cancer cells (Naor et al. 1997; Tanabe et al. 1993). Activated cells and many cancer cells additionally express CD44 variants, such as CD44v3-v10 on keratinocytes and CD44v6 on many transformed cells ((Brown et al. 1991); Wang et al. 2009). CD44-mediated signalling occurs via various pathways. HA binding leads to the activation of several effectors, including c-Src (Ouhtit et al. 2007), Rac1 and RhoA (Bourguignon et al. 2000; Bourguignon et al. 2001). In turn, active Rho and its effector ROCK promote the recruitment of the cytoskeleton-protein ankyrin-1 and engage with the conserved cytoplasmic domain of CD44 and thereby provide a second link between CD44 and the actin cytoskeleton (Singleton and Bourguignon 2004).

In addition to binding to tissue-anchored HA, CD44 immobilizes HA at the cell surface (Rilla et al. 2008). In early cell adhesion, cell-surface-tethered HA captures ECM substrata prior to integrin-mediated focal contact formation (Zimmerman et al. 2002). Cell-surface HA is constitutively present at the tips of cell protrusions, such as pseudopodia and lamellipodia, and engages with extracellular ECM substrate before integrin clustering and the formation of focal adhesions are detectable (Zimmerman et al. 2002; Rilla et al. 2008).

In most 2D haptokinetic migration models, CD44 enhances migration, either directly by mediating attachment to the substrate or by enhancing promigratory signalling. In normal and neoplastic cells, CD44 supports adhesion and migration across HA-coated surfaces (Zhu et al. 2006). Hereby, in contrast to integrins and syndecans, CD44 does not cluster at contact sites but rather seems to form uniform interaction zones to the substrate with a trend for redistribution to the cell rear (Jacobson et al. 1984; Goebeler

et al. 1996; Friedl et al. 1997). In migrating leukocytes, CD44 is virtually excluded from the leading edge and accumulates together with ERM proteins in the posterior uropod, albeit that its function here is unclear (Sanchez-Madrid and del Pozo 1999; Wagner et al. 2008). Many cells, irrespective of adhesion strength and the substrate across which they migrate, release substantial amounts of CD44, the function of which however is unclear, from the rear of the cell (Bazil and Horejsi 1992; Friedl et al. 1997). In addition to an adhesion function, the CD44-HA interaction results in the rapid activation of surface proteolysis via endopeptidases, including MT1- MMP and ADAMs (a disintegrin and metalloproteinase family), which cleave the CD44 ectodomain and thereby limit CD44-mediated cell attachment (Nagano et al. 2004). Thus, the dual role of CD44 comprises cell attachment and the secondary release of CD44-mediated adhesion bonds.

In contrast to *in vitro* findings with respect to the contribution of CD44 to cell migration on an HA substrate, CD44-deficient mice lack obvious defects of development, regeneration and immune function, suggesting intact interstitial cell migration (Protin et al. 1999; Naor et al. 2008). To what extent other adhesion receptors, including β1 integrins, the receptor for hyaluronan-mediated motility (RHAMM) or layilin as alternative receptors for HA compensate for the loss of CD44 remains to be addressed (Protin et al. 1999; Naor et al. 2007; Chen et al. 2008).

In cancer models, the interaction of CD44 variants with HA supports lymphoma and melanoma progression and metastasis, which is prevented by blocking antibodies targeting CD44v4-v10 or by expressing CD44 with an inactive HA-binding domain (Wallach-Dayan et al. 2001). Conversely, over-expression of soluble CD44 ectodomain in malignant melanoma and mammary carcinoma cells inhibits growth, local invasion and metastasis *in vivo*, suggesting a role for the membrane-anchoring of CD44 (Ahrens et al. 2001; Peterson et al. 2000). However, given the lack of a phenotype in CD44-deficient mice, the *in vivo* relevance of CD44-mediated adhesion and migration detected ***in vitro*** remains unclear. Thus, like syndecans, CD44 and its variants provide multiple adhesion and co-signalling functions, the mechanistic contribution of which to cell migration remains incompletely understood.

Concluding remarks

The various adhesion systems expressed by vertebrate cells serve overlapping functions for cell positioning, anchoring and signalling, but simultaneously retain additional independent and unique properties for each receptor. Whereas the molecular structure and associated signalling machinery of each receptor system have been examined in detail, only the role of integrins in cell migration has been conclusively established. Conversely, the functions of syndecans, DDRs and CD44 in the different types of cell migration, their integration into distinct adhesion and de-adhesion functions of the cell, their

functional overlap and their spatiotemporal coordination during cell-matrix interaction and migration within multi-ligand environments remain unknown. Syndecans and DDRs cooperate with integrins synergistically in mediating cell adhesion and migration; this compromises defined experimental control of their functions. In order to experimentally overcome the governance of integrins and to gain better conceptual insights into each adhesion system independently, future strategies will require models of limited integrin availability or integrin deficiency. Integrin-deficient cell models that still retain their cytoskeletal and polarization machinery will be instrumental in addressing specific migration modes and mechanisms and their response to physical tissue properties. To this end, the discrimination of the *bona fide* adhesion function of DDRs, syndecans and CD44 from their other co-receptor functions and from intracellular docking to cytoskeletal and signalling scaffolds, which contribute to cell adhesion and migration by indirect routes, will be of importance. Such approaches will clarify the way that distinct adhesion systems spatio-temorally contribute to the complex process of cell dynamics and of anchoring in multifaceted tissue environments.

References

Abdulhussein R, McFadden C, Fuentes-Prior P, Vogel WF (2004) Exploring the collagen-binding site of the DDR1 tyrosine kinase receptor. J Biol Chem 279:31462–31470, Cell Tissue Res (2010) 339:83–92

Ahrens T, Sleeman JP, Schempp CM, Howells N, Hofmann M, Ponta H, Herrlich P, Simon JC (2001) Soluble CD44 inhibits melanoma tumor growth by blocking cell surface CD44 binding to hyaluronic acid. Oncogene 20:3399–3408

Alves F, Saupe S, Ledwon M, Schaub F, Hiddemann W, Vogel WF (2001) Identification of two novel, kinase-deficient variants of discoidin domain receptor 1: differential expression in human colon cancer cell lines. FASEB J 15:1321–1323

Ballestrem C, Hinz B, Imhof BA, Wehrle-Haller B (2001) Marching at the front and dragging behind: differential alphaVbeta3-integrin turnover regulates focal adhesion behavior. J Cell Biol 155:1319– 1332

Banerji S, Wright AJ, Noble M, Mahoney DJ, Campbell ID, Day AJ, Jackson DG (2007) Structures of the Cd44-hyaluronan complex provide insight into a fundamental carbohydrate-protein interac- tion. Nat Struct Mol Biol 14:234–239

Bazil V, Horejsi V (1992) Shedding of the CD44 adhesion molecule from leukocytes induced by anti-CD44 monoclonal antibody simulating the effect of a natural receptor ligand. J Immunol 149:747–753

Beauvais DM, Burbach BJ, Rapraeger AC (2004) The syndecan-1 ectodomain regulates alphavbeta3 integrin activity in human mammary carcinoma cells. J Cell Biol 167:171–181

Bendall LJ, Nilsson SK, Khan NI, James A, Bonnet C, Lock RB, Papa R, Bradstock KF, Gottlieb DJ (2004) Role of CD44 variant exon 6 in acute lymphoblastic leukaemia: association with altered bone marrow localisation and increased tumour burden. Leukemia 18:1308–1311

Beningo KA, Hamao K, Dembo M, Wang YL, Hosoya H (2006) Traction forces of fibroblasts are regulated by the Rho-dependent kinase but not by the myosin light chain kinase. Arch Biochem Biophys 456:224–231

Bernfield M, Gotte M, Park PW, Reizes O, Fitzgerald ML, Lincecum J, Zako M (1999) Functions of cell surface heparan sulfate proteoglycans. Annu Rev Biochem 68:729–777

Blaser H, Reichman-Fried M, Castanon I, Dumstrei K, Marlow FL, Kawakami K, Solnica-Krezel L, Heisenberg CP, Raz E (2006) Migration of zebrafish primordial germ cells: a role for myosin contraction and cytoplasmic flow. Dev Cell 11:613–627

Bourguignon LY (2008) Hyaluronan-mediated CD44 activation of RhoGTPase signaling and cytoskeleton function promotes tumor progression. Semin Cancer Biol 18:251–259

Bourguignon LY, Zhu H, Shao L, Chen YW (2000) CD44 interaction with Tiam1 promotes Rac1 signaling and hyaluronic acid-mediated breast tumor cell migration. J Biol Chem 275:1829–1838

Bourguignon LY, Zhu H, Zhou B, Diedrich F, Singleton PA, Hung MC (2001) Hyaluronan promotes CD44v3-Vav2 interaction with Grb2–p185(HER2) and induces Rac1 and Ras signaling during ovarian tumor cell migration and growth. J Biol Chem 276:48679–48692

Brown TA, Bouchard T, St John T, Wayner E, Carter WG (1991) Human keratinocytes express a new CD44 core protein (CD44E) as a heparan-sulfate intrinsic membrane proteoglycan with additional exons. J Cell Biol 113:207–221

Buday L, Wunderlich L, Tamas P (2002) The Nck family of adapter proteins: regulators of actin cytoskeleton. Cell Signal 14:723–731 Burbach BJ, Ji Y, Rapraeger AC (2004) Syndecan-1 ectodomain regulates matrix-dependent signaling in human breast carcinoma cells. Exp Cell Res 300:234–247

Burridge K, Chrzanowska-Wodnicka M (1996) Focal adhesions, contractility, and signaling. Annu Rev Cell Dev Biol 12:463–518 Carragher NO, Walker SM, Scott Carragher LA, Harris F, Sawyer TK, Brunton VG, Ozanne BW, Frame MC (2006) Calpain 2 and Src dependence distinguishes mesenchymal and amoeboid modes of tumour cell invasion: a link to integrin function. Oncogene 25:5726–5740

Chalkiadaki G, Nikitovic D, Berdiaki A, Sifaki M, Krasagakis K, Katonis P, Karamanos NK, Tzanakakis GN (2009) Fibroblast growth factor-2 modulates melanoma adhesion and migration through a syndecan-4-dependent mechanism. Int J Biochem Cell Biol 41:1323–1331

Chen Z, Zhuo W, Wang Y, Ao X, An J (2008) Down-regulation of layilin, a novel hyaluronan receptor, via RNA interference, inhibits invasion and lymphatic metastasis of human lung A549 cells. Biotechnol Appl Biochem 50:89–96

Choi S, Kim Y, Park H, Han IO, Chung E, Lee SY, Kim YB, Lee JW, Oh ES, Yi JY (2009) Syndecan-2 overexpression regulates adhesion and migration through cooperation with integrin alpha2. Biochem Biophys Res Commun 384:231–235

Cooke ME, Sakai T, Mosher DF (2000) Contraction of collagen matrices mediated by alpha2beta1A and alpha(v)beta3 integrins. J Cell Sci 113:2375–2383

Curat CA, Eck M, Dervillez X, Vogel WF (2001) Mapping of epitopes in discoidin domain receptor 1 critical for collagen binding. J Biol Chem 276:45952–45958

Deryugina EI, Bourdon MA, Reisfeld RA, Strongin A (1998) Remodeling of collagen matrix by human tumor cells requires activation and cell surface association of matrix metalloproteinase-2. Cancer Res 58:3743–3750

DiMilla PA, Barbee K, Lauffenburger DA (1991) Mathematical model for the effects of adhesion and mechanics on cell migration speed. Biophys J 60:15–37

Echtermeyer F, Streit M, Wilcox-Adelman S, Saoncella S, Denhez F, Detmar M, Goetinck P (2001) Delayed wound repair and impaired angiogenesis in mice lacking syndecan-4. J Clin Invest 107:R9–R14

Entschladen F, Niggemann B, Zanker KS, Friedl P (1997) Differential requirement of protein tyrosine kinases and protein kinase C in the regulation of T cell locomotion in three-dimensional collagen matrices. J Immunol 159:3203–3210

Ewald AJ, Brenot A, Duong M, Chan BS, Werb Z (2008) Collective epithelial migration and cell rearrangements drive mammary branching morphogenesis. Dev Cell 14:570–581

Fackler OT, Grosse R (2008) Cell motility through plasma membrane blebbing. J Cell Biol 181:879–884

Friedl P (2004) Prespecification and plasticity: shifting mechanisms of cell migration. Curr Opin Cell Biol 16:14–23

Friedl P, Brocker EB (2000) The biology of cell locomotion within three- dimensional extracellular matrix. Cell Mol Life Sci 57:41–64 Friedl P, Gilmour D (2009) Collective cell migration in morphogen-

esis, regeneration and cancer. Nat Rev Mol Cell Biol 10:445–457 Friedl P, Weigelin B (2008) Interstitial leukocyte migration and immune function. Nat Immunol 9:960–969

Friedl P, Wolf K (2003) Tumour-cell invasion and migration: diversity and escape mechanisms. Nat Rev Cancer 3:362–374

Friedl P, Wolf K (2009) Plasticity of cell migration modes—a multi-scale tuning model. J Cell Biol (in press)

Friedl P, Maaser K, Klein CE, Niggemann B, Krohne G, Zanker KS (1997) Migration of highly aggressive MV3 melanoma cells in 3- dimensional collagen lattices results in local matrix reorganization and shedding of alpha2 and beta1 integrins and CD44. Cancer Res 57:2061–2070

Friedl P, Entschladen F, Conrad C, Niggemann B, Zanker KS (1998) CD4+ T lymphocytes migrating in three-dimensional collagen lattices lack focal adhesions and utilize beta1 integrin-independent strategies for polarization, interaction with collagen fibers and locomotion. Eur J Immunol 28:2331–2343

Friedl P, Borgmann S, Brocker EB (2001) Amoeboid leukocyte crawling through extracellular matrix: lessons from the Dictyos- telium paradigm of cell movement. J Leukoc Biol 70:491–509

Friedl P, Hegerfeldt Y, Tusch M (2004) Collective cell migration in morphogenesis and cancer. Int J Dev Biol 48:441–449 Cell Tissue Res (2010) 339:83–92

Goebeler M, Kaufmann D, Brocker EB, Klein CE (1996) Migration of highly aggressive melanoma cells on hyaluronic acid is associated with functional changes, increased turnover and shedding of CD44 receptors. J Cell Sci 109:1957–1964

Goodison S, Urquidi V, Tarin D (1999) CD44 cell adhesion molecules. Mol Pathol 52:189–196

Grinnell F (2008) Fibroblast mechanics in three-dimensional collagen matrices. J Bodyw Mov Ther 12:191–193

Grinnell F (2009) Cell migration and signaling in three-dimensional matrix. Annu Rev Cell Dev Biol (in press)

Hegerfeldt Y, Tusch M, Brocker EB, Friedl P (2002) Collective cell movement in primary melanoma explants: plasticity of cell-cell interaction, beta1-integrin function, and migration strategies. Cancer Res 62:2125–2130

Heino J, Kapyla J (2009) Cellular receptors of extracellular matrix molecules. Curr Pharm Des 15:1309–1317

Hienola A, Tumova S, Kulesskiy E, Rauvala H (2006) N-syndecan deficiency impairs neural migration in brain. J Cell Biol 174:569–580

Hood JD, Cheresh DA (2002) Role of integrins in cell invasion and migration. Nat Rev Cancer 2:91–100

Hou G, Vogel WF, Bendeck MP (2002) Tyrosine kinase activity of discoidin domain receptor 1 is necessary for smooth muscle cell migration and matrix metalloproteinase expression. Circ Res 90:1147–1149

Humphries MJ (2000) Integrin structure. Biochem Soc Trans 28:311–339 Humphries MJ, McEwan PA, Barton SJ, Buckley PA, Bella J, Mould AP (2003) Integrin structure: heady advances in ligand binding, but activation still makes the knees wobble. Trends Biochem Sci 28:313–320

Huttenlocher A, Sandborg RR, Horwitz AF (1995) Adhesion in cell migration. Curr Opin Cell Biol 7:697–706

Hynes RO (1992) Integrins: versatility, modulation, and signaling in cell adhesion. Cell 69:11-25

Hynes RO (2002) Integrins: bidirectional, allosteric signaling machines. Cell 110:673–687

Iozzo RV (1998) Matrix proteoglycans: from molecular design tocellular function. Annu Rev Biochem 67:609–652

Iwanicki MP, Vomastek T, Tilghman RW, Martin KH, Banerjee J, Wedegaertner PB, Parsons JT (2008) FAK, PDZ-RhoGEF and ROCKII cooperate to regulate adhesion movement and trailing-edge retraction in fibroblasts. J Cell Sci 121:895–905

Jacobson K, O'Dell D, Holifield B, Murphy TL, August JT (1984) Redistribution of a major cell surface glycoprotein during cell

movement. J Cell Biol 99:1613–1623

Kamohara H, Yamashiro S, Galligan C, Yoshimura T (2001) Discoidin domain receptor 1 isoform-a (DDR1alpha) promotes migration of leukocytes in three-dimensional collagen lattices. FASEB J 15:2724–2726

Khotskaya YB, Dai Y, Ritchie JP, Macleod V, Yang Y, Zinn K, Sanderson RD (2009) Syndecan-1 is required for robust growth, vascularization and metastasis of myeloma tumors ***in vivo***. J Biol Chem 284:26085-26095

Koo DH, McFadden C, Huang Y, Abdulhussein R, Friese-Hamim M, Vogel WF (2006) Pinpointing phosphotyrosine-dependent interactions downstream of the collagen receptor DDR1. FEBS Lett 580:15–22

Lammermann T, Sixt M (2009) Mechanical modes of "amoeboid" cell migration. Curr Opin Cell Biol 21:636–644

Lammermann T, Bader BL, Monkley SJ, Worbs T, Wedlich-Soldner R, Hirsch K, Keller M, Forster R, Critchley DR, Fassler R, Sixt M (2008) Rapid leukocyte migration by integrin-independent flowing and squeezing. Nature 453:51–55

Larsen M, Artym VV, Green JA, Yamada KM (2006) The matrix reorganized: extracellular matrix remodeling and integrin signaling. Curr Opin Cell Biol 18:463–471

Lee JH, Park H, Chung H, Choi S, Kim Y, Yoo H, Kim TY, Hann HJ, Seong I, Kim J, Kang KG, Han IO, Oh ES (2009) Syndecan-2 regulates the migratory potential of melanoma cells. J Biol Chem 284:27167–27175

Legg JW, Lewis CA, Parsons M, Ng T, Isacke CM (2002) A novel PKC-regulated mechanism controls CD44 ezrin association and directional cell motility. Nat Cell Biol 4:399–407

Maaser K, Wolf K, Klein CE, Niggemann B, Zanker KS, Brocker EB, Friedl P (1999) Functional hierarchy of simultaneously expressed adhesion receptors: integrin alpha2beta1 but not CD44 mediates MV3 melanoma cell migration and matrix reorganization within three-dimensional hyaluronan-containing collagen matrices. Mol Biol Cell 10:3067–3079

Midwood KS, Valenick LV, Hsia HC, Schwarzbauer JE (2004) Coregulation of fibronectin signaling and matrix contraction by tenascin-C and syndecan-4. Mol Biol Cell 15:5670– 5677

Midwood KS, Mao Y, Hsia HC, Valenick LV, Schwarzbauer JE (2006) Modulation of cell-fibronectin matrix interactions during tissue repair. J Invest Dermatol Symp Proc 11:73–78

Morgan MR, Humphries MJ, Bass MD (2007) Synergistic control of cell adhesion by integrins and syndecans. Nat Rev Mol Cell Biol 8:957–969

Moser M, Legate KR, Zent R, Fassler R (2009) The tail of integrins, talin, and kindlins. Science 324:895–899

Nagano O, Murakami D, Hartmann D, De Strooper B, Saftig P, Iwatsubo T, Nakajima M, Shinohara M, Saya H (2004) Cell- matrix interaction via CD44 is independently regulated by different metalloproteinases activated in response to extracel- lular Ca(2+) influx and PKC activation. J Cell Biol 165:893– 902

Naor D, Sionov RV, Ish-Shalom D (1997) CD44: structure, function, and association with the malignant process. Adv Cancer Res 71:241–319

Naor D, Nedvetzki S, Walmsley M, Yayon A, Turley EA, Golan I, Caspi D, Sebban LE, Zick Y, Garin T, Karussis D, Assayag- Asherie N, Raz I, Weiss L, Slavin S, Golan I (2007) CD44 involvement in autoimmune inflammations: the lesson to be learned from CD44-targeting by antibody or from knockout mice. Ann N Y Acad Sci 1110:233–247

Naor D, Wallach-Dayan SB, Zahalka MA, Sionov RV (2008) Involvement of CD44, a molecule with a thousand faces, in cancer dissemination. Semin Cancer Biol 18:260–267

Orian-Rousseau V, Chen L, Sleeman JP, Herrlich P, Ponta H (2002) CD44 is required for two consecutive steps in HGF/c-Met signaling. Genes Dev 16:3074–3086

Ouhtit A, Abd Elmageed ZY, Abdraboh ME, Lioe TF, Raj MH (2007) ***In vivo*** evidence for the role of CD44s in promoting breast cancer metastasis to the liver. Am J Pathol 171:2033–2039

Palecek SP, Loftus JC, Ginsberg MH, Lauffenburger DA, Horwitz AF (1997) Integrin-ligand binding properties govern cell migration speed through cell-substratum adhesiveness. Nature 385:537–540

Paluch E, Gucht J van der, Sykes C (2006) Cracking up: symmetry breaking in cellular systems. J Cell Biol 175:687–692

Park H, Kim Y, Lim Y, Han I, Oh ES (2002) Syndecan-2 mediates adhesion and proliferation of colon carcinoma cells. J Biol Chem 277:29730–29736

Peterson RM, Yu Q, Stamenkovic I, Toole BP (2000) Perturbation of hyaluronan interactions by soluble CD44 inhibits growth of murine mammary carcinoma cells in ascites. Am J Pathol 156:2159–2167

Petrie RJ, Doyle AD, Yamada KM (2009) Random versus directionally persistent cell migration. Nat Rev Mol Cell Biol 10:538–549 Ponta H, Sherman L, Herrlich PA (2003) CD44: from adhesion molecules to signalling regulators. Nat Rev Mol Cell Biol 4:33–45

Protin U, Schweighoffer T, Jochum W, Hilberg F (1999) CD44- deficient mice develop normally with changes in subpopulations and recirculation of lymphocyte subsets. J Immunol 163:4917– 4923

Rabinovitz I, Mercurio AM (1997) The integrin alpha6beta4 functions in carcinoma cell migration on laminin-1 by mediating the formation and stabilization of actin-containing motility structures. J Cell Biol 139:1873–1884

Ram R, Lorente G, Nikolich K, Urfer R, Foehr E, Nagavarapu U (2006) Discoidin domain receptor-1a (DDR1a) promotes glioma cell invasion and adhesion in association with matrix metalloproteinase-2. J Neurooncol 76:239–248

Rilla K, Tiihonen R, Kultti A, Tammi M, Tammi R (2008) Pericellular hyaluronan coat visualized in live cells with a fluorescent probe is scaffolded by plasma membrane protrusions. J Histochem Cytochem 56:901–910

Sanchez-Madrid F, Pozo MA del (1999) Leukocyte polarization in cell migration and immune interactions. EMBO J 18:501–511

Shintani Y, Fukumoto Y, Chaika N, Svoboda R, Wheelock MJ, Johnson KR (2008) Collagen I-mediated up-regulation of N- cadherin requires cooperative signals from integrins and dis- coidin domain receptor 1. J Cell Biol 180:1277–1289

Singleton PA, Bourguignon LY (2004) CD44 interaction with ankyrin and IP3 receptor in lipid rafts promotes hyaluronan-mediated Ca^{2+} signaling leading to nitric oxide production and endothelial cell adhesion and proliferation. Exp Cell Res 295:102–118

Stepp MA, Gibson HE, Gala PH, Iglesia DD, Pajoohesh-Ganji A, Pal- Ghosh S, Brown M, Aquino C, Schwartz AM, Goldberger O, Hinkes MT, Bernfield M (2002) Defects in keratinocyte activation during wound healing in the syndecan-1-deficient mouse. J Cell Sci 115:4517–4531

Takada Y, Ye X, Simon S (2007) The integrins. Genome Biol 8:215 Tanabe KK, Ellis LM, Saya H (1993) Expression of CD44R1 adhesion molecule in colon carcinomas and metastases. Lancet 341:725–726

Tkachenko E, Rhodes JM, Simons M (2005) Syndecans: new kids on the signaling block. Circ Res 96:488–500

Tkachenko E, Elfenbein A, Tirziu D, Simons M (2006) Syndecan-4 clustering induces cell migration in a PDZ-dependent manner. Circ Res 98:1398–1404

Trepat X, Wasserman MR (2009) Physical forces during collective cell migration. Nat Physics 5:426–430

van der Flier A, Sonnenberg A (2001) Function and interactions of integrins. Cell Tissue Res 305:285–298

Vicente-Manzanares M, Choi CK, Horwitz AR (2009) Integrins in cell migration–the actin connection. J Cell Sci 122:199–206

Vogel W (1999) Discoidin domain receptors: structural relations and functional implications. FASEB J 13 (Suppl):S77–S82

Vogel W, Gish GD, Alves F, Pawson T (1997) The discoidin domain receptor tyrosine kinases are activated by collagen. Mol Cell 1:13–23

Vogel WF, Abdulhussein R, Ford CE (2006) Sensing extracellular matrix: an update on discoidin domain receptor function. Cell Signal 18:1108–1116

Wagner W, Wein F, Roderburg C, Saffrich R, Diehlmann A, Eckstein V, Ho AD (2008) Adhesion of human hematopoietic progenitor cells to mesenchymal stromal cells involves CD44. Cells Tissues Organs 188:160–169

Wallach-Dayan SB, Grabovsky V, Moll J, Sleeman J, Herrlich P, Alon R, Naor D (2001) CD44-dependent lymphoma cell dissemination: a cell surface CD44 variant, rather than standard CD44, supports *in vitro* lymphoma cell rolling on hyaluronic acid substrate and its ***in vivo*** accumulation in the peripheral lymph nodes. J Cell Sci 114:3463–3477

Wang SJ, Wong G, Heer AM de, Xia W, Bourguignon LY (2009) CD44 variant isoforms in head and neck squamous cell carcinoma progression. Laryngoscope 119:1518–1530

Wolf K, Friedl P (2009) Mapping proteolytic cancer cell-extracellular matrix interfaces. Clin Exp Metastasis 26:289– 298

Wolf K, Wu YI, Liu Y, Geiger J, Tam E, Overall C, Stack MS, Friedl P (2007) Multi-step pericellular proteolysis controls the transition from individual to collective cancer cell invasion. Nat Cell Biol 9:893–904

Wu ZL, Zhang L, Yabe T, Kuberan B, Beeler DL, Love A, Rosenberg RD (2003) The involvement of heparan sulfate (HS) in FGF1/ HS/FGFR1 signaling complex. J Biol Chem 278:17121–17129

Yoshimura T, Matsuyama W, Kamohara H (2005) Discoidin domain receptor 1: a new class of receptor regulating leukocyte-collagen interaction. Immunol Res 31:219–230

Zaidel-Bar R, Itzkovitz S, Ma'ayan A, Iyengar R, Geiger B (2007) Functional atlas of the integrin adhesome. Nat Cell Biol 9:858–867 Zaman MH, Trapani LM, Sieminski AL, Mackellar D, Gong H, Kamm RD, Wells A, Lauffenburger DA, Matsudaira P (2006) Migration of tumor cells in 3D matrices is governed by matrix stiffness along with cell-matrix adhesion and proteolysis. Proc Natl Acad Sci USA 103:10889–10894

Zamir E, Geiger B (2001) Molecular complexity and dynamics of cell-matrix adhesions. J Cell Sci 114:3583–3590

Zhu H, Mitsuhashi N, Klein A, Barsky LW, Weinberg K, Barr ML,

Demetriou A, Wu GD (2006) The role of the hyaluronan receptor CD44 in mesenchymal stem cell migration in the extracellular matrix. Stem Cells 24:928–935

Zimmerman E, Geiger B, Addadi L (2002) Initial stages of cell-matrix adhesion can be mediated and modulated by cell-surface hyaluronan. Biophys J 82:1848–1857

"If we knew what it was we were doing,
it would not be called research, would it?"

Albert Einstein

CHAPTER 3

Readily Accessible Bicyclononynes for Bioorthogonal Labeling and Three-Dimensional Imaging of Living Cells.

Angew. Chem. Int. Ed. 2010, 49, 1-5

Jan Dommerholt[1,], Samuel Schmidt[2,*], Rinske Temming[1], Linda J.A. Hendriks[1], Floris P.J.T. Rutjes[1], Jan C.M. van Hest[1], Dirk J. Lefeber[3], Peter Friedl[2] & Floris L. van Delft[1]*

** These authors contributed equally to this work*

[1] Radboud University Nijmegen Institute for Molecules and Materials Heijendaalseweg 135, 6525 AJ, Nijmegen (The Netherlands), [2] Radboud University Nijmegen, Nijmegen Center for Molecular Life Sciences, Department of Cell Biology, 6500 HB Nijmegen (The Netherlands), [3] Radboud University Medical Center Department of Laboratory Medicine 6525 ED Nijmegen (The Netherlands)

Abstract

A new class of bioorthogonal labeling probes was developed based on Bicyclo[6.1.0] non-4-yne (BCN), a strained cycloalkyne that displays excellent reaction kinetics in cycloadditions with azides and nitrones. Functionalization with Alexa Fluor 555 or biotin facilitated straightforward and highly specific visualization of proteins and glycans, and allowed subcellular-resolved imaging of glycan expression in metastatic melanoma cells during invasive migration into 3D collagen lattices.

The advent of chemical biology tools for imaging and tracking of biomolecules (proteins, lipids, glycans) in their native environment is providing unique insights into cellular processes that are not achievable with traditional biochemical or molecular biology tools.[1] Bioorthogonal labeling of biomolecules has proven particularly useful for the detection and study of glycans[2] and lipids,[3] based on a highly selective reaction between an abiotic functional tag and a designed chemical probe. With respect to the abiotic tag, azide has been used extensively because of its straightforward chemical introduction, small size, and relative inertness.[4] The finding that azides react rapidly and cleanly with terminal acetylenes in the presence of copper(I), the quintessential "click" reaction, has found tremendous application in life and material sciences.[5] However, because up to 20 mol % of copper(I) species is typically used, such click chemistry is not suitable for labeling of living systems without compromising cell function.[6] Apart from that, the presence of copper may induce oligonucleotide[7] and polysaccharide[8] degradation. To avoid the use of toxic metals, several metal-free bioorthogonal labeling reaction have been developed.[9] In particular, phosphines have been used for covalent ligation to azides, a procedure known as Staudinger ligation.[10] However, owing to the oxygen sensitivity of phosphines, recent focus of chemical ligation is shifting towards strain-promoted cycloaddition reactions with cyclooctynes (Scheme 1 a).[11] Most prominently, azides were found to react with cyclooctynes with high reaction rates in a so-called strain-promoted alkyne–azide cycloaddition (SPAAC).[12] The toolbox of metal-free bioorthogonal reactions was most recently further expanded by our research group[13] and others,[14] by demonstrating that cyclooctynes undergo even more rapid strain-promoted cycloaddition with nitrones (SPANC), a procedure that was found suitable for dual, irreversible, and site-specific N-terminal modification of proteins.[13]

The broad application of metal-free cycloaddition in life sciences is, however, hampered by the limited commercial availability and lengthy synthetic routes for preparation of the most common cyclooctynes (Scheme 1 b). For example, eight synthetic steps are required to generate second-generation DIFO (**1**),[15] nine steps for DIBAC (**3**),[16] and seven steps for BARAC (**4**),[17] while yields are usually low (10% for **2**,[18] 16% for **4**). Additional modifications, such as dibenzoannulation (compounds **2–4**), increase lipophilicity and may, therefore lead to non-specific binding to proteins.[17]

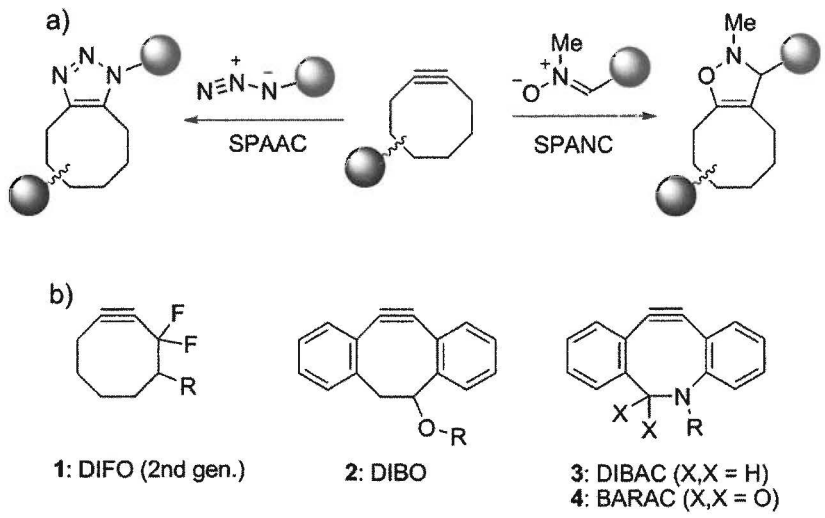

Scheme 1.

Reactions and structures of cyclooctyne compounds for strain-promoted cycloaddition. a) Cycloaddition with azide (SPAAC) or nitrone (SPANC). b) Structures of the most commonly employed cyclooctynes.

Here we report bicycle [6.1.0] nonyne (BCN) as a novel ring-strained alkyne for metal-free cycloaddition reactions with azides and nitrones. Bicyclononyne derivatives, which were obtained in a highly straightforward process through cyclopropanation of 1,5-cyclooctadiene, are C_S symmetrical and display excellent reaction kinetics in strain-promoted cycloaddition reactions. Functionalized derivatives of BCN were applied in the labeling of proteins and glycans, as well as in the three-dimensional visualization of living melanoma cells. Based on the known reactivity enhancement of cyclo-propane fusion,[19] we speculated that analogues of bicycle [6.1.0] nonyne (compound **6**, Scheme 2 a) would form a class of versatile cycloalkynes for bioconjugation by combining relative stability with high reactivity. Thus, the synthesis of BCN started by the dropwise addition of ethyl diazoacetate to a large excess (**8** equiv) of 1,5-cyclooctadiene in the presence of rhodium acetate.[20] The resulting mixture of diastereomeric compounds exo-**5** and endo-**5**, formed in a 2:1 ratio, was readily separated by chromatography on silica gel (combined yield 76%). Next, as exemplified for endo-**5**, the individual stereoisomers were converted into the corresponding hydroxyalkynes by reduction of the ester group, bromination, and elimination—a three-step reaction sequence that was performed within eight hours and required only a single purification step. The desired bicycle [6.1.0] non-4-yn-9-ol (endo-**6**) was thus obtained in 61% overall yield after purification (the diastereomeric exo-isomer of **6** was prepared in 53% yield form exo-**5**). Both exo-**6** or endo-**6** were found sufficiently stable for prolonged storage at -20°C and did not undergo structural change upon stirring in the presence of 5 mm glutathione for 48 hours in CD_3CN/D_2O (1:2).[17]

Next, we investigated the reaction kinetics of **6** in the prototypical SPAAC reaction with benzyl azide. Calculation of second-order reaction kinetics demonstrated that the three-membered ring fusion leads to a near 100-fold rate enhancement over plain cyclooctyne $k \approx 2 \times 10^{-3}\ M^{-1}\ s^{-1}$ measuring $0.14\ M^{-1}\ s^{-1}$ for endo-**6** and $0.11\ M^{-1}\ s^{-1}$ for exo-**6**. Reaction rates increased, as anticipated,[13] in a more polar mixture (CD_3CN/D_2O (1:2)), measuring 0.29 and $0.19\ M^{-1}\ s^{-1}$ for endo-**6** and exo-**6**, respectively, values similar to or better than other cyclooctyne systems.[4, 21] Strain-promoted acetylene–nitrone cycloaddition (SPANC)[13] with nitrone **7** (Scheme 2b) instead of an azide was found to be significantly faster, measuring 1.66 and $1.32\ M^{-1}\ s^{-1}$ for endo-**6** and exo-**6**, respectively. The usefulness of BCN for bioorthogonal functionalization of biomolecules was next investigated in the one-pot SPANC functionalization of a model peptide with an N-terminal serine. Indeed, we observed a clean conversion of FRATtide, a GSK-1 binding peptide that prevents axin binding,[22] into the expected isoxazoline conjugates upon SPANC labeling with endo-**6** or biotinylated BCN conjugate **9**, as judged by mass spectrometric analysis and spot-blot analysis (see the Supporting Information).

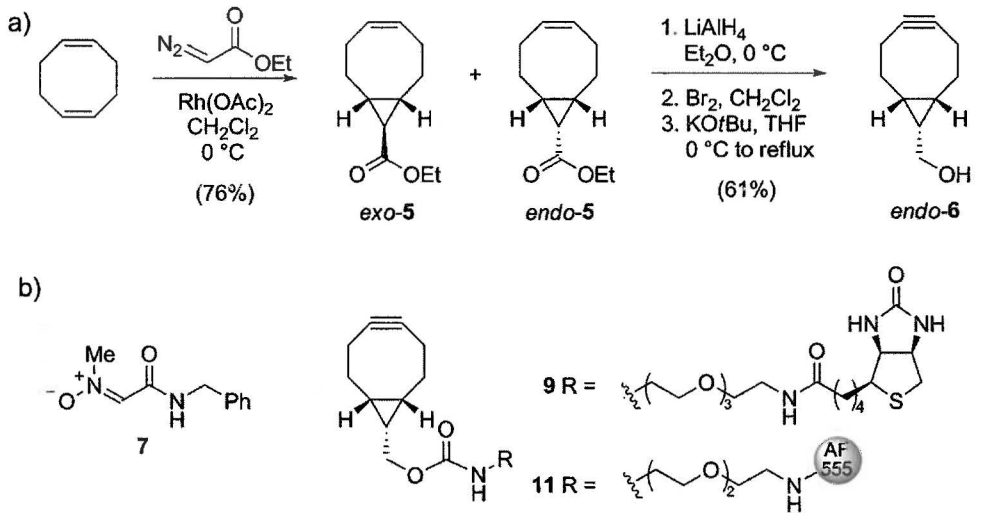

Scheme 2.

a) Synthesis of 9-hydroxymethylbicyclo [6.1.0] nonyne (*endo*-6). b) Structures of BCN conjugated to biotin (9) or Alexa Fluor 555 (11). THF = tetrahydrofuran

We also became interested in whether BCN-conjugates are suitable for labeling of azido-containing proteins. To this end, recombinant virus capsid protein was expressed in auxotrophic E. coli in the presence of azidohomoalanine,[23] thus leading to the introduction of a single azide in nearly 50% of the isolated protein. Without further separation, the mixture of proteins was subjected to strain-promoted functionalization with BCN-Alexa Fluor 555 conjugate **11** by mixing for three hours in a phosphate buffer (pH 7.5). After washing and dialysis, incorporation of **11** was confirmed by sodium dodecyl sulfate polyacrylamide gel electrophoresis (SDS-PAGE; Figure 1 a) and mass spectrometric analysis, which indicated a quantitative mass increase of 1135 Da, that is, the molecular weight of **11** (see the Supporting Information). Next, capsid proteins were assembled into viral capsids by dialysis to a sodium acetate buffer (pH 5.0, 0.01m $CaCl_2$), and subsequently purified by FPLC. A strongly fluorescent peak appeared around 1.2 ml, which is the common elution volume of virus capsid. Finally, the structure of virus capsids was determined by transmission emission spectroscopy (TEM) indicating the structural integrity of the protein capsids after functionalization with **11** (Figure 1 b).

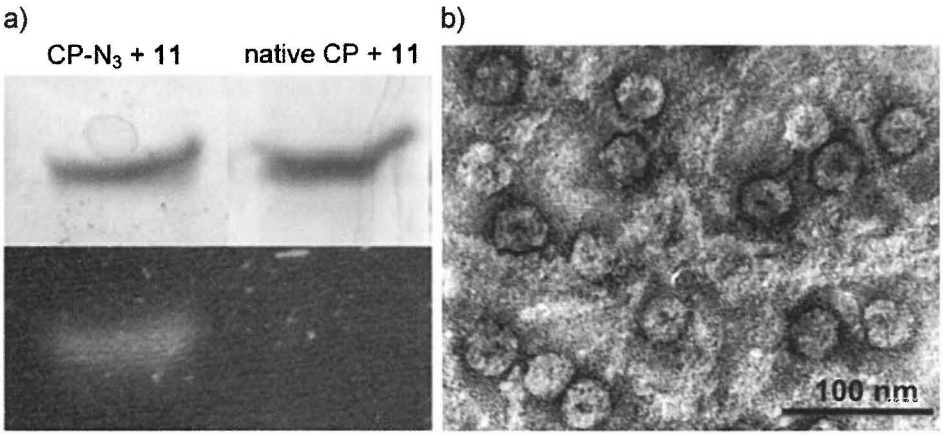

Figure 1.

BCN modification of azido-containing virus capsid protein and assembly into virus capsids. a) SDS-PAGE analysis of reaction of BCN-AF555 conjugate (11) with capsid protein containing azide (left) or without azide (right). Top: Coomassie Brilliant Blue staining, bottom: fluorescence image. b) TEM pictures of fluorescent capsids (images recorded on a JEOL 1010 TEM, the sample was deposited on a hydrophilized Formvar carbon-coated TEM grid and consequently negatively stained with 0.2% uranyl acetate).

The bioavailability and tolerability of labeling surface glycans on living human melanoma MV3 cells was addressed using the chemical reporter strategy.[1b] MV3 melanoma cells are highly invasive and metastatic, and their abundant production of surface glycans was previously implicated in invasion processes.[24] Thus, MV3 cells were incubated with peracetylated N-azidoacetyl-d-mannosamine ($Ac_4ManNAz$), labeled with BCN-biotin conjugate **9**, and stained with streptavidin-Alexa Fluor 488 (Figure 2). To be able to compare the efficiency of labeling of **9** to that of dibenzocyclooctyne (DIBO, **2**), one of the most reactive cyclooctyne systems known to date,[18] cells were also labeled with a DIBO-biotin conjugate. In all cases, cells retained morphological integrity and cell surface fluorescence, with consistently higher labeling for BCN than for DIBO, as detected by confocal microscopy (Figure 2 a) and flow cytometry (Figure 2 b). By using flow cytometry, high monophasic intensities and excellent signal-to-noise ratio (SNR) were found for both DIBO-biotin (SNR = 116) and BCN-biotin (SNR = 221). No signs of label-induced cytotoxicity were detected after propidium iodide staining (see the Supporting Information).

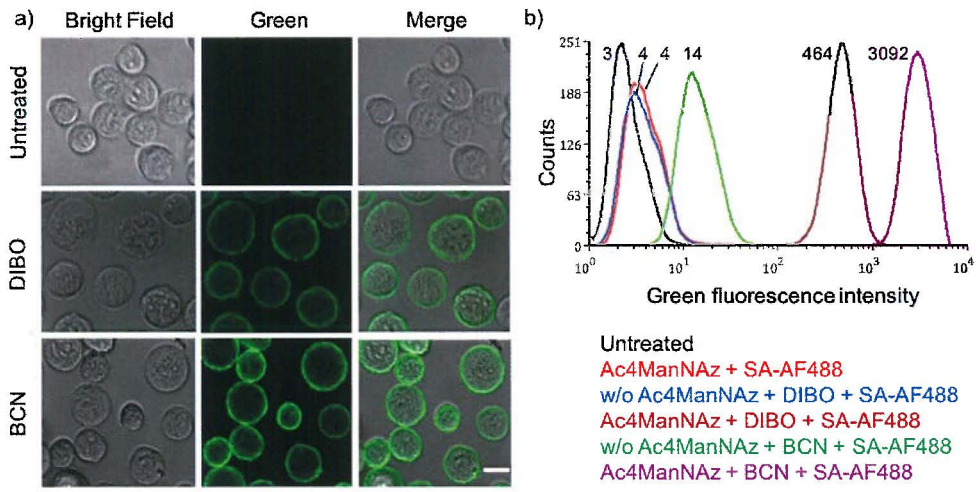

Figure 2.

Surface and total fluorescence intensity of MV3 melanoma, cultured in the absence or presence of $Ac_4ManNAz$ (50 μM), followed by labeling with a cyclooctyne-biotin conjugate and secondary labeling with streptavidin-Alexa Fluor 488 (SA-AF488). a) Representative confocal images of unlabeled cells (top), cells labeled with DIBO-biotin (middle) or BCN- biotin 9 (bottom). Bar: 20 μm. b) Label intensity assessed by flow cytometry, indicated as mean fluorescence intensity (MFI). Numbers denote the average of green fluorescent cells for that particular experiment.

Functional cell integrity was confirmed after incorporating MV3 cells into three-dimensional collagen lattices yielding spontaneous and vigorous invasion. Owing to its high signal-to-noise ratio, labeling with BCN revealed fine, subcellular details, which can discriminate surface glycan distribution states on individual living cells as shown by densitometry experiments (see the Supporting Information). Whereas cells in suspension retain a near-homogeneous distribution of azido-sialic acids on the cell surface (as in Figure 2), invading cells show the redistribution and accumulation of sialic acid at actin-rich contact sites with collagen fibers, consistent with their role in cell adhesion and migration (Figure 3).[25, 26, 27] Thereby, submicron resolution reveals fine surface distribution of sialic acids at leading edge filopodia, focal clusters at actin-rich contact sites to collagen fibers, and substantial glycan-rich deposits into the tissue matrix from the trailing edge (see the Supporting Information).

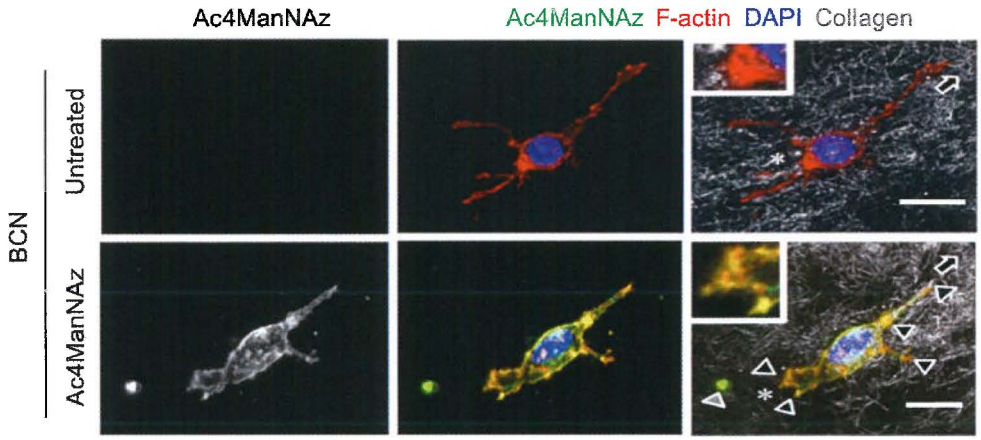

Figure 3.

Live-cell staining and redistribution of glycans during invasive cell migration through a three-dimensional collagen matrix. Focal accumulation of sialic acid on migrating MV3 melanoma cell at interaction sites to collagen fibers and partial colocalization with F-actin. Insets, trailing edge. Direction of migration was determined from retraction fibers (asterisks) and deposited sialic acid-rich material lacking F-actin from the cell rear (gray arrowhead).[28] Bar: 10 µm. Focalized glycan distribution at cell matrix interactions (black arrowheads).

In conclusion, in view of the non-toxic labeling procedure, the tunable fluorescent properties by choice of dye and the high signal-to-noise ratio, BCN will be useful for addressing molecular glycan function studies in live-cell and other systems. A key advantage of BCN over earlier cyclooctynes lies in the combination of its exceptionally easy preparation with high reactivity. Furthermore, it should be noted that the lack of conformational isomerism in bicycle [6.1.0] non-4-ynes[29] leads to sharp peaks in the

^{1}HNMR spectrum, which is further simplified by the C_S symmetry of BCN. An additional advantage of a symmetrical cyclooctyne is the formation of a single regioisomer upon cycloaddition, an aspect of particular advantage in areas where the formation of homogeneous adducts is mandatory.[11] Thus, BCN will allow a broad range of applications that require the highly efficient and metal-free conjugation of two separate molecular entities, for example in life sciences, material science, surface modification, and molecular diagnostics.

Acknowledgement

This research has been financially supported (in part) by the Council for Chemical Sciences of The Netherlands Organization for Scientific Research (NWO-CW, to F.L.D). Dr. G. J. Boons (Complex Carbohydrate Research Center, Athens, GA) is kindly acknowledged for fruitful discussions.

References

[1] a) M. D. Best, Biochemistry 2009, 48, 6571 – 6584 ; b) E. M. Sletten, C. R. Bertozzi, Angew. Chem. 2009, 121, 7108 – 7133 ; Angew. Chem. Int. Ed. 2009, 48, 6974 – 6998.

[2] J. A. Prescher, C. R. Bertozzi, Nat. Chem. Biol. 2005, 1, 13 – 21.

[3] G. Charron, J. Wiljon, H. C. Hang, Curr. Opin. Chem. Biol. 2009,

[12] a) A. T. Blomquist, L. H. Liu, J. Am. Chem. Soc. 1953, 75, 2153 – 2154 ; b) N. J. Agard, J. A. Prescher, C. R. Bertozzi, J. Am. Chem. Soc. 2004, 126, 15046 – 15047.

[13] X. Ning, R. P. Temming, J. Dommerholt, J. Guo, D. B. Ania, M. F. Debets, M. A. Wolfert, G. J. Boons, F. L. van Delft, Angew. Chem. 2010, 122, 3129–3132; Angew. Chem. Int. Ed. 2010, 49, 3065 – 3068.

[14] C. S. McKay, J. Moran, J. P. Pezacki, Chem. Commun. 2010, 46, 931 – 933.

[15] J. A. Codelli, J. M. Baskin, N. J. Agard, C. R. Bertozzi, J. Am. Chem. Soc. 2008, 130, 11486 – 11493.

[16] M. F. Debets, S. S. van Berkel, S. Schoffelen, F. P. J. T. Rutjes, J. C. M. van Hest, F. L. van Delft, Chem. Commun. 2010, 46, 97 – 99.

[17] J. C. Jewett, E. M. Sletten, C. R. Bertozzi, J. Am. Chem. Soc. 2010, 132, 3688 – 3690.

[18] X.Ning,J.Guo,M.A.Wolfert,G.-J.Boons,Angew.Chem.2008, 120, 2285 – 2287; Angew. Chem. Int. Ed. 2008, 47, 2253 – 2255.

[19] H. Meier, C. Schuh-Popitz, H. Peiersen, Angew. Chem. 1981, 93, 286 – 287; Angew. Chem. Int. Ed. Engl. 1981, 20, 270 – 271.

[20] Modern Rhodium-Catalyzed Organic Reactions (Ed. : P. A. Evans), Wiley-VCH, Weinheim, 2005.

[21] N. J. Agard, J. M. Baskin, J. A. Prescher, A. Lo, C. R. Bertozzi, ACS Chem. Biol. 2006, 1, 644 – 648.

[22] G. M. Thomas, S. Frame, M. Goedert, I. Nathke, P. Polakis, P. Cohen, FEBS Lett. 1999, 458, 247 – 251.

[23] A. J. Link, D. A. Tirrell, Methods 2005, 36, 291 – 298.

[24] M. Goebeler, D. Kaufmann, E. B. Brocker, C. E. Klein, J. Cell Sci. 1996, 109, 1957 – 1964.

[25] C. H. Chiang, C. H. Wang, H. C. Chang, S. V. More, W. S. Li, W. C. Hung, J. Cell. Physiol. 2010, 223, 492 – 499.

[26] D. R. Christie, F. M. Shaikh, J. A. Lucas IV, J. A. Lucas III, S. L. Bellis, J. Ovarian Res. 2008, 1, 3.

[27] E. C. Seales, G. A. Jurado, B. A. Brunson, J. K. Wakefield, A. R. Frost, S. L. Beilis, Cancer Res. 2005, 65, 4645 – 4652.

[28] C. Mayer, K. Maaser, N. Daryab, K. S. Zanker, E. B. Brocker, P. Friedl, Eur. J. Cell Biol. 2004, 83, 709 – 715.

[29] C. Antony-Mayer, H. Meier, Chem. Ber. 1988, 121, 2013 – 2018. 13, 382 – 391.

[4] M. F. Debets, C. W. J. van der Doelen, F. P. J. T. Rutjes, F. L. van Delft, ChemBioChem 2010, 11, 1168 – 1184.

[5] M. Meldal, C. W. Tornøe, Chem. Rev. 2008, 108, 2952 – 3015.

[6] A. J. Link, M. K. S. Vink, D. A. Tirrell, J. Am. Chem. Soc. 2004,126, 10598 – 10602.

[7] J. Gierlich, G. A. Burley, P. M. E. Gramlich, D. M. Hammond, T. Carell, Org. Lett. 2006, 8, 3639 – 3642.

[8] E. Lallana, E. Fernandez-Megia, R. Riguera, J. Am. Chem. Soc. 2009, 131, 5748 – 5750.

[9] C. R. Becer, R. Hoogenboom, U. Schubert, Angew. Chem. 2009, 121, 4998 – 5006 ; Angew. Chem. Int. Ed. 2009, 48, 4900 – 4908.

[10] M. Köhn, R. Breinbauer, Angew. Chem. 2004, 116, 3168 – 3178 ; Angew. Chem. Int. Ed. 2004, 43, 3106 – 3116.

[11] J.-F. Lutz, Angew. Chem. 2008, 120, 2212 – 2214 ; Angew. Chem. Int. Ed. 2008, 47, 2182 – 2184.

Supporting Information

Detailed synthetic preparation and structural analysis of compounds 5-11 and cycloadducts.

General methods and procedures

^{1}H NMR spectra were recorded in $CDCl_3$ or CD_3CN/D_2O mixtures on Bruker DMX 300 or Varian Inova-400 spectrometers at 300 K. TMS (δ_H 0.00) or CD_3CN (δ_H 1.94) was used as the internal reference. ^{13}C NMR spectra were recorded in $CDCl_3$ at 75 MHz on a Bruker DMX 300 spectrometer, using the central resonance of $CDCl_3$ (δ_C 77.0) as the internal reference. Mass spectra were obtained on Applied Biosystems Voyager DE-Pro MALDI-TOF (no calibration) or JEOL AccuToF. Chemicals were purchased from Aldrich and used without further purification. CH_2Cl_2, acetonitrile, THF, Et_2O and toluene were obtained dry from a MBRAUN SPS-800 solvent purification system; and CH_3OH was distilled from magnesium and iodine. Aqueous solutions are saturated unless otherwise specified. All reactions were performed under anhydrous conditions under argon and monitored by TLC on Kieselgel 60 F254 (Merck). Detection was by examination under UV light (254 nm) and by charring with 10% sulfuric acid in methanol or with aqueous $KMnO_4$. Silica gel (Acros 0.035-0.070 mm) was used for chromatography.

(1*R*,8*S*,9*r*,*Z*)-Ethyl bicyclo[6.1.0]non-4-ene-9-carboxylate (*exo*-5), and (1*R*,8*S*,9*s*,*Z*)-ethyl bicyclo[6.1.0]non-4-ene-9-carboxylate (*endo*-5)

To a solution of 1,5-cyclooctadiene (19.6 mL, 160 mmol) and $Rh_2(OAc)_4$ (380 mg, 0.86 mmol) CH_2Cl_2 (10 mL) was added dropwise in 3 h a solution of ethyl diazoacetate (2.1 mL, 20 mmol) in CH_2Cl_2 (10 mL). This solution was stirred for 40 h at rt. CH_2Cl_2 was evaporated and the excess of cyclooctadieen was removed by filtration over a glass filter filled with silica and elution with EtOAc:heptane, 1:200 (400 mL). The filtrate was concentrated *in vacuo* and the residue was purified by column chromatography on silica gel (EtOAc:heptane, 1:20) to afford *exo*-**5** (1.10 g, 28%) and *endo*-**5** (2.24 g, 58%) as colorless oils. R_F *exo*-**5** 0.24, R_F *endo*-**5** 0.33 (EtOAc:heptane, 1:20).

exo-**5**: ^{1}H NMR ($CDCl_3$, 400 MHz): d 5.68-5.60 (m, 2H), 4.10 (q, *J* = 7.2 Hz, 2H), 2.35-2.27 (m, 2H), 2.24-2.16 (m, 2H), 2.13-2.04 (m, 2H), 1.59-1.53 (m, 2H), 1.53-1.43 (m, 2H), 1.25 (t, *J* = 7.2 Hz, 3H), 1.18 (t, *J* = 4.8 Hz, 1H). ^{13}C NMR ($CDCl_3$, 75 MHz): d 174.3, 129.8, 60.1, 28.2, 27.8, 27.6, 26.6, 14.2. HRMS (FAB+) *m/z* calcd for $C_{12}H_{19}O_2$ $(M + H)^+$: 195.1385, found: 195.1388.

endo-**5**: ^{1}H NMR ($CDCl_3$, 400 MHz): d 5.65-5.57 (m, 2H), 4.12 (q, *J* = 7.2 Hz, 2H), 2.53-2.46 (m, 2H), 2.25-2.16 (m, 2H), 2.10-2.01 (m, 2H), 1.87-1.79 (m, 2H), 1.70 (t, *J* = 8.8 Hz, 1H), 1.43-1.34 (m, 2H), 1.26 (t, *J* = 7.2 Hz, 3H). ^{13}C NMR ($CDCl_3$, 75 MHz): d 172.2, 129.4, 59.7, 27.0, 24.1, 22.6, 21.2, 14.4. HRMS (FAB+) *m/z* calcd for $C_{12}H_{19}O_2$ $(M + H)^+$: 195.1385, found: 195.1378.

(1*R*,8*S*,9*s*)-Bicyclo[6.1.0]non-4-yn-9-ylmethanol (*endo*-6)

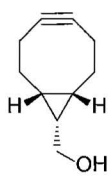

To a suspension of $LiAlH_4$ (90 mg, 2.34 mmol) in Et_2O (10 mL) was added dropwise at 0 °C a solution of *endo*-**5** (520 mg, 2.68 mmol) in Et_2O (10 mL). This suspension was stirred for 15 min at RT, then cooled down to 0 °C, and water was added carefully until the grey solid had turned into white. Na_2SO_4 (2 g) was added, the solid was filtered off and washed thoroughly with Et_2O (100 mL). The filtrate was concentrated *in vacuo*.

Without further purification the alcohol was dissolved in CH_2Cl_2 (20 mL). At 0 °C a solution of Br_2 (151 mL, 2.94 mmol) in CH_2Cl_2 (2 mL) was added dropwise until the yellow color persisted. The reaction mixture was quenched with a 10% $Na_2S_2O_3$-solution (5 mL), and extracted with CH_2Cl_2 (2 x 20 mL). The organic layer was dried (Na_2SO_4) and concentrated *in vacuo* to afford the dibromide (833 mg, quant.).

Without further purification the dibromide (700 mg, 2.24 mmol) was dissolved in THF (25 mL). A solution of KO*t*Bu (7.4 mL, 1 M in THF, 7.40 mmol) was added dropwise at 0 °C. Then the solution was refluxed for 2 h. After cooling down to rt the mixture was

quenched with saturated NH_4Cl-solution (20 mL), and extracted with CH_2Cl_2 (3 x 20 mL). The organic layer was dried (Na_2SO_4) and concentrated *in vacuo*. The residue was purified by column chromatography on silica gel (EtOAc:pentane, 1:1) to afford *endo*-**6** (205 mg, 61%) as a white solid. R_F 0.22 (EtOAc:pentane, 1:1).

^{1}H NMR ($CDCl_3$, 400 MHz): d 3.73 (d, *J* = 8.0 Hz, 2H), 2.35-2.20 (m, 6H), 1.66-1.56 (m, 2H), 1.39-1.30 (m, 1H), 1.18 (bs, 1H), 0.99-0.90 (m, 2H). ^{13}C NMR ($CDCl_3$, 75 MHz): d 98.4, 59.3, 28.5, 21.0, 20.9, 19.5.

(1*R*,8*S*,9*r*)-Bicyclo[6.1.0]non-4-yn-9-ylmethanol (*exo*-6)

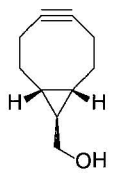

Compound *exo*-**6** was prepared by an identical procedure as described for *endo*-**6**. Final purification by column chromatography on silica gel (EtOAc:pentane, 1:1) afforded *exo*-**6** (128 mg, 53%) as a white solid. R_F 0.23 (EtOAc:pentane, 1:1).

^{1}H NMR ($CDCl_3$, 400 MHz): d 3.54 (d, *J* = 6.4 Hz, 2H), 2.44-2.40 (m, 2H), 2.32-2.25 (m, 2H), 2.18-2.14 (m, 2H), 1.88 (bs, 1H), 1.44-1.34 (m, 2H), 0.74-0.63 (m, 3H). ^{13}C NMR ($CDCl_3$, 75 MHz): d 98.7, 66.9, 33.3, 27.2, 22.5, 21.4.

(1*R*,8*S*,9*s*)-Bicyclo[6.1.0]non-4-yn-9-ylmethyl (4-nitrophenyl) carbonate (8)

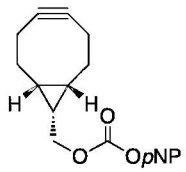

To a solution of *endo*-**6** (32 mg, 0.213 mmol) in CH_2Cl_2 (5 mL) was added pyridine (43 mL, 0.532 mmol) and *p*-NO_2PhOC(O)Cl (53 mg, 0.266 mmol). After stirring for 15 min at RT the mixture was quenched with saturated NH_4Cl-solution (5 mL) and extracted with CH_2Cl_2 (3 x 5 mL). The organic layer was dried (Na_2SO_4) and concentrated *in vacuo*. The residue was purified by column chromatography on silica gel (EtOAc:pentane, 1:5) to afford **8** (52 mg, 77%) as a white solid. R_F 0.30 (EtOAc:pentane, 1:3).

^{1}H NMR ($CDCl_3$, 400 MHz): d 8.28 (d, *J* = 9.2 Hz, 2H), 7.40 (*J* = 9.6 Hz, 2H), 4.41 (d, *J* = 8.4 Hz, 2H), 2.37-2.22 (m, 6H), 1.67-1.57 (m, 2H), 1.56-1.47 (m, 1H), 1.11-1.02 (m, 2H). ^{13}C NMR ($CDCl_3$, 75 MHz): d 155.6, 152.5, 145.3, 125.3, 121.7, 98.7, 68.0, 29.0, 21.3, 20.5, 17.2.

(1*R*,8*S*,9*S*)-bicyclo[6.1.0]non-4-yn-9-ylmethyl12-(+)-biotinylamino-3,6,9-trioxa-dodecyl carbamate (9)

To a solution of **7** (52 mg, 0.165 mmol) in DMF (5 mL) was added (+)-biotin-$(PEO)_4$-NH_2 (69 mg, 0.165 mmol) and NEt_3 (69 mL, 0.495 mmol). After stirring for 2 h at RT the reaction mixture was evaporated to dryness *in vacuo*. The residue was purified by column chromatography on silica gel (acetone:MeOH, 9:1) to afford **9** (68 mg, 69%) as a white solid. R_F 0.22 (acetone:MeOH, 9:1).

^{1}H NMR ($CDCl_3$, 400 MHz): d 6.76-6.69 (m, 1H), 6.61 (bs, 1H), 5.67 (bs, 1H), 5.40-4.34 (m, 1H), 4.52-4.49 (m, 1H), 4.33-4.30 (m, 1H), 4.15 (d, *J* = 8 Hz, 2H), 3.64-3.63 (m, 8H), 3.59-3.54 (m, 4H), 3.46-3.42 (m, 2H), 3.39-3.35 (m, 2H), 3.17-3.12 (m, 1H), 2.90 (dd, *J* = 12.8, 4.8 Hz, 1H), 2.75 (d, *J* = 12.8 Hz, 1H), 2.30-2.21 (m, 8H), 1.80-1.53 (m, 6H), 1.48-1.31 (m, 3H), 0.97-0.92 (m, 2H). HRMS (ESI+) *m/z* calcd for $C_{29}H_{47}N_4O_7S$ $(M + H)^+$: 595.3165, found: 595.3166.

(1*R*,8*S*,9*s*)-bicyclo[6.1.0]non-4-yn-9-ylmethyl 3,6,9-trioxa-12-azadodecylcarbamate (10)

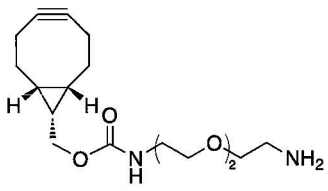

To a solution of **8** (14 mg, 0.044 mmol) in DMF (1 mL) was added 1,8-diamino-3,6-dioxaoctane (38 µL, 0.266 mmol) and NEt_3 (19 µL, 0.133 mmol) and the reaction mixture was stirred at RT for 15 min. The mixture was concentrated under reduced pressure, taken up in CH_2Cl_2 (20 mL) and extracted with 1 N NaOH (2 x 2 mL), followed by water (2 mL). The combined aqueous phases were extracted once with CH_2Cl_2 (10 mL) and extracted with water (2 mL). The combined organic layers were dried over Na_2SO_4 and concentrated *in vacuo*. Silica gel column chromatography (CH_2Cl_2:MeOH, 20:1 → 10:1 → 5:1, 1% Et_3N) and concentration *in vacuo* gave the title compound **10** (12 mg, 83%) as a slightly yellow oil. ^{1}H NMR ($CDCl_3$, 400 MHz): d 5.34 (bs, 1H), 4.15 (d, 2H, *J* = 8.0 Hz), 3.62 (s, 4H), 3.58-3.48 (m, 4H), 3.38 (m, 2H), 2.89 (t, 3H, *J* = 5.2 Hz), 2.32-2.19 (m, 6H), 1.64-1.51 (m, 2H), 1.40-1.31 (m, 1H), 0.96-0.88 (m, 2H). ^{13}C NMR ($CDCl_3$, 75 MHz): d 98.8, 73.4, 70.3, 70.2, 70.1, 62.7, 41.7, 40.8, 29.1, 21.4, 20.1, 17.8. HRMS (ESI+) *m/z* calcd for $C_{17}H_{28}N_2O_4$ $(M + H)^+$: 325.2122, found: 325.2120.

BCN-Alexa Fluor 555 conjugate (11)

To a solution of **10** (0.27 mg, 0.833 µmol) in DMF (1 mL) was added Alexa Fluor 555 carboxylic acid, succinimidyl ester (1 mg, 0.833 µmol). The reaction mixture was stirred for 16 h at RT, and any remaining unreacted Alexa Fluor 555 was quenched with ethanolamine (1 µL, 17 µmol) for 1 h at RT. The reaction mixture was then concentrated *in vacuo*. The crude product was used without any further purification.

((5a*R*,6*S*,6a*S*)-1-benzyl-1,4,5,5a,6,6a,7,8-octahydrocyclopropa[5,6]cycloocta[1,2-*d*][1,2,3]triazol-6-yl)methanol

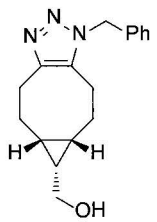

To a solution of *endo*-**6** (24 mg, 0.16 mmol) in a mixture of CH_3CN/H_2O=3/1 (7 mL) was added BnN_3 (19.9 µL, 0.16 mmol). This mixture was stirred for 16 h at RT, and then extracted with CH_2Cl_2 (3 x 5 mL). The organic layer was dried (Na_2SO_4) and concentrated *in vacuo*. The residue was purified by column chromatography on silica gel (EtOAc) to afford the *endo*-cycloadduct (44 mg, 97%) as a white solid. R_F 0.11 (EtOAc).

^{1}H NMR ($CDCl_3$, 400 MHz): d 7.34-7.26 (m, 3H), 7.11-7.09 (m, 2H), 5.52-5.42 (m, 2H), 3.68 (ddd, *J* = 25.7, 11.3, 7.8 Hz, 2H), 3.11 (ddd, *J* = 15.8, 7.3, 3.8 Hz, 1H), 2.91 (ddd, *J* = 15.8, 9.6, 4.0 Hz, 1H), 2.78 (ddd, *J* = 16.1, 6.6, 3.5 Hz, 1H), 2.55 (ddd, *J* = 16.1, 10.3, 3.7 Hz, 1H), 2.25-2.17 (m, 1H), 2.04-1.97 (m, 2H), 1.59-1.41 (m, 2H), 1.19-1.10 (m, 1H), 1.03-0.95 (m, 1H), 0.86-0.78 (m, 1H). ^{13}C NMR ($CDCl_3$, 75 MHz): d 145.1, 135.2, 133.1, 128.8, 128.0, 126.8, 59.5, 51.9, 26.0, 23.1, 22.2, 21.5, 20.9, 19.3, 19.0. HRMS (ESI+) *m/z* calcd for $C_{17}H_{22}N_3O$ $(M + H)^+$: 284.1763, found: 284.1749.

((5a*R*,6*R*,6a*S*)-1-benzyl-1,4,5,5a,6,6a,7,8-octahydrocyclopropa[5,6]cycloocta[1,2-*d*][1,2,3]triazol-6-yl)methanol

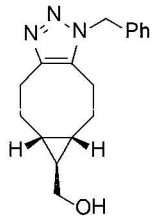

The *exo*-product was prepared by the same procedure as described for the *endo*-cycloadduct. The residue was purified by column chromatography on silica gel (EtOAc) to afford *exo*-cycloadduct (43 mg, 95%) as a white solid. R_F 0.10 (EtOAc).

^{1}H NMR ($CDCl_3$, 400 MHz): d 7.33-7.28 (m, 3H), 7.11-7.09 (m, 2H), 5.46 (s, 2H), 3.50-3.40 (m, 2H), 3.09 (ddd, *J* = 15.9, 7.3, 3.3 Hz, 1H), 2.85 (ddd, *J* = 15.9, 10.1, 3.5 Hz, 1H), 2.73 (ddd, *J* = 16.2, 6.7, 3.0 Hz, 1H), 2.51 (ddd, *J* = 16.1, 10.5, 3.2 Hz, 1H), 2.41-2.33 (m, 1H), 2.22-2.15 (m, 2H), 1.39-1.30 (m, 1H), 1.27-1.18 (m, 1H), 0.83-0.76 (m, 1H), 0.70-0.62 (m, 2H). ^{13}C NMR ($CDCl_3$, 75 MHz): d 145.4, 135.2, 133.3, 128.8, 128.0, 126.8, 66.1, 51.9, 27.6, 27.1, 26.3, 25.8, 22.9, 22.0, 21.9. HRMS (ESI+) *m/z* calcd for $C_{17}H_{22}N_3O$ $(M + H)^+$: 284.1763, found: 284.1746.

(5a*S*,6*S*,6a*R*)-*N*-benzyl-6-(hydroxymethyl)-2-methyl-3,4,5,5a,6,6a,7,8-octahydro-2*H*-cyclopropa[5,6]cycloocta[1,2-*d*]isoxazole-3-carboxamide

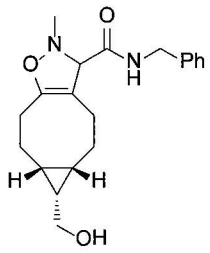

To a solution of *endo*-**6** (54 mg, 0.36 mmol) in a mixture of CH_3CN/H_2O=3/1 (7 mL) was added nitrone **7** (70 mg, 0.36 mmol). This mixture was stirred for 16 h at RT, and then extracted with CH_2Cl_2 (3 x 5 mL). The organic layer was dried (Na_2SO_4) and concentrated *in vacuo*. The residue was purified by column chromatography on silica gel (EtOAc:heptane, 2:1) to afford *endo*-cycloadduct as a mixture of isomers (114 mg, 92%). R_F 0.17 (EtOAc:heptane, 4:1).

^{1}H NMR ($CDCl_3$, 400 MHz): d 7.58-7.52 (m, 1H), 7.34-7.22 (m, 5H), 4.52-4.46 (m, 1H), 4.41-4.34 (m, 1H), 3.93 (s, 0.4H), 3.88 (s, 0.6H), 3.74-3.65 (m, 2H), 2.81-2.73 (m, 1H), 2.69 (2s, 3H), 2.43-2.19 (m, 3H), 2.08-1.94 (m, 3H), 1.65-1.44 (m, 2H), 1.19-1.06 (m, 1H), 1.03-0.95 (m, 1H), 0.90-0.83 (m, 1H). ^{13}C NMR ($CDCl_3$, 75 MHz): d 170.4, 146.3, 146.1, 138.3, 138.2, 128.7, 128.5, 127.5, 127.3, 103.1, 102.8, 79.8, 79.3, 59.7, 46.1, 42.8, 39.1, 25.9, 25.5, 25.2, 21.6, 20.6, 20.5, 19.8, 19.6, 19.2, 18.6, 18.3, 18.1. HRMS (ESI+) ***m/z*** calcd for $C_{20}H_{27}N_2O_3$ $(M + H)^+$: 343.2022, found: 343.2008.

(5a*S*,6*R*,6a*R*)-*N*-benzyl-6-(hydroxymethyl)-2-methyl-3,4,5,5a,6,6a,7,8-octahydro-2*H*-cyclopropa[5,6]cycloocta[1,2-*d*]isoxazole-3-carboxamide

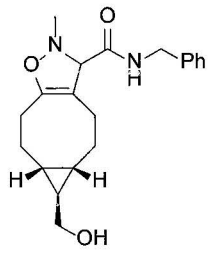

The *exo*-product was prepared by the same procedure as described for *endo*-cycloadduct. The residue was purified by column chromatography on silica gel (EtOAc:CH_2Cl_2, 5:1) to afford the *exo*-cycloadduct as a mixture of isomers (28 mg, 88%). R_F 0.11 (EtOAc:heptane, 2:1).

^{1}H NMR ($CDCl_3$, 400 MHz): d 7.55-7.49 (m, 1H), 7.34-7.24 (m, 5H), 4.52-4.33 (m, 2H), 3.91 (s, 0.5H), 3.87 (s, 0.5H), 3.54-3.40 (m, 2H), 2.78-2.72 (m, 0.5H), 2.69 (2s, 3H), 2.61-2.53 (m, 0.5H), 2.40-2.31 (m, 1H), 2.28-2.11 (m, 4H), 1.50-1.26 (m, 3H), 0.79-0.62 (m, 3H). ^{13}C NMR ($CDCl_3$, 75 MHz): d 170.4, 170.3, 146.3, 138.4, 138.3, 128.6, 128.5, 127.6, 127.4, 127.3, 103.3, 103.0, 80.0, 79.6, 66.6, 46.2, 42.9, 42.7, 26.7, 26.6, 26.4, 25.9, 25.7, 25.4, 25.1, 24.3, 24.2, 21.4, 21.2, 20.9, 20.8. HRMS (ESI+) *m/z* calcd for $C_{20}H_{27}N_2O_3$ $(M + H)^+$: 343.2022, found: 343.2010.

Rate plots for cycloaddition of *endo*-6 and *exo*-6 with benzyl azide

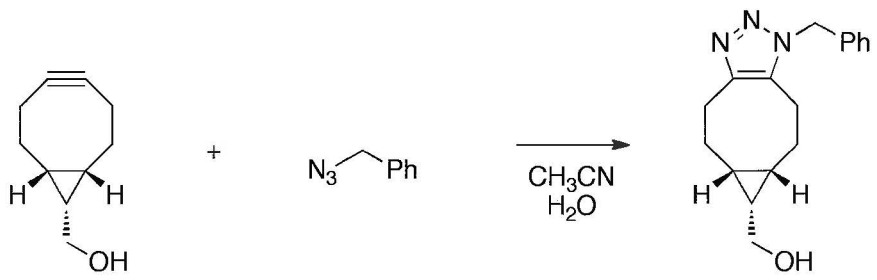

endo-**6**

same for *exo*-**6**

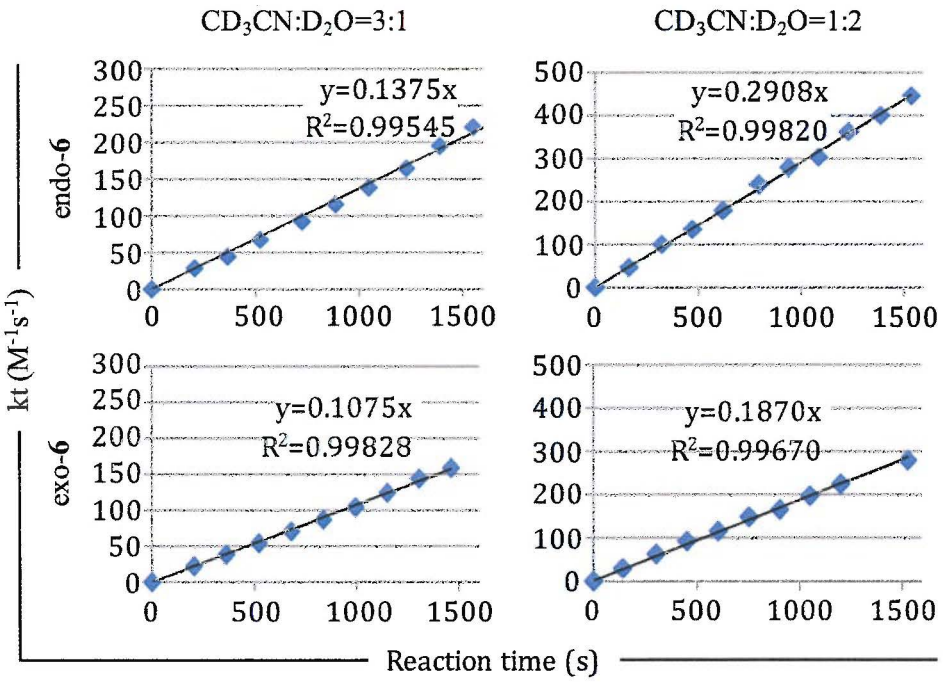

^{1}H-NMR monitoring of cycloaddition of *exo*-**6** or *endo*-**6** with benzyl azide was performed by rapid mixing (t=0) of stock solutions A and B (0.3 mL each) in an NMR tube and immediate insertion into a 400 MHz NMR spectrometer. NMR spectra were measured at preset time-intervals. Each experiment was performed in triplicate.

Stock solution A: alkyne **6** was dissolved in a mixture of CD_3CN and D_2O (ratio 3:1 or 1:2, 10 mL) to give a 36 mM solution.

Stock solution B: benzyl azide was dissolved in a mixture of CD_3CN and D_2O (ratio 3:1 or 1:2, 10 mL) to give a 32.8 mM solution.

All experiments were conducted at 18 mM concentration.
Kinetics of the reaction of *exo*-**6** or *endo*-**6** with benzyl azide were determined by measuring the decrease of the integral of the signal caused by benzyl azide methylene protons, with the integral of the acetonitrile or water solvent-peak as internal standard. A starting value for the integral of the methyl signals was estimated, due to the fact that cycloaddition had already proceeded significantly by the time of the first measurement.

From the conversion plots thus obtained, the second order rate plots were calculated according to equation:

$$kt = \frac{1}{[B]_0 - [A]_0} \times \ln \frac{[A]_0([B]_0 - [P])}{([A]_0 - [P])[B]_0} \quad (1)$$

with k = 2nd order rate constant ($M^{-1}s^{-1}$), t = reaction time (s), $[A]_0$ = the initial concentration of substrate A (mmol/mL), $[B]_0$ = the initial concentration of substrate B (mmol/mL) and $[P]$ = the concentration of product (mmol/mL).

Rate plots for cycloaddition of *endo*-6 and *exo*-6 with nitrone 7

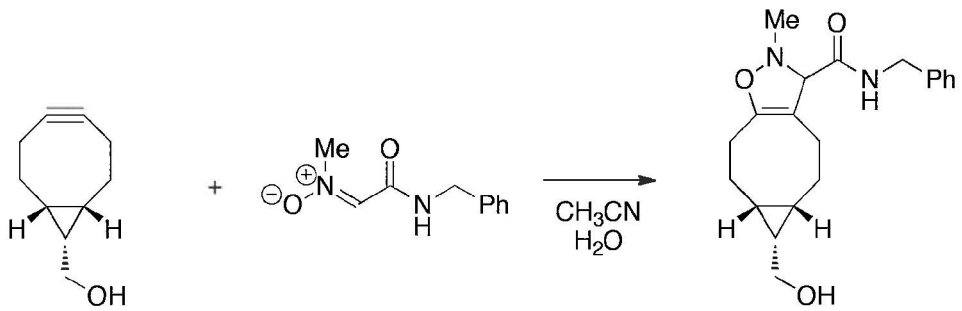

endo-**6** **7**

same for *exo*-**6**

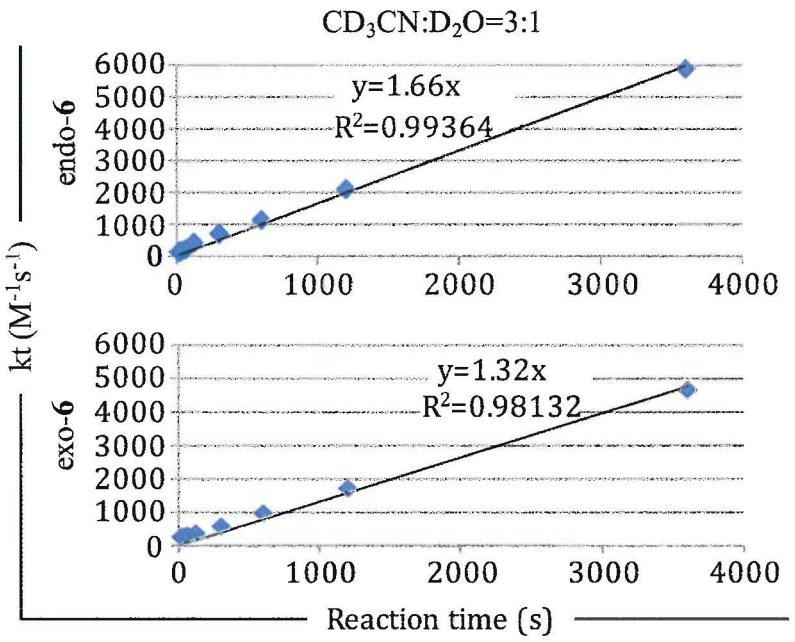

[1]H-NMR monitoring of cycloaddition of *exo*-**6** or *endo*-**6** with nitrone **7** was performed by rapid mixing (t=0) of stock solutions A and B (0.3 mL each) in an NMR tube and immediate insertion into a 400 MHz NMR spectrometer. NMR spectra were measured at preset time-intervals. Each experiment was performed in triplo.
Stock solution A: alkyne **6** was dissolved in a mixture of CD3CN and D2O (ratio 3:1 or 1:2, 10 mL) to give a 36 mM solution.
Stock solution B: *N*-(methyliminoacetyl *N*-oxide)benzylamine (nitrone **7**) was dissolved in a mixture of CD3CN and D2O (ratio 3:1 or 1:2, 10 mL) to give a 32.8 mM solution.

All experiments were conducted at 18 mM concentration in CD3CN:D2O=3:1.
Stock solution B: *N*-(methyliminoacetyl *N*-oxide)benzylamine (nitrone **7**) was dissolved in a mixture of CD_3CN and D_2O (ratio 3:1 or 1:2, 10 mL) to give a 32.8 mM solution.
Kinetics of the reaction of *exo*-**6** or *endo*-**6** with nitrone **7** were determined by measuring the decrease of the integral of the nitrone methyl groups, with the integral of the acetonitrile or water solvent peak as internal standard. A starting value for the integral of the methyl signals was estimated, due to the fact that cycloaddition had already proceeded significantly by the time of the first measurement.

From the conversion plots thus obtained, the second order rate plots were calculated according to equation:

$$kt = \frac{1}{[B]_0 - [A]_0} \times \ln \frac{[A]_0([B]_0 - [P])}{([A]_0 - [P])[B]_0} \quad (1)$$

with k = 2nd order rate constant ($M^{-1}s^{-1}$), t = reaction time (s), $[A]_0$ = the initial concentration of substrate A (mmol/mL), $[B]_0$ = the initial concentration of substrate B (mmol/mL) and $[P]$ = the concentration of product (mmol/mL).

Mass spectrometric analysis of SPANC labeling of FRATtide with *endo*-6 and biotin-conjugate 9.

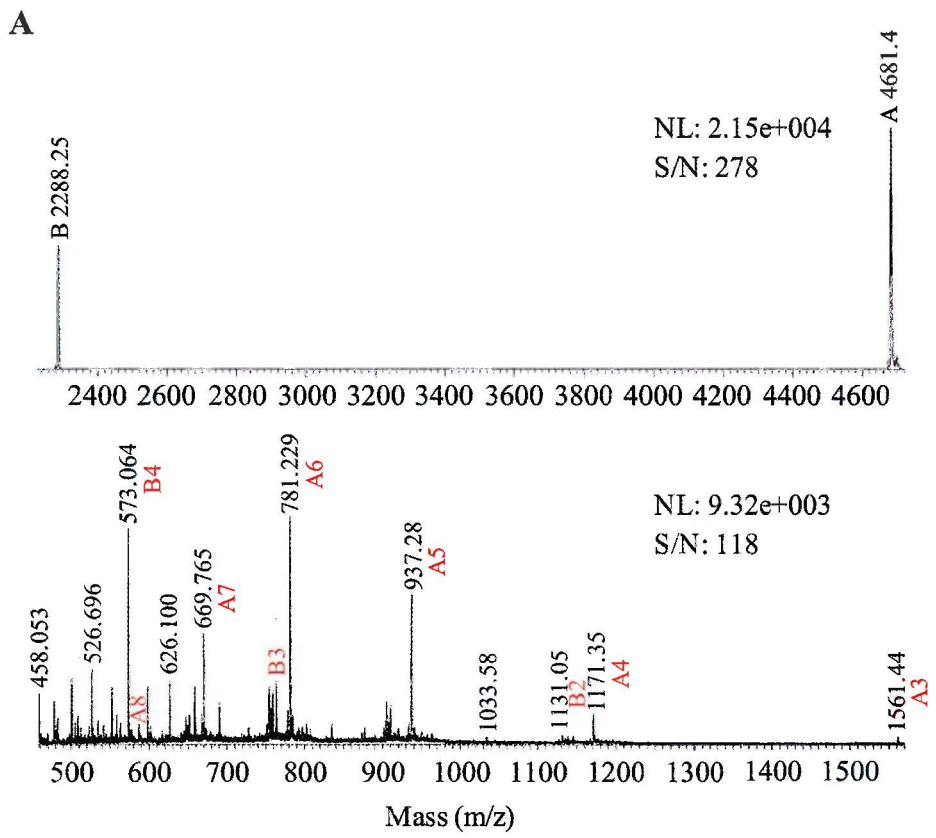

SPANC labeling of FRATtide with *endo*-6 (A)

FRATtide (15.6 µg, 3.4 nmol, 34 µM) was dissolved in 0.1 M NH_4OAc buffer pH 6.9 (100 µL) and $NaIO_4$ (1.1µg, 5.5 nmol, 48 µM) was added. The reaction was allowed to take place at room temperature for 40 min and *p*-methoxybenzenethiol (9.2 µg, 66.0 nmol, 565 µM) was added. The mixture was shaken for 2h at 25 °C and *p*-anisidine (13.5 µg, 109.3 nmol, 845 µM), *N*-methylhydroxylamine hydrochloride (18.2 µg, 218.6 nmol, 1.5 mM), and *endo*-**6** (41.1 µg, 273.3 nmol, 1.8 mM) were added. Finally, the reaction mixture was shaken at 25 °C for 24 h to give the desired conjugate. MS (Accu-TOF) measurement gave 4681.4 Da as the main peak after deconvolution.

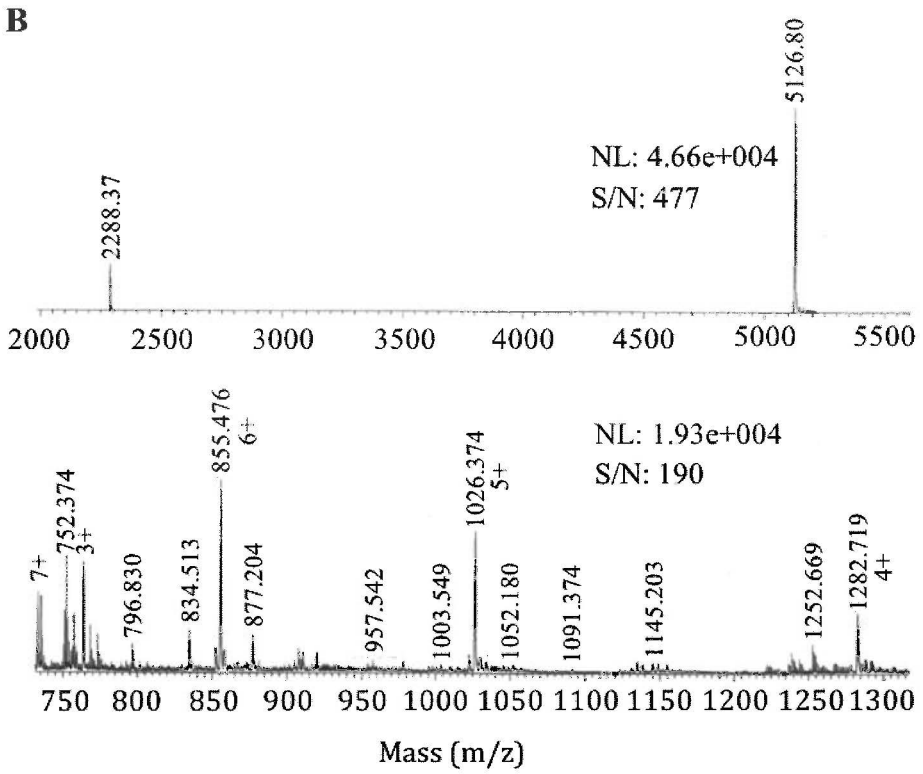

SPANC labeling of FRATtide with BCN-biotin conjugate (B)

FRATtide (9.3 µg, 2.1 nmol, 35 µM) was dissolved in 0.1 M NH_4OAc buffer pH 6.9 (60 µL) and $NaIO_4$ (0.7µg, 3.4 nmol, 52 µM) was added. The reaction was allowed to take place at room temperature for 40 min and *p*-methoxybenzenethiol (5.7 µg, 40.7 nmol, 581 µM) was added. The mixture was shaken for 2 h at 25 °C and *p*-anisidine (8.3 µg, 67.2 nmol, 864 µM), *N*-methylhydroxylamine hydrochloride (11.3 µg, 134.8 nmol, 1.6 mM), and **9** (100.3 µg, 168.6 nmol, 1.7 mM) were added. Finally, the reaction mixture was shaken at 25 °C for 24 h to give the desired conjugate. The residue was purified using an YM-3 millipore microcon centrifugal filter device by centrifuging three times for 30 min at 13,000 x g with 300 µL 0.1 M NH_4OAc buffer pH 6.9. MS (Accu-TOF) measurement gave 5126.8 Da as the main peak after deconvolution.

Spot-blot analysis of biotinylated FRATtide

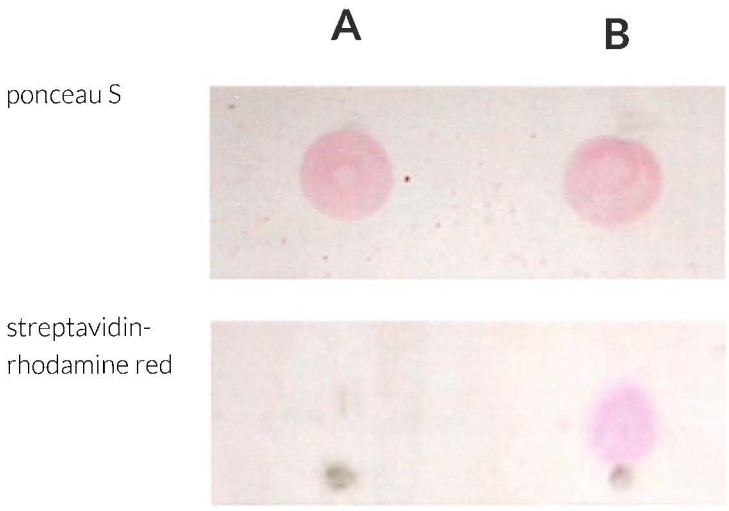

1 µL of native FRATtide (A) or purified FRATtide-BCN-biotin conjugate (B) were spotted on Whatman nitrocellulose membrane. Non-specific sites were blocked using 5% BSA in TBS-T (20 min). Top: proteins were stained using ponceau S. Bottom: proteins were stained with TBS-T solution containing 1% BSA and 0.01% rhodamine red-labeled streptavidin (Invitrogen) for 5 min.

After absorption of the peptide to the membrane, it can be reversibly stained with ponceau S, which stains all peptides and proteins present, showing that there are equal amounts of protein in each spot. Incubation with labeled streptavidin, followed by washing, shows that only the FRATtide-BCN-biotin conjugate (B) binds to the streptavidin, but there is no staining for FRATtide alone (A). This indicates that the conjugation of biotin to the FRATtide was successful and that there is no aspecific absorption taking place at non-functionalized FRATtide.

MS analysis of fluorescence labeling of capsid protein with BCN-Alexa Fluor 555 conjugate 11.

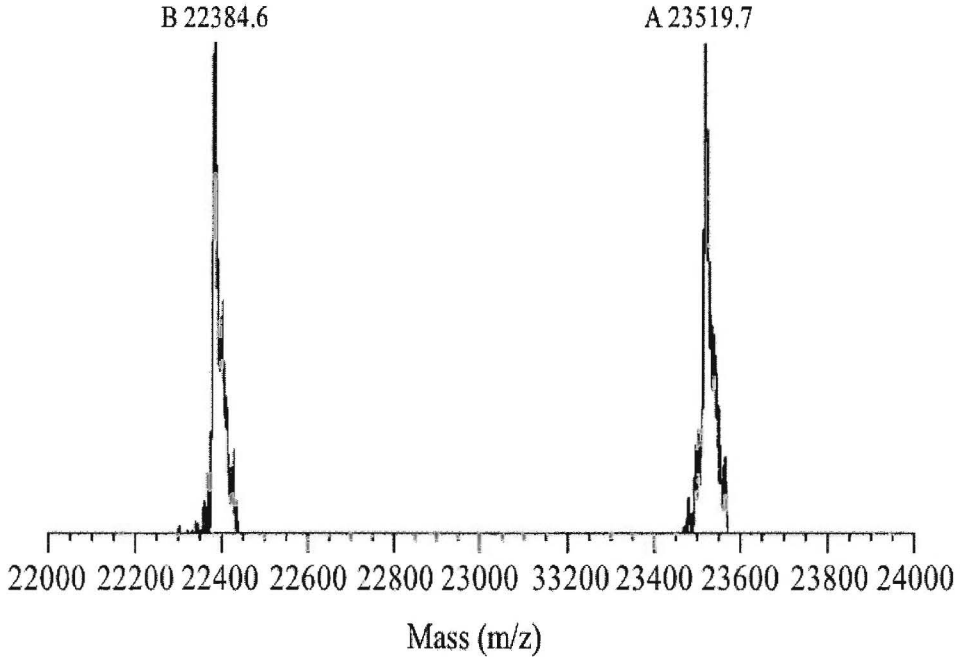

ESI-TOF mass spectrum of capsid protein reacted with **10**. Peak B corresponds to the mass of unreacted CP, while peak A corresponds to the reaction product. The mass difference between the peaks is 1135.1 (expected 1135).

The capsid protein (CP) of Cowpea Chlorotic Mottle Virus (CCMV) was expressed recombinantly in methionine auxotroph *E. coli*. The gene encoding the CP was obtained as described by Minten *et al.*[1] The wild-type CP contains two methionines, Met1 and Met137, and due to the cloning procedure a third methionine was added at the N-terminus of the protein. Site-directed mutagenesis was used to mutate two of these methionines into alanines. First Met137→Ala was mutated with the primer set CGAAAGATGTTGTCGCTGCTGCGTACCCCGAGGCG (mutation site underlined) and its reverse complement using the following PCR program: [95 °C, 1'; 16 cycles of (95 °C, 30"; 55 °C, 1'; 68 °C, 15'); 68 °C, 5']. Consequently Met1→Ala was mutated using the primer-set CGCGGCAGCCATATGGCGTCTACAGTCGGAACAG (mutation site underlined) and its reverse complement using the same PCR program. Both mutations were confirmed by sequence analysis.

Recombinant expression

For recombinant expression, the plasmid containing the CP-gene was transformed to a strain of methionine-auxotroph *E.coli* bacteria (B834 (DE3) pLysS cells, Novagen). The auxotroph expression was performed following the general procedure described by Link *et al.*[2] with some modifications. The bacteria were cultured in LB medium supplemented with ampicillin (100 mg/L) and chloramphenicol (50 mg/L) until an optical density of 0.4 - 0.6 was reached, at which point IPTG (final concentration 1 mM) was added to allow synthesis of T7 polymerase in presence of methionine. After 15 minutes the culture was washed twice by centrifugation and resuspension in 0.9% NaCl, followed by resuspension in M9 minimal medium supplemented with all natural amino acids (40 mg/L each) except methionine, glucose (0.4%), $MgSO_4$ (1 mM), thiamine (0.0005%), ampicillin (100 mg/L) and chloramphenicol (50 mg/L). The bacteria were cultured at 37 °C for 15 minutes before azidohomoalanine (40 mg/L) and IPTG (1 mM) were added to start the production of azido-containing CP. After culturing the bacteria for 18 hours at 30 °C the bacteria were harvested by centrifugation.

The CP was purified by Ni^{2+} NTA affinity chromatography under native conditions (Qiagen, Hilden, Germany). After purification the protein was analyzed by SDS-PAGE and mass spectroscopy, the latter indicating that approximately 50% of the proteins contains an azidohomoalanine instead of a methionine (data not shown). The N-terminal location of this this azide group ensures its positioning on the inside surface of the virus capsid after assembly from the capsid proteins.

Protein functionalization

The mixture of singly functionalized proteins and non-functionalized proteins (1 mg/ml in 0.1M phosphate buffer pH 7.5, 1M NaCl) was mixed with 4 equivalents of Alexa Fluor-BCN conjugate 11, which was dissolved in a minute amount of water. After mixing for 3 hours at RT, the reaction product was analyzed on a 12% SDS PAGE gel, of which a fluorescence image was obtained before staining it with Coomassie Blue stain. As control reaction Alexa Fluor-BCN conjugate 11 was mixed with non-functionalized CP protein in exactly the same conditions as the reaction. The absence of fluorescence in the fluorescence image shows that there is neither a side reaction nor any non-covalent adhesion of the dye to the protein.

To obtain a mass spectrum of the reaction product, the product was dialyzed to 0.1% formic acid in water (using Microcon® centrifugal filter units, 10 kDa, Millipore) before injecting it into the ESI-TOF (JEOL AccuTOF) mass spectrometer. Deconvolution of the raw data resulted in the spectrum displayed in Figure 5.

FPLC trace of the reaction mixture after assembly of fluorescent capsids by dialysis

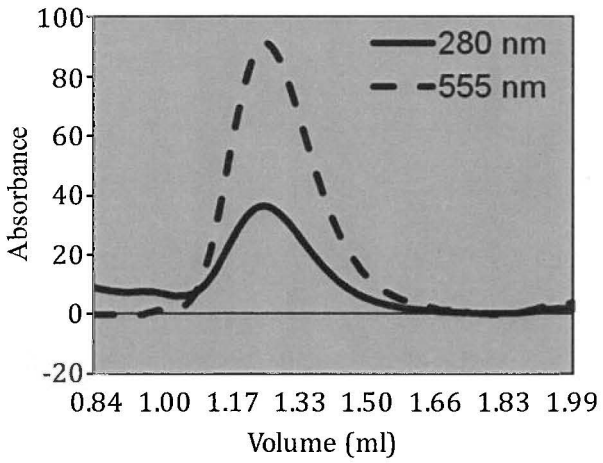

FPLC trace of the reaction mixture after assembly of the capsids by dialysis. The peak at 1.2 ml corresponds to 28 nm capsids, the 555 nm-absorbance shows that the capsid protein-AF555 conjugate is present in the capsids.

Capsid assembly

Self-assembly of the functionalized capsid protein was performed by 18 hour dialysis of the crude reaction mixture to a slightly acidic buffer (pH 5.0, 50 mM NaOAc; 1 M NaCl; 10 mM $CaCl_2$), which induces the formation of 28 nm sized spherical particles.[3,4] FPLC size exclusion analysis on a Superose 6 column showed an absorption peak at 280 nm at an elution volume of 1.2 ml, indicating the formation of 28 nm-sized capsids. The overlapping absorbance at 555 nm indicated the presence of Alexa dye in the capsids.

Transmission electron microscopy

An FPLC sample of the 1.2 ml peak was loaded on a TEM-grid, which was subsequently stained with 0.2% uranyl acetate in water. Analysis of the grid clearly shows the presence of spherical particles with a size of approximately 28 nm, the expected size for virus capsids.

Flow cytometry of glycan labeling

Cell culture procedure

Invasive and metastatic human melanoma cells (MV3)[5] were maintained in culture medium RPMI 1640, containing 10% fetal calf serum, penicillin/streptomycin (each 50U/ml) in a 5% CO_2 water-saturated atmosphere.

Cell surface azide labeling

MV3 cells were cultured for 6 days in the absence or presence of Ac_4ManNAz (50 µM). Medium and compound change was performed after 3 days. For live-cell labeling, cells were detached using EDTA (1 mM), washed and centrifuged three times (PBS, 300 x G, 5 min, 4 °C), resuspended in PBS and incubated in BCN-biotin **8** (60 µM), DIBO-biotin (60 µM), or buffer (1 h, 20 °C), washed three times (PBS, 300 x G, 2 min, 4 °C), resuspended in ice-cold PBS containing Alexa Fluor 488-conjugated streptavidin (5 µg/ml, Invitrogen; final volume 200 µl). After incubation (30 min, 4 °C), cells were washed three times, resuspended in PBS (200 µl, 4 °C) for further cell-function studies.

Flow cytometry

Flow cytometry was performed on a BD Biosciences FACS-Calibur flow cytometer using the 488 nm argon laser and data were analyzed with FCS Express version 3 research edition (De Novo Software, Los Angeles, CA). Per sample, $2x10^4$ morphologically intact cells were analyzed in the presence of propidium idodide (2.5 µg/ml).

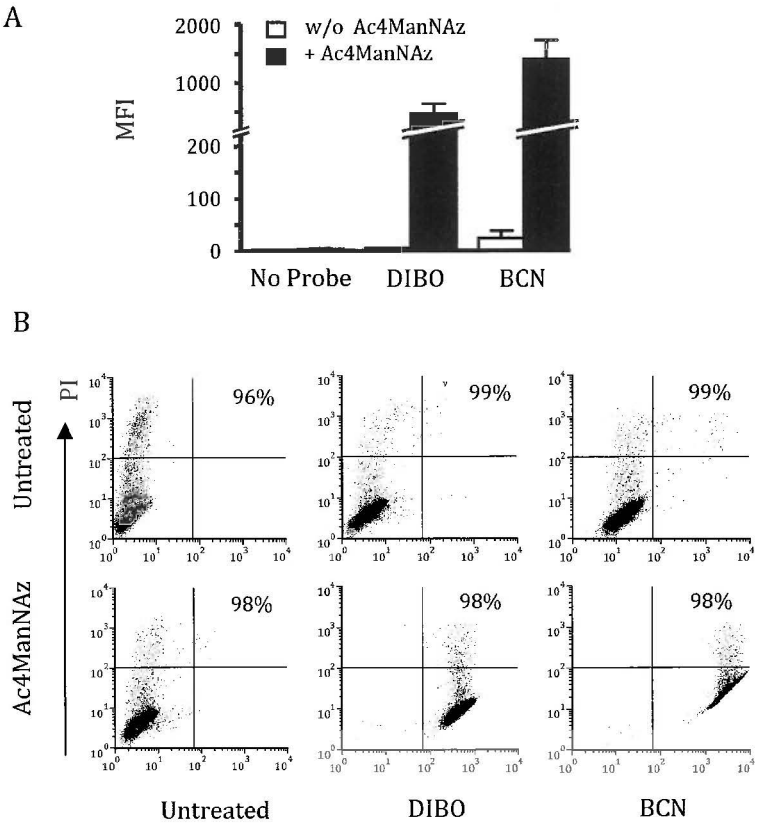

Fluorescence intensities and cell viability after cell labeling with Ac_4ManNAz and detection with DIBO- or BCN-biotin and secondary Alexa Fluor 488-conjugated streptavidin. (A) Mean intensities for green fluorescence (Alexa Fluor 488) and standard deviations (SD) from four independent experiments. (B) Intact cell viability after glycan labeling. Green fluorescence (Alexa Fluor 488) and propidium iodide (PI) label. Numbers indicate the percentage of PI-negative, viable cells.

Procedure for confocal microscopy and 3D imaging of glycan redistribution during invasive cell migrations

For confocal microscopy, azido-labeled cells were resuspended in normal culture medium, transferred to a 6 well plate and incubated for 30 min at 37 °C. Life cell imaging of MV3 cells was performed on a Olympus FV1000 confocal laser scanning microscope using excitation at 488 nm and emission detection of 520/50 nm.

Distribution studies of azido sialic acids were performed in 3D cell migration assays. Labeled MV3 cells were incorporated into 3D collagen I lattices and incubated for 90 min at 37°C, subsequently fixed with paraformaldehyde (4% in 0.1 M phosphate buffer) for 30 min at 37 °C and washed three times (PBS). Finally F-actin was stained with phalloidin Alexa Fluor 568 (Invitrogen, 2 U/ml) and nucleus with DAPI (Roche Diagnostics, 2,5 µg/ml).

Imaging of MV3 cells was performed as described above, using an additional excitation at 559 nm and emission detection of 647 nm and excitation at 405 nm and emission detection of 422 nm.

Pixel densitometry

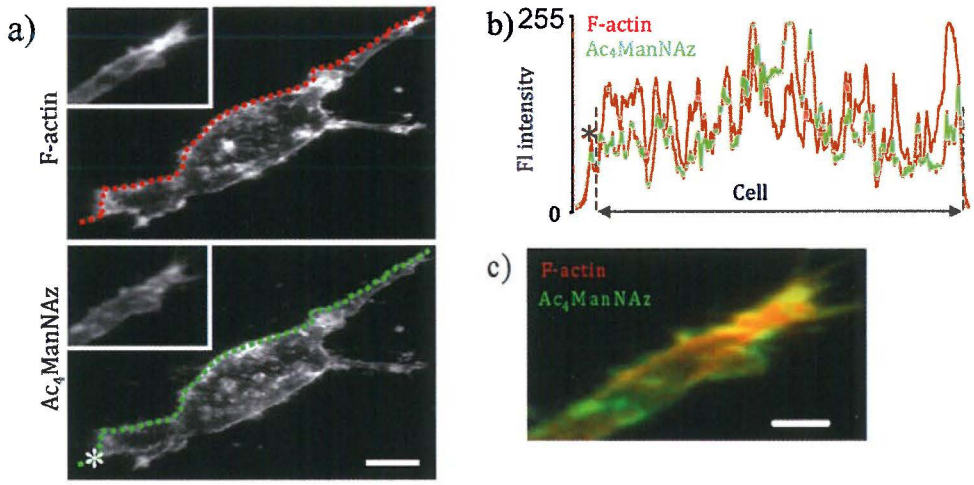

Intensity measurements of sialic acid and F-actin distribution at the cell surface. a) Region of interest for densitometric analysis. Bar 2 µm. b) Fluorescence intensity for sialic acid and F-actin from the leading to trailing edge. c) Two-channel detail of the leading pseudopod, revealing partial colocalization (yellow) in the sub-micron range. Asterisk, sialic acid containing deposited cell surface material. Bar 2 µm.

Literature references

[1] Minten, I. M., Hendriks, L. J. A., Nolte, R. J. M. & Cornelissen J. J. L. M. Controlled encapsulation of multiple proteins in virus capsids. *J. Am. Chem. Soc.* **131**, 17771 (2009).

[2] Link, A. J. & Tirrell, D. A. Reassignment of sense codons *in vivo*. *Methods* **36**, 291–298 (2005).

[3] Verduin, B. J. M. The preparation of CCMV-protein in connection with its association into a spherical particle. *FEBS Lett.* **45**, 50–54 (1974).

[4] Comellas-Aragones, M., Engelkamp, H., Claessen, V. I.; Sommerdijk, N., Rowan, A. E., Christianen, P. C. M., Maan, J. C., Verduin, B. J. M., Cornelissen, J. J. L. M. & Nolte, R. J. M. *Nat. Nanotechnol.* **2**, 635 (2007).

[5] Maaser, K. *et al.*, "Functional hierarchy of simultaneously expressed adhesion receptors: integrin alpha2beta1 but not CD44 mediates MV3 melanoma cell migration and matrix reorganization within three- dimensional hyaluronan-containing collagen matrices," *Mol. Biol. Cell.* **10**, 3067 (1999).

"If everything worked the first time they would call it 'search'"

Patti Giblin and Carolyn Bertozzi

CHAPTER 4

Quantitative Removal of Multiple Glycan Species from Live Cells. *(in preparation)*

Samuel Schmidt[1,2] *and Peter Friedl*[2,3,4]

[1] Radboud University Medical Centre, Department of Biochemistry, Nijmegen, (Netherlands); [2] Radboud University Medical Centre, Department of Cell Biology (Nijmegen, (Netherlands); [3] Cancer Genomics Center, (Netherlands); [4] The University of Texas MD Anderson Cancer Center, Department of Genitourinary Medical Oncology, Houston, Texas, (United States)

Abstract

Tumor development is marked by alterations in glycosylation patterns but the functional significance of glycosylation in biological processes including cell adhesion and migration is not well understood. Over the last decades technologies have been developed to perturb glycan biosynthesis and address their functional role. However, tools like natural inhibitors are often limited in their utility due to their impact on intracellular glycosylation and their strong off-target effects. There is a strong need for tools that allow the study of the dynamics in glycan functions that can be met in complex biological systems. We here introduce a protocol for the efficient enzymatic digestion of cell surface glycosylation using a two-step procedure that allows a separate digestion of distinct glycan epitopes using high-purity glycosidases while maintaining cell viability and integrity. Furthermore, we describe procedures for detecting the successful digestion of enzyme-selected glycan chains and moieties using antibodies, lectins and bioorthogonal labeling. Excellent cellular viability was maintained after applying the approach to the cells, which allows the subsequent functional analyses of targeted glycans and their roles in dynamic biological contexts such as cell adhesion and migration.

Introduction

Glycosylation of proteins is one of the most important posttranslational modifications, with more than half of all human proteins estimated to be glycosylated.[1] Cell surface glycans are components of glycoproteins, glycolipids, and proteoglycans, forming an outer layer of a phylogenetically old and molecularly complex scaffold, the so-called glycocalyx. These biopolymers play key roles in numerous biological processes[2] such as cell-cell and cell-matrix interactions involved in embryonic development[3], leukocyte homing[4], adhesion, migration and invasion.[5] Furthermore, glycans serve additional functions including modulation of protein structure, sorting and targeting of proteins within the cell and modulation of enzyme activity. [6] An increasing number of studies attempt to determine the molecular glycan-mediated mechanisms that underlie these processes, but the wide range of functions and contrasting results make a comparative evaluation often a challenge. For example high expression of some glycosyl epitopes promotes invasion and metastasis, leading to shorter 5-10 year survival rates of patients, whereas expression of some other glycosyl epitopes suppresses tumor progression, leading to higher postoperative survival rates.[7] In recent decades increasing progress has been made in the development of analytical tools for the study of cellular glycosylation and corresponding defects, including high performance anion-exchange chromatography of glycans after deglycosylation and purification[8] or mass spectrometry.[9] Using these techniques it has become possible to screen patient material from complex cell lysates or bodily fluids and detect potential glycosylation anomalies and thereby identify new clinical biomarkers. Regrettably, analyzing glycans in living systems is a challenge for which these experimental approaches are not suited, as they provide only a snapshot of glycosylation at a certain state. Tumor development including invasion and metastasis is an extremely complex and dynamic process, that requires a steadily adaptation of cells in response to environmental determinants, including availability of nutrients and accessibility of ligands within the tissue. Thus, it is difficult if not even impossible to study the context dependent functions of glycosylation during tumor progression in isolation. Rather a means is required to study these biopolymers both as individual glycans and glycan ensembles in physiologically relevant context to relate this impact. Consequently, efforts have been made to investigate potential functions of glycosylation in living systems, such as perturbing glycan strategies using small molecule inhibitors of glycan biosynthesis that target glycosyltransferases. Natural inhibitors including tunicamycin block the biosynthesis of N-linked glycan precursors[10] and serve as useful tool for efficient inhibition of glycosylation in biological systems as it is selective for its target and active in living cells. Tunicamycin has been widely employed to study the effects of glycosylation on protein function.[11] However, the use of tunicamycin is limited as it interferes also with intracellular glycosylation and feature strong off-target effects.[11a-c, 12] Thus, an induced impact on cellular function cannot be correlated to missing glycan

residues on the cell surface but might result from an affected intracellular mechanism that depends on accessible N-glycosylation. Recently, new inhibitors and approaches including modified sugars known as "primers of glycosylation" have been developed that are supposed to disrupt glycosylation in a more refined fashion than tunicamycin.[13] However, there are more than 100 glycosyltransferase families predicted in mammalians[14] with structural homology and functional overlap which makes inhibition of individual glycosyltransferases still a challenge. Approaches that use enzymes, including exo- and endoglycosidases to interfere with cell surface glycosylation have received more attention during the last years. However, in most of the enzymes often require reaction milieus with pH values and buffer conditions that are inappropriate for functional studies in live cells.[15] Nevertheless, in case one could optimize that approach for an application in living systems, the spatial orientation of glycosidase treatment to the cell surface through externally administered enzymes, makes such an approach the most promising tool to study the function of cell surface glycans while largely maintaining intracellular glycosylation and accompanied mechanisms such as protein conformation and stability.[16] We developed an approach for enzymatic digestion of the main part of cell surface glycan chains and moieties while retaining cell viability. Aim was to generate a protocol that combines optimal enzyme efficacy with a mild treatment of cells under physiological conditions to maintain cellular integrity. We achieved optimal enzyme conditions by decreasing the serum concentration in the incubation medium, that contains amongst growth factors also proteolytically active enzymes and inhibitors[17] to a level that compromises its potential impact on enzyme activity[18] while providing crucial ingredients required for cell survival. Using high-purity glycosidases enables a targeted enzymatic treatment and thereby allows the incubation under conditions that can be tolerated by cells. Furthermore, incubation with high purity enzymes in a two-step procedure allows a separate digestion of distinct glycan epitopes that is prerequisite for a selective analysis of their functions. We developed this approach with the purpose to provide evidences for a direct relation between the glycocalyx polarity and integrin independent cell adhesion to collagen I fibers. To perform these studies, cells need an excellent viability to define a functional impairment as a result of a degraded glycan chain or moiety and not of the treatment. We controlled the cell viability using propidium iodide (PI). When applying the digestion protocol, the targeted glycan classes and moieties were efficiently removed from the cell surface with more than 95 % decrease in signal as approved by staining procedures using glycan targeting antibodies, lectins and bioorthogonal labeling. The epitope specificity of the glycosidases was approved using lectins recognizing glycan residues that were not addressed by the used enzymes. Finally, this protocol could be implemented into functional assays to study the role of the glycocalyx in cell adhesion and migration ***in vitro*** and ***in vivo***. The here presented strategy provides an innovative tool to interfere spatially with cell surface glycosylation using high-purity glycosidases for an efficient and selective digestion of individual and multiple

glycans. Furthermore, it facilitates subsequent functional analyses of targeted glycans in dynamic biological contexts such as cell adhesion and migration.

Materials

Reagents

- Fetal bovine serum (FBS, PAA Laboratories, Cat. No. A15-101)
- RPMI1640 (1×, liquid, GlutaMAX, 2,000 mg/L D-glucose, Gibco, Cat. No. 21875-034)
- L-glutamine (4 mM, 100×; PAN, Cat. No. P04-80100)
- Penicillin (10,000 U/ml) - streptomycin (10,000 µg/ml) (100×, Gibco, Cat. No. 15140-122)
- Sodium pyruvate (1 mM, Invitrogen, Cat. No. 11360)
- Phosphate-buffered saline containing Ca2 + and Mg2 + (PBS) (1x, Gibco, Cat. No. 14040-117)
- EDTA (1 M; PAN Biotech, Cat. No. P10-026500)
- 3,8-Diamino-5-[3-(diethylmethylammonio)propyl]-6-phenylphenanthridinium-diiodide (PI) (50 mg/ml, Sigma Aldrich, Cat. No. P4170)
- Hyaluronidase from bovine testes, Type I-S (275-550 U/ml, Sigma-Aldrich, Cat. No. H9910) hydrolyzes 1,4-linkages between N-acetyl-β-D-glucosamine and D-glucuronate residues in hyaluronate.
- Heparitinase I from Flavobacterium heparinum (10 mU/ml, Seikagaku, Cat. No. 100704) hydrolyses α-N-acetyl /-sulfo-D-glucosaminidic linkage in heparansulfate and reacts with chondroitin sulphate A (0.1 %), B (1.0 %), C (0.1 %), Hyaluronic acid (0.1 %) and Heparin (1.0 %).
- Chondroitinase ABC from Proteus vulgaris (100 mU/ml, Sigma-Aldrich, Cat. No. C3667) acts on chondroitin 4-sulfate, chondroitin 6-sulfate, and dermatan sulfate and acts slowly on hyaluronate.
- Neuraminidase from Clostridium perfringens (C. welchii), Type V (100 mU/ml, Sigma-Aldrich, Cat. No. N2876) cleaves terminal sialic acid residues which are α-2,3- α-2,6- or α-2,8-linked to Gal, GlcNac, GalNAc, AcNeu, GlcNeu, oligosaccharides, glycolipids or glycoproteins.
- β-1,4 galactosidase (150 mU/ml, QA-Bio, Cat. No. E-BG07), recognizes specifically non-reduced terminal β-1,4-galactose. According to the manufacturer, the production host strain has been extensively tested and does not produce any other detectable glycosidases.
- Anti-heparan sulfate (HS) single chain Fv fragment-vsv-g-tag antibodies (HS4C3)[20]
- Anti-dermatan sulfate (DS) single chain Fv fragment-vsv-g-tag antibodies (LKN1)[20b, 21]

- Anti-chondroitin sulfate (CS) single chain Fv fragment-vdv-g-tag antibody (IO3H10)[20b,22]
- Monoclonal mouse anti-vsv-g (clone P5D4) IgG (Sigma-Aldrich, Cat. No. V5507)
- Goat-anti-mouse IgG Alexa Fluor 488-conjugated antibody (2 mg/ml, Invitrogen, Cat. No. A-11029)
- Peracetylated N-azidoacethylmannosamine (Ac4ManNAz, 50 mM stock in DMSO, Sigma-Aldrich, Cat. No. A-7605) **CRITICAL** Store at -20 °C or -80°C
- Biotin-conjugated Bicyclo [6.1.0] nonyne (BCN-POE_3-NH-biotin, 10 mM stock in MilliQ, SynAffix, Oss, The Netherlands) **CRITICAL** Store at -20°C.
- Alexa Fluor 488-conjugated Streptavidin (2 mg/ml, Invitrogen, Life Technologies, Carlsbad, USA, Cat. No. S32354) **CRITICAL** Store at -20°C.
- Biotin-conjugated *Maackia amurensis* agglutinin (MAA) (1 mg/ml, EY Laboratories, INC., Cat. No. BA-7801-5) **CRITICAL** Store at -20°C.
- FITC-conjugated *Arachis hypogaea* (peanut) Agglutinin (PNA) (5 mg/ml, Sigma Aldrich, Cat. No. L7381) **CRITICAL** Store at -20°C.
- Human MV3 melanoma (provided by G. van Muijen, Dept. of Pathology, RadboudUMC Nijmegen, The Netherlands)
- Human T-leukemia cell-line Molt-4 (ACC362; DSMZ Braunschweig, Germany)
- Human MV3 melanoma (provided by G. van Muijen, Dept. of Pathology, RadboudUMC Nijmegen, The Netherlands)[23]
- Human T-leukemia cell-line Molt-4 (ACC362; DSMZ Braunschweig, Germany)

Equipment

- FACS-Calibur (BD Biosciences, Erembodegem, Belgium) flow cytometer, 488 nm line argon ion laser, emission 530/40 (Alexa Fluor 488), 620/50 (PI)
- FACS tubes (Micronic, Lelystad, The Netherlands, Cat. No. M32000)
- Greiner CELLSTAR 96 round bottom well plates (Sigma Aldrich, Cat. No. M9311)
- Flow cytometry analysis DeNovo FCS 5.0 (De Novo Software, Glendale, USA)

Reagent Setup

Cell detachment buffer (2 mM EDTA/1xPBS, pH 7.4) Add 200 µl EDTA to 98 ml PBS **CRITICAL** To prevent cleavage of protein cores and bound glycan chains of proteoglycans and glycoproteins in an uncontrolled manner that may affect cell functions do not use trypsine for cell detachment.

MV3 and Molt4 cell culture medium Add 50 ml FBS, 5 ml sodium pyruvate, 5 ml L-glutamine and 5 ml penicillin-streptomycin to 435 ml RPMI1640. The medium can be stored for several weeks at 4 °C.

MV3 and Molt-4 low serum medium Add 5 ml FBS, 5 ml sodium pyruvate, 5 ml L-glutamine and 5 ml penicillin-streptomycin to 435 ml RPMI1640. The medium can be stored for several weeks at 4 °C **CRITICAL** To prevent proteolytic degradation of used glycosidases through serum-containing proteases, it is essential to administer serum only at low concentrations.

Hyaluronidase digestion medium Weigh 2.75 mg hyaluronidase and add 5 mL low serum medium yielding 275-550 U/ml **CRITICAL** Hyaluronidase digestion medium needs to be prepared freshly prior to the digestion experiment.

Pre-cocktail digestion master-mix Add 4 µl heparitinase (20 mU/ml), 2 µl chondroitinase ABC (200 mU/ml) and 1.8 µl neuraminidase (200 mU/ml) to 92,2 µl hyaluronidase digestion medium (100 µl master-mix)

Maxi-cocktail digestion master-mix Add 4 µl heparitinase (20 mU/ml), 2 µl chondroitinase ABC (200 mU/ml), 1.8 µl neuraminidase (200 mU/ml) and 10 µl β-1,4 galactosidase (300 mU/ml) to 83,2 µl hyaluronidase digestion medium (100 µl master-mix).

CRITICAL Used enzyme volumes are two-fold administered in the master-mix and will be finally diluted 1:2 with hyaluronidase digestion medium including cells to achieve 200 µl digestion volume. To ensure that experiments are performed in a near-physiological environment, it is essential to maintain cells at 37 °C and physiological pH conditions (7.4). Control the approximate pH prior to each treatment using indicator paper.

Digestion control medium Add MilliQ at equal volumes to low serum medium instead of master-mix enzymes.

Heparan sulfate (HS) staining solutions Add 5 µl HS4C3 to µl PBS.

Dermatan sulphate (DS) staining solutions Add 20 µl LKN1 to 80 µl PBS.

Chondroitin sulphate (CS) staining solutions Add 20 µl IO3H10 to 80 µl PBS.

CRITICAL Keep all antibody solutions on ice.

P5D4 IgG staining solution Add 10 µl P5D4 IgG to 90 µl PBS.

Goat anti mouse- Alexa Fluor 488 IgG staining solution Add 0.5 µl to 99.5 µl PBS (10 µg/ml working solution).

Ac4ManNAz incubation medium Add 1 µl Ac4ManNAz to 999 µl cell culture medium (50 µM working solution). **CRITICAL** Medium needs to be prepared freshly on the day of administration and kept at 37 °C.

BCN-biotin solution Add 6 µl BCN-biotin to 994 µl PBS (60 µM working solution) **CRITICAL** Keep the solution at room temperature.

Streptavidin- Alexa Fluor 488 staining solution Add 0.5 µl Streptavidin- Alexa Fluor 488 to 99.5 µl PBS (10 µg/ml working solution) **CRITICAL** Keep the solution temperature at 4 °C.

MAA-biotin staining solution Add 10 µl MAA-biotin to 90 µl PBS (100 µg/ml working solution) **CRITICAL** To minimize uptake of MAA by cells during the incubation period, it is essential to keep the solution temperature at 4 °C.

PNA-FITC staining solution Pre-dilute the PNA-FITC stock solution in PBS to achieve a concentration of 1 mg/ml prior to the incubation experiment. Add 10 µl MAA-biotin to 90 µl PBS (100 µg/ml working solution) **CRITICAL** To minimize uptake of MAA and PNA by cells during the incubation period, it is essential to keep the solution temperature at 4 °C. **Staining control solution** Add MilliQ in equal volumes to PBS instead of antibodies, probes or lectins

Procedure

Cell culture TIMING ~1 h

1 Culture MV3 and Molt-4 cells in cell culture medium (see REAGENT SETUP) in T75 flasks at 37 °C, 5 % CO_2.

2 Passage cells 1:10 every third day at about 70 % confluence, for MV3 cells according to the following protocol (Steps 3-6). For Molt-4 cells transfer 1 ml to a flask pre-filled with 10 ml cell culture medium. **CRITICAL STEP** Split the cells before they reach 70 % confluency to prevent contact inhibition in adherent cells.

3 Aspirate the cell culture medium, wash the cells with 10 ml PBS and aspirate to remove traces of old media.

4 Harvest MV3 cells by incubation with 3 ml 2 mM EDTA/PBS for about 2 min.

5 Add 7 ml cell culture medium and transfer the cells into a 15-ml conical tube.

6 Add 1 ml of the cell suspension into a new T75 flask pre-filled with 10 ml HeLa cell culture medium.

7 For metabolic labelling experiments, inoculate 2×10^5 cells in Ac_4ManNAz incubation medium (see REAGENT SETUP) in T25 flasks 72 h before the glycosidase digestion experiment **PAUSE POINT** Culture cells for 72 h at 37 °C, 5 % CO_2.

Preparation of cells for enzymatic digestion with glycosidase cocktails TIMING ~1h

8 At 1 h before the glycosidase digestion experiments, aspirate the MV3 cell culture medium from the T25 flasks (prepared in Step 6 and 7). Thereafter, briefly wash the cells with 5 ml PBS and aspirate to remove traces of old media. For Molt-4 cells transfer cells into a 15 ml conical tube and continue with step 11.

9 Harvest MV3 cells by incubation with 3 ml 2 mM EDTA/PBS for about 2 min.

10 Add 3 ml cell digestion medium (see REAGENT SETUP) in T75 and T25 flasks and transfer the cells into a 15 ml conical tube.

11 Spin down the cells by centrifugation at 400g for 5 min, room temperature.

12 Carefully remove the supernatant and resuspend the cells in digestion medium (for control cells) or Hyaluronidase digestion medium (for digestion cells)

13 Repeat steps 11 and 12 once **CRITICAL STEP** Wash cells carefully to dispose residual compounds from the cell culture medium including 10 % FBS.

14 Resuspend cells in digestion medium (for control cells) or Hyaluronidase digestion medium (for digestion cells) (see REAGENT SETUP), count them using a Neubauer counting chamber and adjust the cell number to 5×10^5 cells/ml in 15 ml conical tubes.

Enzymatic digestion with glycosidase cocktails TIMING ~6 $^1/_2$ h

15 Transfer 100 µl Pre-cocktail und Maxi-cocktail master-mix (see REAGENT SETUP) into each conical Eppendorf tube. For Control cells transfer 100 µl digestion control medium (see REAGENT SETUP) into each conical Eppendorf tube.

16 Add 100 µl cell suspension (Step 14) to each conical Eppendorf tube.

17 Cover the upper side of the Eppendorf tubes with parafilm and prick in a tiny hole with a needle or a yellow pipette tip **CRITICAL STEP** The perforated parafilm allows sufficient gas exchange for oxygenation, thus avoid closing the tubes with the plastic lid.

18 Incubate the cells for 6 h at 37 °C, 5 % CO_2. Mix the cell suspension every 2 h gently with a pipette and place them immediately back in the incubator. Prevent air-bubbles **CRITICAL STEP** Every 2 h transfer a drop of cell suspension from each tube on an object slide and mount it on a light microscope. Monitor cells in digestion medium and compare them carefully with the control cells regarding cell morphology.

Preparation of cells for immuno-stainings and confocal microscopy TIMING ~40 min

19 Transfer the cell suspensions into 96 well plates with round bottom.

20 Spin down the cells by centrifugation at 400g for 5 min, room temperature.

21 Carefully remove the supernatant and resuspend the cells in PBS.

22 Repeat steps 20 and 21 three times **CRITICAL STEP** Wash cells carefully to dispose residual compounds from the glycosidase cocktail medium.

23 After the last centrifugation step remove the supernatant and continue with 24, 40 or 51.

Immuno-fluorescence with GAG recognizing antibodies TIMING ~2 $^1/_2$ h

24 Transfer the 1st antibody HS, DS and CS staining solutions (see REAGENT SETUP) to the appropriate wells on the 96 well plate (prepared in steps 19-23). For Control cells transfer the staining control solution with appropriate volume (see REAGENT SETUP).

25 Incubate the cells for 45 min at 20°C.

26 Spin down the cells by centrifugation at 400g for 5 min, room temperature.

27 Carefully remove the supernatant and resuspend the cells in PBS.

28 Repeat steps 26 and 27 twice **CRITICAL STEP** Repeating the steps is essential to dispose antibody residuals.

29 Transfer the 2nd antibody P5D4 IgG staining solution (see REAGENT SETUP) to the appropriate wells on the 96 well plate.

30 Incubate the cells for 30 min at 4°C on ice.

31 Spin down the cells by centrifugation at 400g for 5 min, 4°C.

32 Carefully remove the supernatant and resuspend the cells in PBS.

33 Repeat steps 31 and 32 twice.

34 Transfer the 3rd antibody Goat anti mouse- Alexa Fluor 488 IgG staining solution (see REAGENT SETUP) to the appropriate wells on the 96 well plate.
35 Incubate the cells for 30 min at 4°C on ice **CRITICAL STEP** Cover the tubes with aluminium foil to keep them dark and prevent photo-bleaching.
36 Spin down the cells by centrifugation at 400g for 5 min, 4°C.
37 Carefully remove the supernatant and resuspend the cells in PBS.
38 Repeat steps 36 and 37 twice.
39 After the last centrifugation step, resuspend the cells in cold PBS, transfer the cells into conical FACS tubes, put them on ice and continue with step 62 **CRITICAL STEP** Cover the tubes with aluminium foil to keep them dark and prevent photo-bleaching.

Bioothogonal labelling of SiaNAz using strain-promoted alkyne-azide cyclo-addition (SPAAC)[24] TIMING ~2 h

40 Transfer the BCN-biotin solution (see REAGENT SETUP) to the appropriate wells on the 96 well plate (prepared in steps 19-23). For Control cells transfer the staining control solution with appropriate volume (see REAGENT SETUP).
41 Incubate the cells for 1 h at room temperature.
42 Spin down the cells by centrifugation at 400g for 5 min, room temperature.
43 Carefully remove the supernatant and resuspend the cells in PBS.
44 Repeat steps 42 and 43 twice **CRITICAL STEP** Repeating the steps is essential to dispose antibody residuals.
45 Transfer the Streptavidin- Alexa Fluor 488 staining solution (see REAGENT SETUP) to the appropriate wells on the 96 well plate.
46 Incubate the cells for 30 min at 4°C on ice **CRITICAL STEP** Cover the tubes with aluminium foil to keep them dark and prevent photo-bleaching.
47 Spin down the cells by centrifugation at 400 g for 5 min, 4°C.
48 Carefully remove the supernatant and resuspend the cells in PBS.
49 Repeat steps 42 and 43 twice.
50 After the last centrifugation step, resuspend the cells in cold PBS, transfer the cells into conical FACS tubes, put them on ice and continue with step 62 **CRITICAL STEP** Cover the tubes with aluminium foil to keep them dark and prevent photo-bleaching.

Fluorescence with Gal β-1,4 recognizing *Maackia amurensis* agglutinin and Gal β-1,3 GalNAc recognizing *Arachis hypogaea* (peanut) agglutinin TIMING ~ 2 h

51 Transfer the MAA-biotin and PNA-FITC staining solution (see REAGENT SETUP) to the appropriate wells on the 96 well plate (prepared in steps 19-23). For Control cells transfer the staining control solution with appropriate volume (see REAGENT SETUP).

52 Incubate the cells for 20 min at 4°C on ice.

53 Spin down the cells by centrifugation at 400 g for 5 min, 4 °C.

54 Carefully remove the supernatant and resuspend the cells in PBS.

55 Repeat steps 52 and 53 twice **CRITICAL STEP** Repeating the steps is essential to dispose antibody residuals.

56 Transfer the Streptavidin- Alexa Fluor 488 staining solution (see REAGENT SETUP) to the appropriate wells on the 96 well plate.

57 Incubate the cells for 30 min at 4°C on ice **CRITICAL STEP** Cover the tubes with aluminium foil to keep them dark and prevent photo-bleaching.

58 Spin down the cells by centrifugation at 400 g for 5 min, 4°C.

59 Carefully remove the supernatant and resuspend the cells in PBS.

60 Repeat steps 57 and 58 twice.

61 After the last centrifugation step, resuspend the cells in cold PBS, transfer the cells into conical FACS tubes, put them on ice and continue with step 62 **CRITICAL STEP** Cover the tubes with aluminum foil and keep them dark to prevent photo-bleaching.

Flow cytometry TIMING ~1 h

62 Add propidium iodide (PI) to each FACS tube shortly before the measurement with a final concentration of 2.5 µg/ml. Mix cell suspension gently **CRITICAL STEP** PI needs to be added to each tube independently, because it is potentially toxic by intercalating into the DNA in small amounts and harming replicating / dividing cells.

63 Perform measurements with the appropriate parameters (488 nm line argon ion laser, emission 530/40 (Alexa Fluor 488), 620/50 (PI)).

64 At the end export the datasets for data analysis.

Data analysis of flow cytometry experiments TIMING ~2 h

65 Import datasets, usually as fsc format, in analysis software, e.g. FCS Express and perform data analysis.

Timing

Steps 1-7, Cell culture: 1 h
Step 8-14, Preparation of cells for enzymatic digestion with glycosidase cocktails: 1 h
Step 15-18, Enzymatic digestion with glycosidase cocktails: ~ 6 $^{1}/_{2}$ h
Step 19-23, Preparation of cells for immuno-stainings: ~ 40 min
Step 24-39, Immuno-stainings with GAG recognizing antibodies: ~ 2 $^{1}/_{2}$ h
Step 40-50, Bioorthogonal labelling of SiaNAz using SPAAC: ~ 2 h
Step 51-61, Immuno-stainings with Gal β-1,4 recognizing *Maackia amurensis* agglutinin and *Arachis hypogaea* (peanut) agglutinin recognizing Gal β-1,3 GalNAc: ~ 2 h
Step 62-64, Flow cytometry: ~ 1 h
Step 65, Data analysis of flow cytometry experiments: ~ 2 h

Troubleshooting

Troubleshooting advice can be found in **Table 1.**

Step	Problem	Possible reason	Solution
18	Cells do not appear healthy during the incubation	Cells are sensitive to the treatment (low serum, long incubation, enzyme cocktails)	Prepare a time series, e.g. 2 h, 4 h, 6 h and monitor the cells carefully at each time point. Alternatively, reduce the glycosidase concentration for a certain enzyme or for the complete enzyme collection or increase the serum concentration. Primary cells such as activated T cells or primary fibroblasts but also cell lines that experienced additional stress e.g. in a transfection procedure prior to the glycosidase treatment may react to the slightest changes in culture conditions.
51-61	Glycan removal incomplete	Cells express different or additional glycan residues e.g. in response to cell culture environmental cues[28]	Prepare a separate staining procedure using an appropriate lectin or modified sugar for metabolic labeling. Some glycosidases do not digest the target sugar at all or not efficiently. β-1,4 Galactosidase will not digest β-1,4 coupled galactose if the adjacent sugar, N-acetyl-glycosamine (GlcNAc) comprises an 1-3 glycosidic bond to L-Fucose, commonly found in sialyl Lewis^{x} or Lewis^{x}.[25] We recommend to stain either with sialyl Lewis^{x} recognizing *Aleuria aurantia* agglutinin (AAA) or *Lotus tetragonolobus* agglutinin (LTL-A) which recognises Lewis^{x}.[26] Alternatively perform a bioorthogonal labelling assay using 6-azido-Fucose to determine the fucosylation status of the used cells.[27]

Anticipated Results

One should note that the glycocalyx composition is not uniform among cell types and hence expression levels of certain glycan chains show enormous variations. This was shown particularly for the glycosaminoglycans (GAGs) on MV3 and Molt-4 cells (Fig. 1a, b). When measuring the expression patterns of surface glycans on cells to approve the digestion of cell surface glycan chains and moieties, fluorescence signals measured by flow cytometry showed an efficient decrease in intensity. The digestion efficiency exceeded 90% for the applied glycosidases in most cases (Fig. 1, 2, blue and green curves/bars) while maintaining excellent cell viability as approved by staining with propidium iodide (PI) (Fig. 2b). The successful digestion of glycosaminoglycans and sialic acids (Fig. 1a, b) could be additionally validated by MAA and PNA (Fig. 2a, c, blue curves and bars). The increase of fluorescent signals is due to exposed non-reduced epitopes below the GAG layer and downstream of sialic acids that are accessible for the lectins. Furthermore, using PNA lectin, which recognizes an epitope different from the target sequences of the applied glycosidases approved the high purity of enzymes. As depicted in Fig. 2c, the PNA epitope Gal β-1,3 GalNAc was not digested, but rather more accessible for the lectins. This was even more pronounced after digestion with the β-1,4 galactosidase (blue and green curves/bars).

Figures

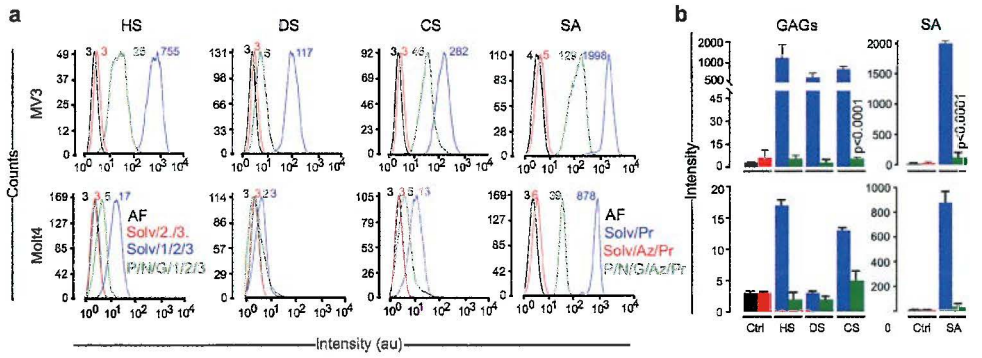

Figure 1

Enzymatic digestion and profiling of GAGs and sialic acids in MV3 and Molt-4 cells by flow cytometry. Cells were digested (step 15-18), stained with GAG recognizing antibodies (step 24-39) or bioorthogonal labeled using BCN for sialic acids (step 40-50) and measured by flow cytometry. (a) Flow cytometry histograms of one representative experiment; (b) Average intensities and standard errors (SEM) of three (MV3) and two (Molt-4) independent experiments. Statistical analysis was obtained by the non-paired, nonparametric Mann-Whitney t-test.

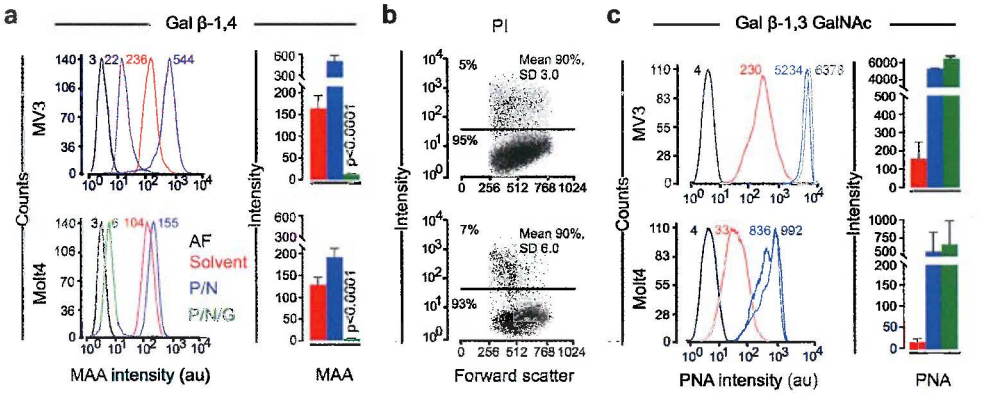

Figure 2

Enzymatic digestion and profiling of Gal β-1,4, Gal β-1,3 GalNAc and viability in MV3 and Molt-4 cells by flow cytometry. Cells were digested (step 15-18), stained with MAA or PNA lectin (step 51-61) or and measured by flow cytometry. (a) MAA flow cytometry histograms of one representative experiment and corresponding bar diagrams for average intensities and standard errors (SEM) of three independent experiments; (b) Scatterplot presenting the distribution of alive and dead cells after enzyme treatment and administration of propidium iodide (PI). Mean percentage of cell viability and standard deviations (SD) of three independent experiments. (c) PNA flow cytometry histograms of one representative experiment and corresponding bar diagrams for average intensities and standard errors (SEM) of two independent experiments. Statistical analysis was obtained by the non-paired, nonparametric Mann-Whitney t-test.

Acknowledgments

This work was supported by the Netherlands' Science Organization (NWO-VICI-918.11.626) and the Cancer Genomics Center, The Netherlands and further was supported by the European Research Council (617430-DEEPINSIGHT) and the Horizon 2020 consortium MULTIMOT (634107-2).

Author Contributions

S.S. and P.F. designed the study; S.S. designed, performed experiments; S.S. and P.F. analyzed the data. Both authors interpreted the data and wrote the article.

Competing Financial Interests

The authors declare no competing financial interests.

References

[1] R. Apweiler, H. Hermjakob, N. Sharon, *Biochim Biophys Acta* **1999**, *1473*, 4-8.

[2] aK. Ohtsubo, J. D. Marth, *Cell* **2006**, *126*, 855-867; bJ. R. Bishop, M. Schuksz, J. D. Esko, *Nature* **2007**, *446*, 1030-1037.

[3] R. S. Haltiwanger, J. B. Lowe, *Annual review of biochemistry* **2004**, *73*, 491-537.

[4] S. D. Rosen, *Annual review of immunology* **2004**, *22*, 129-156.

[5] aM. M. Fuster, J. D. Esko, *Nat Rev Cancer* **2005**, *5*, 526-542; bJ. W. Dennis, M. Granovsky, C. E. Warren, *Biochim Biophys Acta* **1999**, *1473*, 21-34; cH. Ghazarian, B. Idoni, S. B. Oppenheimer, *Acta Histochem* **2011**, *113*, 236-247.

[6] aD. F. Wyss, G. Wagner, *Curr Opin Biotechnol* **1996**, *7*, 409-416; bT. Muramatsu, *J Biochem* **2000**, *127*, 171-176; cJ. Roth, C. Zuber, S. Park, I. Jang, Y. Lee, K. G. Kysela, V. Le Fourn, R. Santimaria, B. Guhl, J. W. Cho, *Molecules and cells* **2010**, *30*, 497-506; dA. Larkin, B. Imperiali, *Biochemistry* **2011**, *50*, 4411-4426.

[7] aS. Hakomori, *Cancer Res* **1996**, *56*, 5309-5318; bT. Muramatsu, *Glycobiology* **1993**, *3*, 291-296.

[8] J. S. Rohrer, L. Basumallick, D. Hurum, *Biochemistry (Mosc)* **2013**, *78*, 697-709.

[9] H. Kalay, M. Ambrosini, P. H. van Berkel, P. W. Parren, Y. van Kooyk, J. J. Garcia Vallejo, *Anal Biochem* **2012**, *423*, 153-162.

[10] aA. Takatsuki, K. Arima, G. Tamura, *J Antibiot (Tokyo)* **1971**, *24*, 215-223; bA. Takatsuki, K. Kohno, G. Tamura, *Agricultural and Biological Chemistry* **2014**, *39*, 2089-2091; cJ. S. Tkacz, O. Lampen, *Biochem Biophys Res Commun* **1975**, *65*, 248-257.

[11] aC. H. Damsky, A. Levy-Benshimol, C. A. Buck, L. Warren, *Exp Cell Res* **1979**, *119*, 1-13; bD. Duksin, P. Bornstein, *Proc Natl Acad Sci U S A* **1977**, *74*, 3433-3437; cK. Olden, R. M. Pratt, K. M. Yamada, *Int J Cancer* **1979**, *24*, 60-66; dK. Olden, R. M. Pratt, C. Jaworski, K. M. Yamada, *Proc Natl Acad Sci U S A* **1979**, *76*, 791-795.

[12] S. B. Atienza-Samols, P. R. Pine, M. I. Sherman, *Dev Biol* **1980**, *79*, 19-32.

[13] aM. Sobue, H. Habuchi, K. Ito, H. Yonekura, K. Oguri, K. Sakurai, S. Kamohara, Y. Ueno, R. Noyori, S. Suzuki, *Biochemical Journal* **1987**, *241*, 591; bS. F. Kuan, J. C. Byrd, C. Basbaum, Y. S. Kim, *J Biol Chem* **1989**, *264*, 19271-19277.

[14] aI. Brockhausen, *Frontiers in immunology* **2014**, *5*, 492; bL. L. Lairson, B. Henrissat, G. J. Davies, S. G. Withers, *Annual review of biochemistry* **2008**, *77*, 521-555.

[15] D. Schomburg, Salzmann, M., in *Springer International Publishing, Vol. 4*, **1991**.

[16] M. Bektas, D. S. Rubenstein, *J Biomed Res* **2011**, *25*, 227-236.

[17] aJ. F. Morgan, H. J. Morton, R. C. Parker, *Proc Soc Exp Biol Med* **1950**, *73*, 1-8; bH. Otsuka, *J Cell Sci* **1972**, *10*, 137-152; cT. Kimura, K. Miyazaki, K. Mashima, J. Yamashita, T. Horio, T. Kakuno, *J Biochem* **1991**, *110*, 423-428; dO. Barta, R. A. Nelson, Jr., C. Y. Kuo, *Immunological communications* **1976**, *5*, 75-86.

[18] M. Kosuge, T. Takeuchi, I. Nakase, A. T. Jones, S. Futaki, *Bioconjugate chemistry* **2008**, *19*, 656-664.

[19] M. Hricovini, *Curr Med Chem* **2004**, *11*, 2565-2583.

[20] aT. H. van Kuppevelt, M. A. Dennissen, W. J. van Venrooij, R. M. Hoet, J. H. Veerkamp, *The Journal of biological chemistry* **1998**, *273*, 12960-12966; bN. C. Smits, J. F. Lensen, T. J. Wijnhoven, G. B. Ten Dam, G. J. Jenniskens, T. H. van Kuppevelt, *Methods Enzymol* **2006**, *416*, 61-87.

[21] J. F. Lensen, T. J. Wijnhoven, L. H. Kuik, E. M. Versteeg, T. Hafmans, A. L. Rops, M. S. Pavao, J. van der Vlag, L. P. van den Heuvel, J. H. Berden, T. H. van Kuppevelt, *Matrix Biol* **2006**, *25*, 457-461.

[22] T. F. Smetsers, E. M. van de Westerlo, G. B. ten Dam, I. M. Overes, J. Schalkwijk, G. N. van Muijen, T. H. van Kuppevelt, *J Invest Dermatol* **2004**, *122*, 707-716.

[23] G. N. van Muijen, K. F. Jansen, I. M. Cornelissen, D. F. Smeets, J. L. Beck, D. J. Ruiter, *Int J Cancer* **1991**, *48*, 85-91.

[24] J. Dommerholt, S. Schmidt, R. Temming, L. J. A. Hendriks, F. P. J. T. Rutjes, J. C. M. van Hest, D. J. Lefeber, P. Friedl, F. L. van Delft, *Angewandte Chemie-International Edition* **2010**, *49*, 9422-9425.

[25] S. Sakamoto, T. Watanabe, T. Tokumaru, H. Takagi, H. Nakazato, K. O. Lloyd, *Cancer Res* **1989**, *49*, 745-752.

[26] T. Haselhorst, T. Weimar, T. Peters, *J Am Chem Soc* **2001**, *123*, 10705-10714.

[27] aS. T. Laughlin, C. R. Bertozzi, *Nat Protoc* **2007**, *2*, 2930-2944; bD. Rabuka, S. C. Hubbard, S. T. Laughlin, S. P. Argade, C. R. Bertozzi, *J Am Chem Soc* **2006**, *128*, 12078-12079.

"I liked the lab culture: the freedom, flexibility, challenges, and the late-night experimental marathons."

Carolyn Bertozzi

CHAPTER 5

Glycocalyx-mediated Integrin-independent Amoeboid Cell Migration

Nature (in revision)

Samuel Schmidt[1,2], Bettina Weigelin[1,4], Neda Daryab[3], Joost te Riet[1], Mariska te-Lindert[1], Barbara Lelli[8], Lorenz Rognoni[7], Marina Krause-Vortmeyer[1], Luisa Bracci[8,9], Kay-Eberhard Gottschalk[6,7], Stephan Kissler[10], Jack Fransen[1], Martin J. Humphries[5] & Peter Friedl[1,3,4]

[1] Microscopical Imaging of the Cell, [2] Biochemistry of Integrated Systems, RIMLS, Radboud University Medical Centre, P.O. Box 9101, 6500 HB Nijmegen, The Netherlands; [3] Rudolf Virchow Center for Experimental Biomedicine and Department of Dermatology, University of Würzburg, Josef-Schneider-Str. [2], 97080 Würzburg, Germany; [4] The University of Texas MD Anderson Cancer Center, Houston, Texas, USA; [5] Wellcome Trust Centre for Cell-Matrix Research, Faculty of Life Sciences, Univ. of Manchester, Manchester M13 9PT, UK; [6] Institute for Experimental Physics, University of Ulm, 89069 Ulm, Germany [7] Institute for Applied Physics, Ludwig Maximilians University, 80799 München, Germany; [8] Department of Medical Biotechnologies, University of Siena, 53100 Siena, Italy; [9] Laboratorio di Patologia Clinica, Azienda Ospedaliera Universitaria Senese, 53100 Siena, Italy; [10] Joslin Diabetes Center, Harvard University, MA 02215 Boston, Massachusetts, USA

Abstract

The migration of cells through the extracellular matrix (ECM) of tissues and organs critically contributes to morphogenesis, tissue repair and, in its deregulated form, cancer invasion and metastasis. Adhesion molecules of the integrin family are the dominant cell system to bind extracellular matrix proteins and generate force for migration[1,2]. In addition, experimental models which disable integrin function have revealed alternative low-adhesive types of mechanotransduction that can sustain cell movement[3-6], however the organization of integrin-independent adhesion sites and their mechanisms for force coupling remain unclear. Using multi-enzymatic digestion of sugar moieties on the surface of mesenchymal cells after interference with integrin function as well as on leukocytes that intrinsically migrate integrin-independently, we show that the surface glycocalyx generates cell attachment to ECM ligands in the 100-500 pN force range and mediates amoeboid migration in 3D ECM-based models in vitro and in vivo. By combining glycan removal with 3D confocal and electron microscopy, identified glycan-based adhesions consist of actin-rich complex-shaped imprint-like membrane appositions along ECM topologies associated with filopods and bleb-like interactions. The data suggest that, by shape-adaptive scaffolding combined with generic stickiness, the glycocalyx mediates multivalent nanotopologies between the cell surface and ECM to enable mechanocoupling and cell migration. Because integrin- and glycan-mediated mechanotransduction occur in parallel modulation of each adhesion system may adjust cell-matrix interaction and migration programs, including the mesenchymal-to-amoeboid transition.

To mediate cell migration across surfaces, integrins form transient focalized actin-containing adhesion and signalling complexes that provide mechanotransduction as well as intracellular signals that control cytoskeletal organization, cell shape, and gene expression[1,2,7-10]. In cancer metastasis, integrins mediate cell invasion and represent candidate targets for pharmacological interference[8,11-13]. In contrast to 2D migration models, interference with β1 integrin function in 3D models, where cells migrate through substrate of complex geometry and confinement, provides only incomplete inhibition of migration, depending on the cell model.[6,14-17] We thus aimed to identify the cellular and molecular mechanisms of integrin-independent cell-matrix interaction, force generation, and migration within interstitial tissue *in vitro* and *in vivo*.

Fibrillar collagen is the predominant scaffold in mammalian tissues recognized with high affinity by integrins α1β1, α2β1, and α11β1, and weakly by αVβ3[10,18]. Invasive MV3 melanoma cells express β1 and aV but lack all other integrin β-chains (Extended Data Fig. 1a, h). MV3 cells utilize α2β1 integrins for efficient migration within 3D collagen lattices[9] and for collagen matrix remodeling[19,20]. The majority of MV3 cells is elongated and spindle-shaped during migration at speeds similar to *in vivo* movement of mesenchymal cells[20], yet a fraction (10-20 %) fails to elongate during migration (Extended Data Fig. 1b, dashed box). Graded interference with β1 integrins either by adhesion-perturbing mAb 4B4 at concentrations saturating the epitope up to 90% (Extended Data Fig. 1c-e) or by stable β1/β3 integrin downregulation with an efficiency between 93% (Extended Data Fig. 1f, westernblot) and 99% demonstrated by antibody competition followed by flow cytometry (Extended Data Fig. 1g) reduced migration rates but failed to cause immobilization, so that most cells continued to move at lower speed and partially reduced directional persistence (Fig. 1a, Extended Data Fig. 2a, b). Interference with β1 integrins further caused changes in how the cells were moving. First, the spindle-shaped, elongated morphology was abandoned and an ellipsoid shape with multiple dynamic blebs and few filopodia at the surface was gained (Fig. 1b). Second, focalized β1 integrin and filamentous actin at sites of interaction with collagen fibres converted towards cortical diffuse distribution when β1 integrins were inhibited using mAb 4B4 (Fig. 1b, arrowheads). Third, interference with β1 integrin impaired the ability to contract free-floating collagen lattices, which is a measure for traction force in 3D ECM (Extended Data Fig. 2c). Abrogated matrix contraction and cell elongation were concurrent, suggesting that impaired traction force and cell rounding during migration were coupled.

These findings support concepts that mammalian cells maintain different molecular motility programs[12,21]. Mesenchymal migration of fibroblasts and some cancer cell types results from elongated spindle-shaped morphology, focalized adhesion sites, and high traction force towards the ECM[7,9,12]. Conversely, amoeboid migration displayed by leukocytes and other cells generates weak mechanotransduction by means of poorly focalized adhesion sites and actin cytoskeleton[6,14,21-23].

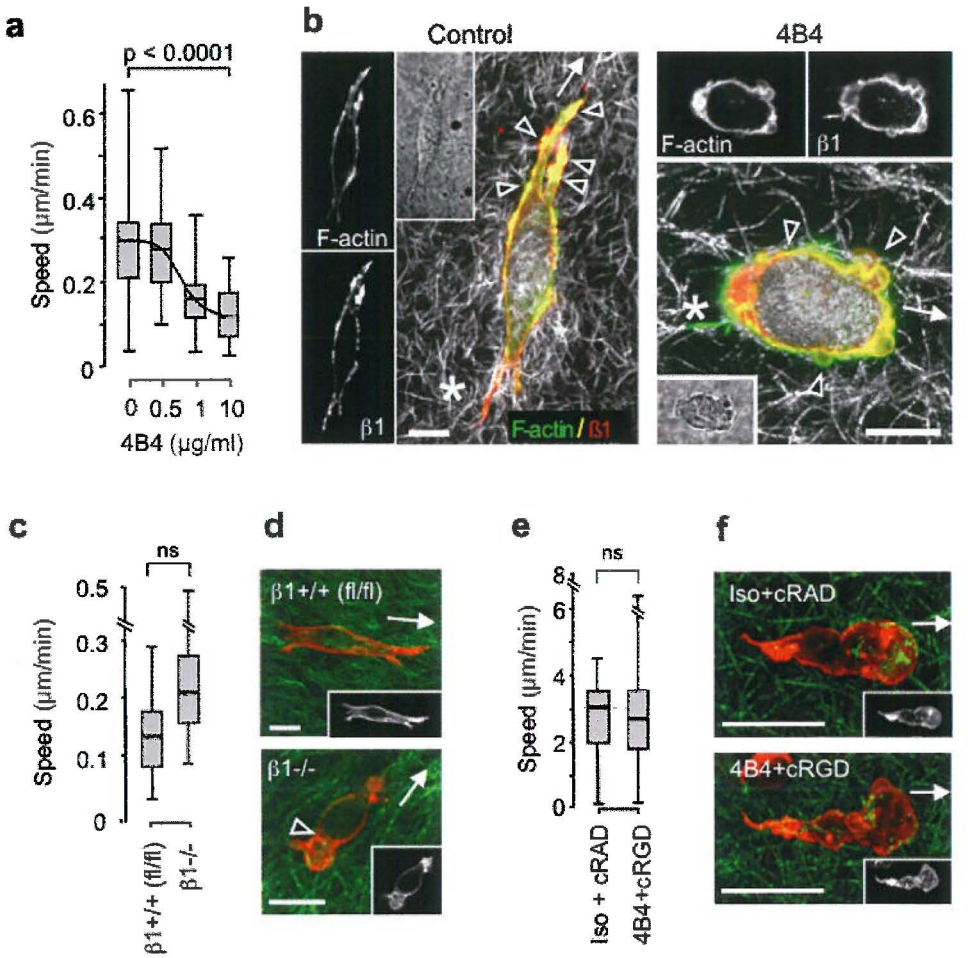

Fig. 1 Conversion to amoeboid migration in mesenchymal tumor cells and fibroblasts after interference with integrins.

(a-c) Mesenchymal-amoeboid transition in MV3 melanoma cells after interference with β1 integrin function using anti-β1 integrin mAb 4B4. (a) Speed change with increasing doses of mAb 4B4. Data show the population speed obtained by single cell tracking for an 18h observation period (120 cells, 3 independent experiments). (b) Cell morphology, F-actin and β1 integrin distribution (arrowheads) for control and mAb 4B4 treatment condition. Arrows, direction of migration, based on retraction fibres from the cell rear (asterisks). (c-d) Mesenchymal-amoeboid transition in murine embryonic fibroblasts after interference with β1 integrin function. Amoeboid migration in β1-deficient embryonic murine fibroblasts. (c) Migration speed and (d) morphology of wild-type and β1-/- MEFs. Bars (b), 10 µm. F-actin (red, grey insets), collagen fibres (green; reflection), and constriction rings (arrowheads). Bars (d), 100 µm. (e-f) Constitutive amoeboid migration in human Molt-4 leukemia cells in control cells and after interference with β1 and β3 integrin function using mAb 4B4 and cyclic RGD (cRGD). Migration speed (e) and morphology (f) of Molt-4 control cells and in the presence of β1 and cRGD. F-actin (red, grey insets), collagen fibres (green; reflection) and direction of migration (arrows). Bars, 20 µm.

β1-/- MEFs employed a rounded amoeboid migration type with increased speed, compared with β1+/+(fl/fl) MEFs (Fig. 1c, d), slightly diminished directional persistence (Extended Data Fig. 2d, e) and impaired ability to generate traction force in 3D ECM (Extended Data Fig. 2f). This amoeboid phenotype in β1-/- MEFs was reversible after reintroduction of β1 integrin (Extended Data Fig. 2g, h), suggesting amoeboid-mesenchymal transitions as a direct function of β1 levels.

As confirmatory model, integrin-independent migration of human T-leukemia cells (Molt-4) was equally amoeboid with rounded shape and an elongated uropod in both, control cells and interfering with β1 and aV integrins using mAb 4B4 and cRGD (Fig. 1f, Extended Data Fig. 2i, j) with similar migration speeds (Fig. 1e).

These results confirm for 3D fibrillar collagen that eukaryotic cells posses largely integrin-independent interaction mechanisms to maintain migration. The expression of a set of alternative collagen receptors[24-29], that might compensate the loss of integrin-mediated adhesion and migration was measured in MV3, including syndecan-4 (SDC-4), discoidin domain receptors (DDR) 1 and 2 and proteoglycan CD44. DDR-1 and -2 or SDC-4 were not expressed by MV3 cells (Extended data Fig.3a) and CD44 was expressed, however CD44 perturbing antibody did not affect the migration of MV3 cells in 3D fibrillar collagen[9] (Extended data Fig.3b), excluding these known collagen receptors as to mediate amoeboid movement in these cells.

In contrast to mammalian cells which express integrins together with ECM proteins, the lower eukaryote *Dictyostelium discoideum* is an amoeba without known collagen receptor[30-33], which interacts with surrounding substrates via a cellulose-based surface coat („slime")[34]. As a 'natural' model of collagen receptor-independent movement, *D. discoideum* efficiently migrates into and within 3D collagen lattices (Extended data Fig.3c,d). We thus hypothesized that non-specific low-affinity interaction with collagen fibres could result from surface glycans[35-37] or even non-adhesive cell extensions and shape change[38].

In mammalian cells, the glycocalyx forms a thick, polar layer[39,40], which is composed of various classes of glycoconjugates, including glycosaminoglycan (GAG) chains of the proteoglycans heparan sulfate, chondroitin sulfate, dermatan sulfate as well as N- and O- linked glycans of the glycoproteins and glycolipids coupled to the cell membrane (Extended data Fig. 5a). Highly sulfated glycoconjugate side chains of proteoglycans are known to interact with ECM components, including fibrillar collagen[35,36,41]. MV3 cells expressed an about 200 nm thick glycan layer at the cell surface (Fig. 2a, b) but depending on the cell type the glycocalyx may reach hundreds of nanometers up to several micrometers in thickness[42-45].

To address the role of surface glycans in cell migration, protein- and lipid-linked glycoconjugates were enzymatically removed from the surface of live cells by using a cocktail of glycosidases, including GAG digesting enzymes hyaluronidase, heparitinase, chondoritinase, neuraminidase and galactosidase recognizing β-1,4 coupled galactose

residues in N- and O-linked glycans and glycolipids. The enzymatic digestion of GAG chains lowered heparan- and chondroitin sulfate by ~98% and dermatan sulfate by ~95% (Extended data Fig. 5g), which together with sialic acid removal by neuraminidase resulted in an exposure of subjacent β-1,4 coupled galactose residues (Fig. 2d, Extended data Fig. 5 d, P/N). Additional treatment with β 1-4 galactosidase removed β 1-4 coupled galactose by >90% in MV3 β1/β3KD, >98% MEF β1-/- and >94% Molt-4 cells without negative impact on cell viability (Extended data Fig. 5 d). The loss of cell surface β-1,4 galactose was maintained for at least 6-9h (MV3), 24-92 h (MEF β1-/-) and 5-6 h (Molt-4) followed by a stepwise recovery (Extended data Fig. 5 e, f).

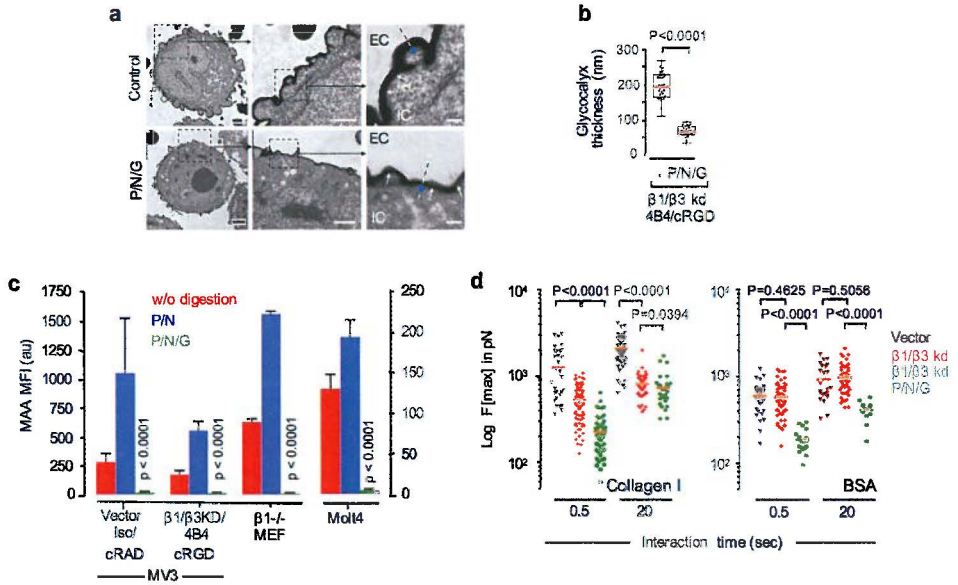

Fig. 2. Enzymatic digestion of the glycocalyx to probe glycan-mediated cell binding to collagen.

(a) Transmission electron microscopy and quantitative image densitometry (b) of the glycocalyx thickness. MV3 β1β3KD cells before and after glycan removal with P/N/G glycosidase cocktail. Detection of surface glycans with Ruthenium red. Bars, 1 µm (left), 1 µm (middle), 200 nm (right). (a) Blue dot, position of the plasma membrane. Dashed lines, cross-sections perpendicular to the plasma membrane used for image analysis from 10 cells of 2 independent experiments (see densitometry profiles in Extended data Fig. 5b). P values, non-paired Mann-Whitney test for independent means. (c) Population-based analysis of digestion efficacy of glycans moities on the surface of living MV3, β1-/- Mef and Molt-4 cells. β-1,4 galactose was detected with Maackia amurensis agglutinin and fluorescence intensity was assessed by flow cytometry (means and SD from 3 independent experiments). (d) Live-cell atomic force microscopy and spectroscopy. Interaction forces of MV3 control cells and cell after β1/β3 KD and additional treatment with P/N/G glycosidase treatment to a fibrillar collagen I surface after 0.5 s or 20 s interaction time. Pooled median values of maximum retraction forces shown as Log F_{max} for 21 (Collagen I) and 15 cells (BSA) from 3 independent experiments. Data sets were compared using ANOVA followed by post-hoc Bonferroni correction. Bar, 20µm.

To verify that the digestion procedure was non-toxic and further did not compromise the basic cell function and migration ability, β1/β3 integrin-expressing MV3 control cells treated with GAG, sialic acid and β-1,4 galactose digesting enzymes (P/N/G) together with isotype and cRAD showed normal baseline migration, mesenchymal phenotype, and focalized cell-matrix interactions (Fig. 3a-d, Fig. 4 a, b, Extended data Fig. 8a, 8 I, II). Likewise, β1-/- but β3 integrin-expressing MEFs developed similar morphological phenotypes and migration speeds after treatment with glycosidases when compared with β1+/+(fl/fl) MEFs (Fig. 1c, Fig. 3d, Fig. 4a, b). These data exclude even subtle cell perturbation by the glycosidase treatment and further show that the glycocalyx has no detectable contribution to mesenchymal migration.

However, when glycan removal was combined with interference of integrin expression and function, cell migration and persistence were severely compromised across the studied cell models. Cells were immobilized and completely rounded, despite ongoing cytoskeletal activity ("running on the spot"), for time periods of 6-9h in MV3 (Fig. 3a-c, Extended data Fig. 8a, b, e), at least 24h in β1-/- MEFs (Fig. 3d, Extended data Fig. 8a, c) and for 5-6 h in Molt-4 cells (Fig. 3e, Extended Data Fig. 7a, d, f). The subsequent stepwise recovery of migration was consistent with the re-onset of β-1,4 galactose expression (Extended data Fig. 5 e, f). Strikingly, the enzymatic removal of GAGs and neuraminic acids alone (P/N) did not influence migration of MV3 β1/β3KD cells significantly (Fig. 3c), whereas the migration of Molt-4 cells were partly compromised (Fig. 3e, P/N), indicating a more pronounced impact of changes in the glycosylation of T cells[46], e.g. in sialylation on cell migration[47] compared with MV3 cells.

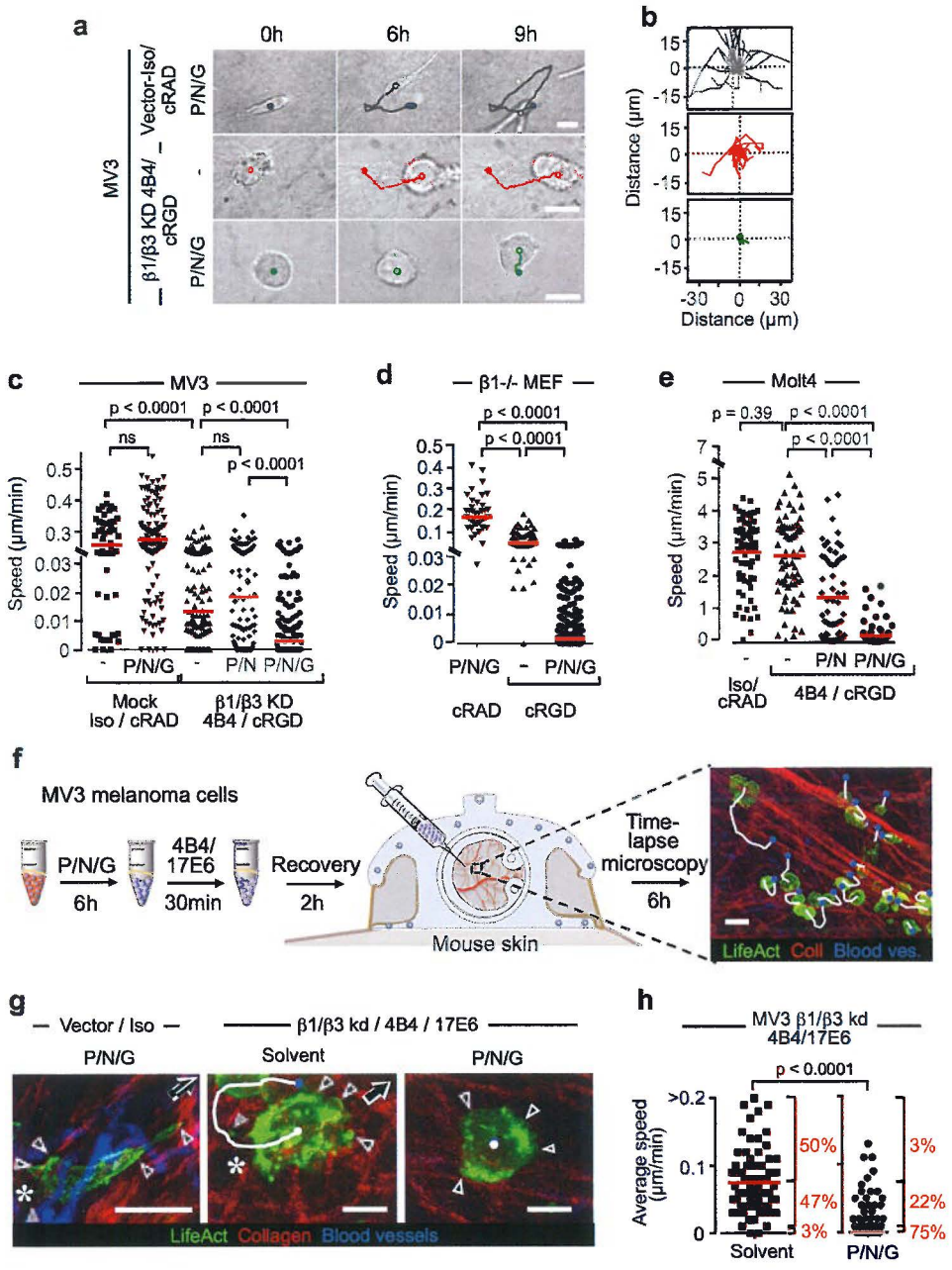
a
0h
6h
9h
MV3
Vector-Iso/ cRAD
β1/β3 KD 4B4/ cRGD
P/N/G
b
Distance (µm)
Distance (µm)
c
MV3
p < 0.0001
p < 0.0001
ns
ns
p < 0.0001
Speed (µm/min)
P/N/G
P/N P/N/G
Mock Iso / cRAD
β1/β3 KD 4B4 / cRGD
d
β1-/- MEF
p < 0.0001
p < 0.0001
Speed (µm/min)
P/N/G
P/N/G
cRAD
cRGD
e
Molt4
p = 0.39
p < 0.0001
p < 0.0001
Speed (µm/min)
P/N P/N/G
Iso/ cRAD
4B4 / cRGD
f
MV3 melanoma cells
P/N/G
6h
4B4/ 17E6
30min
Recovery
2h
Mouse skin
Time-lapse microscopy
6h
LifeAct Coll Blood ves.
g
Vector / Iso
β1/β3 kd / 4B4 / 17E6
P/N/G
Solvent
P/N/G
LifeAct Collagen Blood vessels
h
MV3 β1/β3 kd 4B4/17E6
p < 0.0001
Average speed (µm/min)
50%
47%
3%
3%
22%
75%
Solvent
P/N/G

Fig. 3. Surface-glycan dependent cell migration in vitro and in vivo.

(a-e) MV3 melanoma cells, murine β1-/- embryonic fibroblasts and Molt-4 T lymphoma cells were subjected to enzymatic surface-glycan removal using P/N/G followed by analysis of migration rates in 3D collagen lattices in vitro. (a) Time-lapse sequences (bright-field microscopy), (b) migration paths and (c) single-cell speed distributions of MV3 vector control and β1/β3KD cells in the presence of mAb 4B4 and cRGD for control conditions or after glycan removal by P/N or P/N/G. Glycan-dependent migration of (d) β1 -/- MEF (e) Molt-4 cells. (f) Workflow of orthotopic injection into the collagen-rich deep mouse dermis followed by intravital time-lapse microscopy of LiveAct-expressing MV3 vector control and MV3 β1/β3KD cells without or after glycan removal. (g) Zooms showing example cells with typical morphology. White lines represent migration paths after 8-9h. Arrows, direction of migration. Grey arrowhead, microparticle released from the cell rear (Asterisk). (g, I) Bar, 20 µm, (g, II-III) Bar, 10µm. (h) Migration speed of MV3 β1/β3KD cells additionally treated with mAb 4B4 and 17E6. Data represent 30 cells from 3 independent experiments.

As in 3D collagen *in vitro*, MV3 β1/β3KD cells that were additionally pretreated with integrin-blocking mAbs 4B4 and 17E6 injected into the deep mouse dermis and monitored by intravital multiphoton microscopy developed blebbing amoeboid movement (Fig. 3f, g; Extended data Fig. 9 III, IV), whereas MV3 vector control cells retained spindle-shaped morphology (Fig. 3g, Extended data Fig. 9 I, II). This shows that lowering adhesion in otherwise mesenchymal cells yields similar amoeboid movement in different 3D environments, including fabricated microfluidic channels[48] or cell confiner[5], 3D fibrillar collagen and complex connective tissue. After glycan-removal, cells underwent complete rounding with near-complete migration arrest despite oscillatory shape change (Fig. 3g, h, Extended data Fig. 9 V, VI). Thus, an intact surface glycocalyx is required to maintain amoeboid migration in collagen-rich tissue when integrin functions are perturbed.

To directly address whether the glycocalyx might support cell-ECM adhesion, atomic force microscopy (AFM) was used to probe the binding of synthetic glycans as well as of intact cells to fibrillar collagen. The tip of the cantilever was functionalized with simple-structured amylose and cellulose polymers that lack modifications such as sulfation or acetylation and the forces to break the bonds upon cantilever retraction were recorded (Extended data Fig. 7a). With increasing amylose density on the cantilever, the binding to collagen was dose-dependently strengthened (Extended data Fig. 7b). Besides the majority of background-level, weak bonds (40-120 pN), amylose or cellulose prompted subsets of stronger bonds with unbinding forces in the high pN range (Extended data Fig.4c-e). Similar concentration dependent increase in binding affinities between glycan and collagen fibers was detected when amylose polymer binding to immobilized collagen was probed by surface plasmon resonance (SPR) (Extended data Fig. 7f). After binding, affinity bonds were stable for >15 min at any amylose concentration that were disrupted by the wash-out during the regeneration phase (Extended data Fig. 7g, h). Thus, multivalent polysaccharides in the absence of additional positive or negative side chain charges provide significant interaction strength to fibrillar collagen.

To determine binding forces between the glycocalyx and collagen I, AFM-based single-cell force spectrocopy (SCFS) was exploited. A living MV3 cell was mounted to the tip of a cantilever and binding forces between cell and substrate were recorded upon cantilever

retraction (Extended data Fig. 6a). To determine the appropriate interaction times that would discriminate fast receptor-independent from slow receptor-dependent bond formation, interaction times from 0.5 s up to 20 s with a collagen I matrix were used. In control cells with integrins expressed, short interaction times (0.5 s) enabled variable interaction forces from 400 pN up to 2 nN (Fig. 2d, Extended data Fig. 6e), indicating the coexistence of low (400 pN - 800 pN) and high-avidity interactions (above 800 pN) when adhesion is initiated[49,50]. Multiple single rupture events (jump events), i.e. the smallest detectable force units, reached 200 pN which represent multiple-bond ruptures already after short contact times in the presence of integrins (Extended data Fig. 6c, d). After 20s contact time, binding forces were strongly increased and retraction curves showed a sharp peak, that can be assigned to multiple single-integrin binding events[51,52] to collagen I at the extracellular binding sites and to actin at the cytoplasmatic tail as well as early cooperative integrin engagement. Weak interactions (<1 nN) were largely abandoned (Fig. 2d, Extended data Fig. 6e), indicating time-dependent cooperation and reinforcement of adhesion[50]. After interference with integrins cells lacked strong binding events but retained peak forces that reached 500 pN and included small jump events (<50 pN) (Fig. 2c,d, Extended data Fig. 6d-f). The broadened retraction profile after 20s of contact (Fig. 2d, Extended data Fig. 6e, f) might result from time-dependent adhesion events, such as intercalation of collagen fibers between plasma membrane blebs or engagement of slower but weak adhesion systems. Additional glycosidase treatment resulted in a substantial reduction of both peak force and a shift to single-bond rupture events of <30 pN (Fig. 2c, d, Extended data Fig. 6d-f). To rule out intermittent parameters, such as receptor activation, cytoskeletal reinforcement or epitope saturation due to receptor shedding, repeated probing conditions were verified. The results clearly show similar magnitudes of generated forces at each binding event and equal force distribution between a cell and collagen (Extended data Fig. 6b, e lower panel). The loss of binding forces after glycosidase treatment was reverted by increasing the contact time (Fig. 2d, Extended data Fig. 6e, f), suggesting maturation-dependent additional binding events. The glycocalyx is thus suited to support very fast binding to collagen in the pN range when integrin function is marginalized.

To test, whether besides collagen, any substrate would be bound by the glycocalyx, protein-inert BSA was used as non-specific counterpart ligand. The results clearly show that integrin binding was lost but glycan binding retained, with similar forces compared to collagen binding (Fig. 2d, Extended data Fig. 6e, g). Glycosidase treatment of integrin knockdown cells resulted in a similar loss of unspecific adhesion to BSA as it was shown for collagen I for short contact times (Fig. 2d, Extended data Fig. 6e, g), which assigns the residual forces to glycans.

Thus, the data indicate that the glycocalyx functions as an independent low-level adhesion system to a broad range of substrates.

To map the transitions after limiting integrin availability, as a basis for identifying the ECM-binding contact structures enabled/mediated by surface glycans towards collagen fibrils, cell morphologies were classified as mesenchymal (type I), amoeboid-moving with actin-rich protrusions and well-developed filopodia (IIa), polarized surface blebs (IIb), or an elongated uropod (IIc), or non-polarized, concentric with microruffles (IIIa) or microblebs (IIIb) (Fig. 4a). MV3 cells and MEFs developed a mesenchymal migrating phenotype, which converted to bleb-like (MV3 and Molt-4 cells) or filopodal (β1-/- MEFs) amoeboid movement with integrin function impaired but surface glycans available. After interference with both integrins and surface glycans only small subsets of bleb-like (MV3 cells) and a mix of filopodal and blebbing amoeboid movement (MEF cells) were retained. Molt-4 cells were constitutively amoeboid, dominated by an elongated uropod with occasional blebs (Fig. 4b) and interference with integrin and surface glycans resulted in only a small subset of filopodal, blebbing and uropodal amoeboid migration phenotype (Fig. 4b, asterisks indicate amoeboid subsets). Thus, when integrin-mediated force generation is disabled, filopod-like protrusions and blebs are retained to engage with extracellular structures.

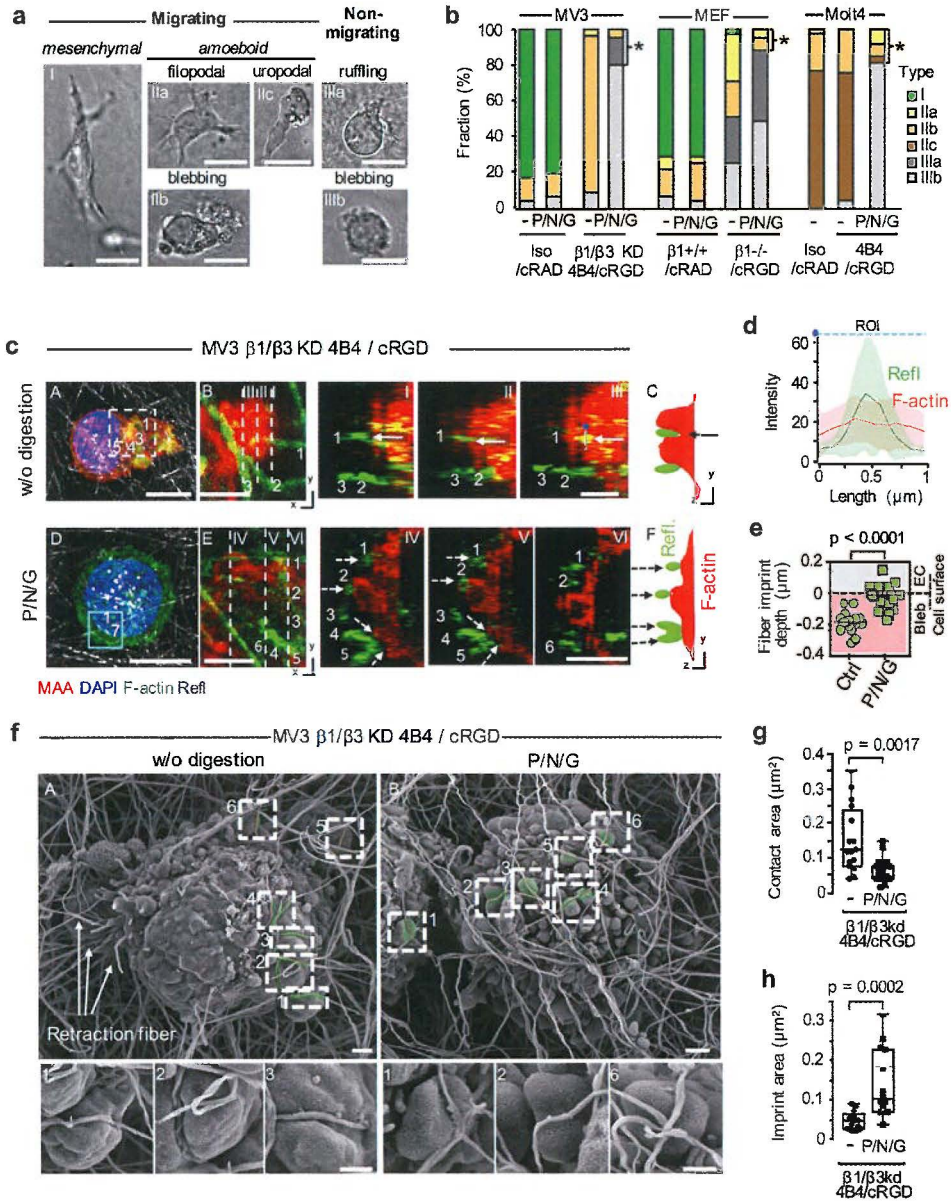
a
Migrating
Non-migrating
mesenchymal
amoeboid
filopodal
uropodal
ruffling
blebbing
blebbing
b
MV3
MEF
Moit4
Fraction (%)
Type
I
IIa
IIb
IIc
IIIa
IIIb
- P/N/G
- P/N/G
- P/N/G
- P/N/G
- P/N/G
Iso /cRAD
β1/β3 KD 4B4/cRGD
β1+/+ /cRAD
β1-/- /cRGD
Iso /cRAD
4B4 /cRGD
c
MV3 β1/β3 KD 4B4 / cRGD
w/o digestion
P/N/G
MAA DAPI F-actin Refl
d
ROI
Refl
F-actin
Intensity
Length (μm)
e
p < 0.0001
Fiber imprint depth (μm)
Bleb
EC
Cell surface
Ctrl
P/N/G
f
MV3 β1/β3 KD 4B4 / cRGD
w/o digestion
P/N/G
Retraction fiber
g
p = 0.0017
Contact area (μm²)
- P/N/G
β1/β3kd 4B4/cRGD
h
p = 0.0002
Imprint area (μm²)
- P/N/G
β1/β3kd 4B4/cRGD

Fig 4. Organization of glycan-dependent cell-matrix interactions.

(a) Morphological phenotypes in migrating and non-migrating cells according to shape and polarity. MV3 cells were fixed after 2h of culture in 3D collagen lattices. (b) Phenotype frequencies in MV3, MEF and Molt-4 cells after interference with integrins and surface glycans (97 (MV3), 100 (MEF), 92 (Molt-4) cells from 3 independent experiments). Asterisks, amoeboid migrating subsets. Bars, 20µm. (c) Maackia amurensis agglutinin (MAA) staining of cell surface β-1,4 galactose residues (red signal), F-actin (green signal), collagen I (reflection) and (c: B, E) F-actin (red signal), collagen I (green reflection) in MV3 β1/β3KD control cell (c, A-C) and after P/N/G digestion (c, D-F). Cells were embedded in 3D collagen and fixed after 90 min. Because of the resolution limit of ~200 nm, these confocal reconstructions do not resolve the nanometer-scale exclusion of F-actin by imprinting fibers. (c, A,D) XY and (c, B,E) XZ projections of F-actin and confocal reflection (fiber) signal from serial positions indicated in (c, B,E; dashed lines). (c, C,F) Schematic representation of the YZ projections shown in I-III and IV-VI. Arrows, collagen fibers located with overlap to glycan-enriched blebs. Dashed arrows, collagen fibers laterally intercalating between blebs. Numbers indicate collagen fibers engaged with the cell surface. (d) Averaged densitometry curves of a bleb cross section with F-actin residues (red, 35 curves) and collagen I (green, 26 curves) and (e) calculation of the fiber imprint depth based on 17 bleb cross sections from 3 independent experiments. (f) Scanning electron microscopy and quantification of the area of membrane-collagen fiber contact (g) and imprint area (h) of MV3 β1/β3KD cells before and after treatement with P/N/G glycosidase cocktail. MV3 cells were fixed after 2h of culture in 3D collagen lattices. (f: A, B) Regions of interest (numbered dashed boxes) depicted as representative zooms of the contact area between cell membrane (green area) and collagen fibers (red), used for calculating the 3D cell-surface/collagen fiber contact (g) and peri-imprint area (h). Bars, 10 µm (c: A, D), 2 µm (c: B, E), 1 µm (f: A, B), 0.5 µm (f: A, B ROIs). Statistical analysis was obtained using the non-paired Mann-Whitney test.

To define the adhesion topologies when engaging with collagen fibers, we performed 3D confocal microscopy in fixed and live cells after integrin targeting and simultaneously detected the surface glycocalyx by staining with fluorescent lectins ConA and MAA. MV3 β1/β3KD (Fig. 4c, Extended data Fig. 10a) and Molt-4 cells (Extended data Fig. 10e) formed actin-rich filopodal or bleb-like protrusions engaging with collagen fibers which both retained a linear glycan-collagen fiber interface. Whereas filopodia of MEF cells formed a defined longitudinal interface with collagen fibers which is resolved by diffraction-limited microscopy (Extended Data Fig. 10.2a-c), bleb-collagen fiber contacts were topologically complex and more varied. In MV3 cells individual blebs contained filamentous actin and uniform, non-focalized galactosyl-rich surface overlapped with the reflection signal from collagen fibers in xyz direction (Fig. 4c,d, Extended data Fig. 10a, b, e-g) with stretches from sequential sections located near-inside the bleb and depth overlap ranging from few to 200 nm or more (Fig. 4e, Extended data Fig. 10c, d, h). Both, galactosyl-residues and overlap between bleb and fiber were lost after glycan removal (Fig. 4c, e, Extended data Fig. 10e, h), implicating the glycocalyx in providing particularly tight apposition between surface blebs and fibrils with "imprint-like" topology. Bleb-rich contact types persisted as abortive, non-polarized structures in immobilized cells, which differs from apoptotic cell detachment by an intact nuclear morphology (Fig. 4c, Extended data Fig. 10a, e) and uncompromised viability after cell retrieval from the collagen lattice. To resolve the 3D organization of glycan-mediated contacts, scanning electron microscopy was used for cells located inside the collagen after exposure by mechanically ripping the gels apart at mid-level. Blebs located towards the polar front of MV3 β1/β3KD

cells underwent a complex-shaped, indentation in direct contact with a collagen fiber, forming a "grip-like" tight interphase of complex geometry with typical half-cylindrical shape and a variable contact area ranging from 0.05 up to 0.4 μm^2 as a function of bleb size, fiber calibre and indentation depth (Fig. 4f, A, Extended data Fig. 11a, A, B 4-6). These interactions typically withstood mechanical disruption of the collagen lattice during sample preparation, but occasional disruptions of the bond with displaced collagen fibril uncovered the half-cylindrical grove inside the bleb matching the calibre of the collagen fibre (Extended data Fig. 11a, B, C). This indicates very tight "grip-like" apposition of the cell surface and collagen fibre. Possibly, the minimal 50 pN adhesion unit detected by AFM in MV3 β1/β3KD cells (Extended data Fig. 6c, inset) corresponds to the disruption of individual bleb-based contacts to collagen fibrils (Fig. 4e, Extended data Fig. 10d, h, 11d).

Enzymatic digestion of cell surface glycans disabled the tight surface apposition between bleb and fibril, resulting in near-ablated direct contacts but largely increased peri-imprint area adjacent to the fiber contact (Fig. 4f-h, Extended data Fig. 11a, D, b 3-5, d). This identifies the glycocalyx as glue-like scaffold mediating complex-shaped membrane topologies in close apposition with irregular-shaped extracellular topologies. Additional interaction types detected by SEM irrespective of glycan availability included intercalation of collagen fibers between blebs and other protrusions (Fig. 4c, Extended data Fig. 10a, e, 11c, dashed arrows). Together these data implicate the glycocalyx in supporting fast, low- to moderate-adhesive facilitation of membrane apposition along extracellular interfaces allowing the cell-surface to adopt complex nanotopology (Extended data Fig. 12a). Thus, by mediating adhesion through adaptive interfaces, we here identify a complementary adhesion principle which typically acts in parallel to integrin-mediated mechanocoupling but also may occur independently, when integrin functions are disabled. Thus, the glycocalyx provides generic low-affinity but high avidity adhesion through adaptive interfaces to mediate integrin-independent mechanocoupling and cell migration in 3D tissue environments.

High- and low-adhesive interactions coexist, overlap and substitute for each other (Extended data Fig. 12b). Focalized integrin-mediated cell-matrix adhesions transmit dedicated mechanotransduction, mesenchymal migration and further support the ability to reorganize ECM[7,9,19]. When integrins are downregulated or disabled, glycan-based adhesions depend upon actin-rich filopodal or bleb-like protrusions which support tight membrane apposition towards extracellular topologies and shape the cell surface accordingly (Extended data Fig. 12a, b).

Albeit the interaction of blebs with collagen fibers is largely sensitive to glycan removal, surface blebs provide a degree of roughness anchoring the cell surface into ECM discontinuities in an intercalating manner and provide residual non-adhesive cell migration via the stiff yet dynamic cell cortex[53]. Thus, even more weakly adhesive or non-adhesive cell-matrix interactions likely sustain a basal migration level by propulsive shape

change[22,38]. Because integrin- and glycan-dependent adhesion and migration strategies overlap, increasing or lowering integrin engagement towards the 3D ECM scaffold results in gradual transitions from mesenchymal to amoeboid migration. Consequently, complete immobilization in 3D collagen lattices requires the simultaneous interference with integrin- and glycan-mediated matrix binding, yet neither interference strategy alone is sufficient to abrogate cell movement in 3D ECM.

The role of the glycocalyx in amoeboid movement indicates an evolutionary ancient physiochemical mechanism for substrate binding which may be retained in mammalian cells, in reminiscence of cellulose-based substrate binding by ***Dictyostelium***[31,34]. Mesenchymal-to-amoeboid transition might thus reflect an experimentally induced 'step backwards in evolution time' towards less specific mechanisms of cell-tissue interaction. Glycans provide promiscuous cell-substrate interactions to nearly any substrate of the living and non-living nature. In addition, as revealed here, the lattice-like bonds support the shape adaptation of the plasma membrane to collagen fibers and complex-shaped topologies. Combining the generic stickiness with shape alignment of the membrane and the underlying cortical actin cytoskeleton, extremely flexibly and mechanically robust adhesions are being generated. In conclusion, the transition between integrin- and glycan-mediated as well as 'physical' cell-tissue interaction may underlie phenotypic and functional transitions of cell migration during differentiation and invasion.

Methods

Reagents. The following primary antibodies were used: mouse anti-human β1 integrin 4B4 and K20 (Beckman Coulter); rat anti-mouse β1 integrin mAb KMI6 (BD-Pharmingen); mouse anti-human β3 integrin mAb Y2/51 (AbD Serotec); mouse anti-human αV mAb 272-17E6 (Abcam), anti-GAG single-chain antibodies carrying a VSV-tag for recognition by a secondary antibody (kind gift from Toin van Kuppevelt, Radboudumc Nijmegen), including anti-heparan sulphate (HS) antibody (HS4C3)[54,55], anti-dermatan sulphate (DS) antibody (LKN1)[56] and the anti-chondroitin sulphate (CS) antibody (103H10)[57]; rabbit anti-human discoidin domain receptor (DDR1) pAb IgG C-20 (Santa Cruz BioTech); rabbit anti-human discoidin domain receptor (DDR2) pAb IgG H-108 (Santa Cruz BioTech); mouse anti-human CD44 blocking mAb (5F12) (ThermoFischer Scientific). The following isotype control was used: mouse IgG1 Ab-1 (clone: NCG01) isotype (Neomarkers). The following secondary and tertiary antibodies were used: mouse anti-VSV mAb P5D4 from hybridoma culture supernatant (ATCC), goat anti rabbit IgG (H+L) (Molecular Probes), AlexaFluor 488-conjugated goat-anti-mouse IgG antibody (Invitrogen). The following lectins and secondary probes were used: Rhodamine-RedX-conjugated concanavalin A (Invitrogen), Biotin-labeled Maackia amurensis agglutinin (EY Laboratories), Alexa Fluor 488 or 647-conjugated streptavidin

(Invitrogen); cyclic tripeptide arginine-glycine-aspartic acid (cRGD; Arg-Gly-Asp-D-Phe-Val) and cRAD control peptide (Arg-Ala-Asp-D-Phe-Val) (Bachem; purity >95 %). DAPI (Roche) was used for nucleus staining.

Cells. Metastatic human MV3 melanoma cells stem from a spontaneous lung metastasis after subcutaneous implantation in nude mice[20]. For generation of β1/β3 integrin double knockdown cells shRNA sequences targeting ITGB1 (β1 integrin; AGCCACAGACATTTACATTAAA) and ITGB3 (β3 integrin; AAGTCACTTTCTTCTTCTTAAA) for gene silencing by RNA interference were cloned into the lentiviral vector pLBM either containing a puromycin (p-puro) or a neomycin (p-neo) cassette. Lentiviral particles were produced and concentrated by ultracentrifugation, as described[58]. MV3 parental cells were infected with p-puro and p-neo viruses (vector controls), or with ITGB1 (on p-puro) and additionally ITGB3-targeting (on p-neo) pLBM viruses. Stable MV3 β1/β3 knockdown cells were maintained in medium supplemented with puromycin (5 µg/ml) and G418 sulfate (400 mg/ml). Stable LifeAct-eYFP expressing MV3 melanoma cells were obtained as follows. A fragment spanning the pMSCV-hygro (Addgene) Hygromycin B resistance cassette was PCR-amplified (primer sequences available upon request) and inserted into KpnI-digested pLenti6.2/V5-DEST (Invitrogen), replacing the Blasticidin resistance cassette and rendering pLenti6.2_Hygro/V5-DEST. A BglII-NotI fragment, containing the LifeAct-eYFP open reading frame, was then isolated from plasmid pEYFP-N1-ΔATG-Lifeact[59] and cloned into BamHI/NotI-digested pENTR4 (Addgene). Using Gateway recombinase-mediated transfer the pENTR4-LifeAct-eYFP insert was subsequently introduced in pLenti6.2_Hygro/V5-DEST. Stable LifeAct-eYFP expressing MV3 cells were obtained following lipofectamine 2000 transfection of the resulting plasmid, subsequent hygromycin B (Invitrogen) selection (200 µg/ml) and final fluorescence-activated cell sorting.
Immortalised β1-/- murine embryonic fibroblasts (MEFs) were obtained by crossing Immorto mice (Charles River Laboratories, Wilmington, USA) carrying the thermolabile large T antigen H-2KtsA58[60] with mice, in which exon 1 of the β1 integrin gene was flanked by loxP sites[61] and genotyped by tail-tip PCR. Mice that were homozygous for the β1 wild-type or floxed allele and carried at least one Immorto allele were interbred and E13.5 embryos dissected for MEF preparation. Isolated MEFs were cultured at 33°C in the presence of IFNg for five passages until all non-immortalized cells had senesced. Adenovirus-Cre (AdCreM1; Microbix Inc) (MOI 40) was added overnight to subconfluent cultures of a random subset of cells derived of β1 (fl/fl)/Immorto embryos. Deletion of β1 expression was monitored by flow cytometry with mAb KMI6 and confirmed by PCR and Western blot (Extended data Fig.4a,b). Clones from both the parental floxed β1 (β1(fl/fl)) and β1-/- cells were derived by limited dilution, and expression levels of β1 integrins were detected by flow cytometry using mAb KMI6 (Extended data Fig.4c, d). In control cultures using non-floxed immortalised MEFs, Adeno-Cre caused no alteration

of migration rates and mesenchymal phenotype (data not shown). For rescue of β1 in β1-/- MEFs, full-length β1/GFP fusion protein was stably reintroduced at moderate expression level, as described[62] The human T-leukemia cell line Molt-4 was kindly provided by Blanca Scheijen, Laboratory of pediatric oncology, Radboud Institute for Molecular Life Sciences, Nijmegen).
Unless stated otherwise, cells were maintained in RMPI 1640 (Gibco) (MV3, Molt-4) or DMEM (Gibco) (MEF) containing 10 % fetal calf serum (Sigma-Aldrich), penicillin/streptomycin 100 U/ml penicillin and 100 µg/ml streptomycin (PAA), l-glutamine (2mM), sodium pyruvate (1mM) (both Invitrogen) and detached from the culture plate by EDTA (2mM) (Invitrogen). Molt-4 cells were cultured in RPMI 1640 (PAN Biotech GmbH) supplemented with 10 % fetal calf serum (Aurion), penicillin and streptomycin (both 100 µg/ml; PAN) at 37 °C in a humidified 5 % CO_2 atmosphere.

Flow cytometry. Cells were washed three times with PBS by centrifugation (MV3 MEF and Molt cells, 180 g for 5 min). For cell viability analysis, cells were enzymatically digested out of 3D collagen I using collagenase I and washing steps were omitted to prevent the loss of dead cells by centrifugation. After resuspension the cell-associated fluorescence was measured using a FACSCalibur_flow cytometer (BD Biosciences, Erembodegem, Belgium). Data were analyzed using FCS Express (Version 5 Research Edition; De Novo Software, Los Angeles, CA). Per sample, 10.000 morphologically intact and alive cells were gated based on forward and sideward scatter and propidium-iodide negativity.

Cell sorting. MV3 cells were detached by EDTA, washed, stained with FITC-conjugated anti-β1 integrin mAb K20 and subjected to cell sorting for high and low surface label (cut-offs: 5th and 95th percentile; FACS DiVa, BectonDickinson). After up to three passages and complete loss of residual FITC-fluorescence, sorted cells were used for migration and confocal analysis.

Westernblot. β1 knockdown efficiency determined by Western blot (detection Ab 18; BectonDickinson) from whole cell lysates (>90 %) or flow cytometric analysis of β1 integrin surface levels (> 80 %).

Cell migration in 3D collagen lattices, cell tracking and persistence measurements. Integration of cells into 3D pepsin-digested bovine dermis collagen lattices containing 98% type I and 2.8% type III (Vitrogen; Nutracon), time-lapse microscopy and computer-assisted cell tracking[9,63] and morphometric analysis of mesenchymal and amoeboid phenotypes[21] were performed as described. The collagen was native, based on its sensitivity to cleavage by MMP-14 and resistance to degradation by trypsin[64]. Cell migration experiments were performed at 37°C (MV3, Molt-4, MEF parental) and 33°C (Mef β1 -/- cells) for up to 108h. Multicellular spheroids were generated by overnight

culture of MEFs on dishes coated with poly-2-hydroxyethyl methacrylate (0.33 %; Sigma), individually transferred by the tip of a pipette and incorporated into collagen solution prior to polymerization. The population speed was derived from the individual tracks of randomly selected cells for 24 h observation periods. Persistence was calculated as mean for each cell from the continuous-time quotient of direct distance between the end-points divided by the actual track length over a 6 h and 9 h period, excluding phases of immobilization. Box and whisker plots show the median population speed, 25-75 percentiles (box) and minimum and maximum values (whiskers). Statistical analysis was obtained by the non-paired Kruskal-Wallis test for independent samples including post-hoc Bonferoni adjustment. For interference with integrin-mediated adhesion, mAb 4B4 was used at maximum concentration of 10 and 40 µg/ml and cRGD peptide (2 or 10 µM) in addition to stable β1/β3 integrin knockdown.

Collagen contraction assay. Cells were incorporated into 3D collagen lattices in non-adhesive 24-well plates pre-coated with poly-2-hydroxyethyl methacrylate (0.33 %). Contraction was quantified as pixel count representing the matrix area after 24 h.

Confocal microscopy. Confocal fluorescence and reflection microscopy were performed as described[9,21]. Cells in 3D collagen lattices were fixed in de-polymerized 4 % para-formaldehyde at 37 °C, washed, and stained with biotinylated Maackia amurensis agglutinin (MAA) and secondary Alexa Fluor 647 conjugated streptavidin and combined with Alexa Fluor 488 conjugated phalloidin and DAPI. Confocal z-reconstruction was performed on a TCS SP8 confocal microscope (Leica Microsystems, Mannheim, Germany) equipped with an HCX PL APO 63x 1.2 N.A. water immersion lens and on a Leica SP2 scanner for each emission separately and displayed by maximum intensity projection of selected slices. Image analysis was performed using the Fiji ImageJ software from native slices (V1.51d V1.67 and 2.0 NIH, Bethesda).

Imprint depth. Confocal microscopy cross sections were used to determine the imprint depth of the collagen fibers into the glycocalyx layer (MAA) and cortical actin (phalloidin) of cell membrane blebs. Two measuring lines of constant length (8 µm) and width (5 pixels) were set adjacent to both lateral sides of a collagen fiber and two additional lines were set within the collagen fiber. Intensities of the MAA, phalloidin and collagen I signal were determined along these lines by densitometry and exported as table of values. Subsequently, values of both lines were averaged and plotted as overlay. The half-maximum intensities ($Max_{1/2}$) of MAA, phalloidin and collagen and the corresponding x-values were read off the curves followed by the subtraction of the x-values of the collagen I from the values of MAA and the F-actin. The imprint depth (ID) was calculated based on the equation:

$$ID\,(\mathrm{nm}) = \frac{(\text{x-value MFI}_{[\mathrm{Max1/2}]} - \text{x-value Reflection}_{[\mathrm{Max1/2}]})}{PSF}$$

For this the differential values of MAA or F-actin fluorescence and collagen reflection were divided by the YZ point spread function (PSF, 3.64).

Glycan removal. Cells from subconfluent cultures were first detached using 2 mM EDTA (MV3, MEF), transfered into 2 ml Eppendorf tubes and washed twice with culture medium containing 1 % FCS. Molt-4 cells were directly transfered into 2 ml Eppendorf tubes and washed equally to MV3 and MEF. Subsequently cells were simultaneously incubated with glycosidase cocktail (P/N), containing hyaluronidase at 275-500 U/ml (Sigma Aldrich), heparitinase I at 10 mU/ml (Seikagaku), chondroitinase ABC at 100 mU/ml (Sigma Aldrich) and neuraminidase type V at 100 mU/ml (Sigma Aldrich) targeting both distal glycosaminoglycan chains of proteoglycans (P) and terminal sialic acids / neuraminic acid (N) of glycoproteins and glycolipids and a cocktail (P/N/G) containing additionally β-1,4 galactosidase at 150 mU/ml (Sigma Aldrich) cleaving proximal β-1,4 galactose (G) of glycoproteins and glycolipids (37 °C, pH 7.0-7.4, 6 h). Afterwards, cells were washed three times and further studied. Because latent cytotoxicity negatively impacts migration rates, non-damaging conditions were monitored by different approaches. After glycan removal, cells were collected, stained by propidium iodide, and analyzed by flow cytometry. Unaffected cell viability was routinely confirmed by propidium iodide staining and flow cytometry before and after time-lapse microscopy and cell retrieval by collagen digestion (type I collagenase, Sigma; 100 U/ml, 15 min, 37 °C) as well as unaltered intact nuclear morphology after fixation *in situ* and DAPI staining.

Transmission electron microscopy (TEM). Detection of the surface glycocalyx using TEM was performed largely based on Cox et al[65]. MV3 cells were detached from the culture plate by EDTA, pelleted and fixed with Ruthenium Red containing fixatives for transmission electron microscopy. Cells were washed twice with DMEM (without FCS). Supernatant was removed and fixative 1 [0.1 M PHEM Buffer (PIPES, HEPES, EGTA, MgCl2), 0.075 % ruthenium red, 3 % glutaraldehyde] was applied to the cell pellet. The samples were wrapped with parafilm and incubated on a shaker at RT for 1 h. After incubation, cells were centrifuged (1200 rpm; 5 min and washed with washing buffer [0.1 M PHEM Buffer (PIPES, HEPES, EGTA, MgCl2) 0.075 % ruthenium red three times for 15 minutes. After postfixation with fixative 2 [0.1 M PHEM Buffer (PIPES, HEPES, EGTA, MgCl2), 0.075 % Ruthenium Red, 1 % Osmium Tetroxide (OsO4)] for 2h at RT (2h at RT) cells were washed three times with 0.1 M PHEM buffer, resuspended in 0.1 M PB and centrifuged (13.000 rpm; 30 seconds). Supernatant was removed and 4 % agar (pre-warmed, boiled first in advance) was applied. Samples were then incubated for 2-5 minutes at 45 °C. Afterwards, cells were immediately centrifuged (before the agar

solidified) at 13.000 rpm for 30 seconds and put in an ice bucket. After 2-5 minutes, the cell pellet was cut out of the eppendorf tube and carefully chopped up into very small slices using a razor blade. The slices were put in to 2 % paraformaldehyde / 0,1 M PB and left at RT for 2 h. After washing 3 times in 0,1 M PB the samples were dehydrated through a graded ethanol serie (50 %, 70 %, 80 %, and 96 % respectively for 5 min each and 2x 15 min in ethanol 100 % P.A.). Afterwards, samples were washed with propylene oxide for 2 x 20 minutes at room temperature. Propylene oxide was then discarded and replaced by a mixture of 1:1 epon:propylene oxide and left in this mixture for at least 2 h at room temperature. Epon:propylene oxide mixture was replaced by pure epon and left for at least 2 h (preferably overnight) at room temperature. An embedding mold was prepared and the samples were carefully placed in the embedding mold (1 slice per hole). Fresh epon was added until the hole was slightly overfilled (because of shrinkage of epon during polymerization). The mold was placed in an incubator at 37 °C. After at least 2 h, temperature was raised to 60 °C to polymerize the epon (epon polymerization is an irreversible reaction, once epon has polymerized, it cannot be depolymerized). After polymerization, the samples were removed from the embedding mold and semi-thin sections (1 µm thick) were cut on an ultramicrotome, stained with a 1 % Toluidin blue solution and examined under a light microscope to select the area of interest. Excess epon/ tissue was trimmed off by hand with a razor blade and ultrathin sections (50 – 80 nm) were cut with a diamond knife and collected on formvar coated copper grids. Sections were stained with 4 % uranyl acetate for 20 minutes at room temperature, washed 3 times with MILL-Q water and stained with lead citrate solution (2.66 % lead nitrate and 3.52 % sodium citrate) for 10 minutes at room temperature. Afterwards sections were washed 3 times with MILL-Q water, dried and examined on a Jeol 1010 TEM.

Scanning electron microscopy (SEM). Following the treatment with glycosidases or solvent, MV3 cells were embedded into 3D bovine fibrillar collagen I lattice for 90 min. Subsequently, the collagen lattices were fixed in 2 % glutaraldehyde in 0.1M Cacodylate-buffer for 1 h at 37 °C, washed, post-fixed for 1 h in 1 % OsO4 in 0.1M Cacodylate-buffer, followed by dehydration in a graded ethanol series and Critical Point Dried. Dried samples were mounted on stubs and then coated with 5nm Chromium in a Quorum Q150TS (Quorum Technologies Ltd, East Sussex, UK). Images were made with a Zeiss (Carl Zeiss AG, Jena Germany) Sigma 300 Scanning Electron Microscope operating at 3 kV.

Imprint area and contact area. Scanning electron microscopy pictures were used to determine the imprint area. First, the area between the convex maxima of the bleb-membrane, defined as total area $Area_{Total}$ and the area covered by the collagen fiber defined as $Area_{Fiber}$ was determined using Fiji/ImageJ (http://pacific.mpi-cbg.de/wiki/index.php/Fiji). Subsequently the imprint area was calculated by subtracting the $Area_{Fiber}$

from the $Area_{Total}$. To determine the contact area, the lateral surface area of the fiber was calculated and the bleb-free fiber area subtracted.

Atomic force microscopy (AFM). The forces between carbohydrate polymers and collagen fibres were determined by atomic force microscopy (AFM). Flat collagen lattices (1.6 mg/ml, 40 µm thick) mounted on a 1.5 mm thick glass cover slip (PLANO) were probed using a NanoWizard AFM (JPK Instruments, Berlin, Germany) mounted on an Axiovert 200 inverted microscope (Carl Zeiss, Jena, Germany). The cantilever was functionalized with either bovine serum albumin (3 %, 2 h, 20 °C), Bis-NHS-polyethylen glycol (5 % w/w, 200000 g/mol, Nektar, Huntsville, AL), amylose (carboxymethyl amylose, Sigma) or cellulose (carboxymethylcellulose, Sigma) at the indicated weight percentage. After UV-irradiation (10 min), silicon nitride cantilevers (MLCT, Veeco Probes) with a spring constant of 60 pN/nm were functionalised by N1-[3-(trimethoxysilyl)propyl] diethylenetriamine (Aldrich; 30 min, RT) followed by heating (30 min, 80 °C), incubation in sodium borate buffer (60 min; RT), and either Bis-NHS-PEG solution, amylase, or cellulose solution in N-hydroxysuccinimide (NHS; Aldrich; 100 mM) and 1-ethyl-3-(3-dimethylaminopropyl)carbodiimide (EDC, Sigma; 100 mM, 90 min, RT)[66]. System position and sensitivity were calibrated before each measurement, as described by Puech et al[67]. The spring constants ranged from 50 to 80 (median 60) pN/nm (thermal noise method). All interaction measurements were performed in PBS/BSA (0.4 %) at RT (set point of 200 pN for approach curve; dwell time 0.1 s). For each measurement, 1600 to 10000 force curves were obtained for a retract velocity of 10 µm/s from different spots within a 40 x 40 µm collagen surface area. The force curves were analyzed with a customized software and statistical analysis was obtained by the software package R, version 1.22 (R Foundation for Statistical Computing). After UV irradiation (10 min), the silicon nitride cantilevers were functionalized with (3-Glycidoxypropyltrimethoxysilane (98 %, Sigma Aldrich) at 80 °C for 30 min, incubated in sodium-borate buffer for one hour at RT, functionalized with NH2-PEG(3000)-COOH (Rapp Polymers) in 50 mM sodium borate buffer for one hour at RT. Then 1 % (w/w) BSA was coupled to the PEG for one hour at RT with 1-ethyl-3-(3-dimethylaminopropyl) carbodiimide (EDC, Sigma Aldrich, 100 mM) and N-hydroxy-succinimide (NHS; Sigma Aldrich; 100 mM). The measurement was performed without BSA in solution.

Single cell force microscopy and spectroscopy (SCFM/SCFS). The interaction strength between cell surface glycans and 3D collagen I fibers was determined by single-cell force spectroscopy (SCFS), using a combined Catalyst AFM (Bruker) and inverted 3-channel Leica TCS SP5 II confocal laser-scanning microscope equipped with 10 × 0.4 NA, 20 × 0.70 NA, and 40 × 0.85 NA air objectives and Hamamatsu (ORCA-05G) brightfield camera. Unlabeled or TAMRA-labeled 3D Collagen I (1.6 mg/ml, 40 µm thick) and BSA coating (2 % in TSM solution, containing 20 mM Tris-HCl, 150 mM NaCl, 1 mM $CaCl_2$,

2 mM $MgCl_2$ at pH 8.0, incubated 24 h at 4 °C) were made on glass-bottomed dishes (55-mm Willco dish), using a 150-mm thick four-segment polydimethylsilane (PDMS) mask that was fused to the glass directly after treating the glass and mask for 30 s in a plasma cleaner/sterilizer (PDC- 32G, Harrick Plasma)[68] Cells were attached to a tippless AFM cantilevers NP-0 (type D; nominal spring constant of 0.06 Nm^{-1} (Bruker) coated with concanavalin A (ConA) (Sigma)[69]. ConA-coated cantilevers were prepared as follows: cantilevers were cleaned by immersion in pure 18 M sulphuric acid (Sigma) for 1 h and then thoroughly rinsed with Milli-Q water followed by ethanol and, after a final rinse in Milli-Q water, left to dry. Following an overnight incubation at 4 °C in ConA (2 mg/ml in PBS), the cantilevers were rinsed and stored in PBS for no more than 1 day. The spring constant of each cantilever was calibrated before cell attachment using the thermal noise method[70] To adhere a single cell to the AFM cantilever, cells were seeded from suspension in the perfusion chamber in culture medium without FBS but with 0.5 % antibiotic-antimycotic at pH 7.4 (+10 mM HEPES). The ConA-coated cantilever was pushed softly (< 3 nN) onto the cell for <10 s. Upon retraction of the cantilever, the detachment of the cell was monitored by using brightfield microscopy. Thereafter, the cell was allowed to adhere strongly to the cantilever for 5–10 min. When cells (partly) detached from the cantilevers during experiments, cantilevers and data were discarded. Possible sink function of cell surface glycans towards the ConA coated cantilever, the contact area of the cells (133 μm^2) realtive to the total cell surface (1.385 μm^2) was determined with a ratio of 9.6 % and thus could be ruled out. Adhesion of the cantilever-bound cell to different substrates was measured after pushing the cell into contact with the substrate, applying 2 nN contact aquisition for predefined time intervals (0.5, 5 and 20 s). Subsequently, the cell was retracted at 5 µm/s and allowed to recover for a time period equal to that of the contact time with the substrate[69,71]. Since the number of matrix contacts, which can be done by SCFS with a single cell depends on the contact time[52], acquisition of binding forces was limited to maximal 15 measurements per cell to prevent cell deformation. The sequence of contact time measurements was varied and performed in different areas of the substrate. Repeated probing on one spot was limited to a maximum of 5 times in a row. The maximum detachment force F [max] was calculated from the peak of the retraction curves to background level (Extended data Fig. 6c, f, g).

Surface plasmon resonance (SPR). The binding affinities between amylose polymers and collagen fibres were monitored by surface plasmon resonance (SPR) using a Biacore T100 instrument (GE Healthcare). All materials were purchased from GE Healthcare whereas not specified. For the preparation of the analyte, amylose type III (Sigmal Aldrich) was dissolved using 200 mM NaOH and subsequently neutralization with 200 mM HCl. The resulting Amylose - NaCl solution was diluted in Biacore running buffer (HBSN, 10 mM Hepes, 150 mM NaCl, pH 7.4). For the preparation of the ligand collagen was immobilized via amino groups on the dextran surface of a CM5 sensor chip The

amylose solution at concentration ranging from 300 µg/ml to 12 µg/ml was injected over the immobilized collagen or a control flow cell at the flow rate of 50 µl/min, 25 °C. Regeneration was achieved with a short pulse of 100 mM NaOH. No binding is observed with PEG dissolved in HBSN and injected in the same way. The negligible non-specific binding on the empty flow cell was substracted from measured specific binding affinity. Kinetics were analyzed throught Biacore T100 evaluation 1.1.1 software using Langmuir model 1:1 for fitting curves. For the global fitting, we chose the the theoretical molecular weight of 8000 for amylose. We also calculated the sole dissociation rates, that is only time-dependent and not influenced by the the analyte molecular weight.

Intravital multiphoton microscopy. All intravital imaging experiments were approved by the Ethical Committee on Animal Experiments and performed in the Central Animal Laboratory of the Radboud University, Nijmegen (RU-DEC 2009-174, 2011-298), in accordance with the Dutch Animal Experimentation Act and the European FELASA protocol (www.felasa.eu/guidelines.php).

LifeAct-YFP expressing MV3 control and β1/β3 integrin knockdown cells were incubated with anti-β1 integrin mAb 4B4 (10 µg/ml) and anti-αV integrin mAb 272-17E6 (10 µg/ml) and glycans were digested. The cells were then injected as single cell suspension ($2*10^4$ cells / mouse) into the deep dermis of Balb/c nu/nu mice (Charles River) carrying a dorsal skin-fold chamber. To ensure complete integrin blocking, mice received i.p. injections of 4B4 (5 µg/g) and 17E6 (5 µg/g) 2 h before cell injection.

Intravital multiphoton microscopy was performed 1-2 h after cell injection on anesthetized mice (1-3 % isoflurane in oxygen) on a temperature-controlled stage (37°C). Blood vessels were labeled by intravenous injection of AlexaFluor750-labeled 70kD dextran (2 mg/mouse; Invitrogen).

Imaging was performed on a customized near-infrared/infrared multiphoton microscope (TriMScope-II, LaVision BioTec, Bielefeld, Germany), equipped with three tunable Ti:Sa (Coherent Ultra II Titanium:Sapphire) lasers and an Optical Parametric Oscillator (OPO). 4D time-lapse recordings were acquired by sequential scanning with 960 nm (YFP, 10 - 20 mW) and 1090 nm (AI750 and SHG, 30-60 mW) with a sampling rate of 1 frame / 10 min over periods of up to 8 h.

Image processing and quantification. Images were processed using Fiji/ImageJ (http://pacific.mpi-cbg.de/wiki/index.php/Fiji). Drifts in time-lapse recordings were corrected using the StackReg plugin[72]. To avoid tissue regions perturbed by the injection procedure, migration analysis was performed in intact collagen-rich loose connective tissue identified by second harmonic generation. Quantitative analysis of tumor cell migration

was performed using the FIJI manual tracking plugin (Fabrice P. Cordelières, rsb.info.nih.gov/ij/plugins/track/track.html). To control for small local tissue drifts, particularly important for analyzing the residual migration after glycan removal, movements of 3 tissue structures in close proximity to each analyzed cell were recorded and used to correct individual cell migration tracks.

Acknowledgements

We thank Monika Kuhn, Ute Eifert, Martina Jossberger, Margit Ott and Kathrin Bührle for expert technical assistance; Irmgard Schwarte-Waldhoff, Christian Linden, Kimberly Burns, and Ute Schwab for technical advice; Jan Schepens and Wiljan Hendriks for generating the Lifeact-eYFP expressing cells; Zena Werb for helpful discussions; and Martin Lohse and Rex Chisholm for comments on the manuscript. This work was supported by the DFG Transregio-SFB 17, (to P.F.), and the Welcome Trust (to M.J.H.), and the Center for NanoScience (L.R. and K.E.G) and the Fonds der Chemischen Industrie (Liebig Felloship to K.E.G.). J.t.R. is supported by the Netherlands Organisation for Scientific Research (NWO) (Veni Grant No. 680-47-421). The AFM work was supported by NWO Medium Sized Investment (Grant No. NWO-ZonMW 91110007). The authors furthermore thank the RIMLS Microscopic Imaging Center for the use of their facilities.

Author contributions

S.S., P.F., M.J.H., and K.E.G. designed the experiments, S.S, P.F. and N.D. performed migration and immunostaining experiments, S.S and B.W, performed in vivo imaging experiments, S.S., L.R., K.E.G. and J.t.R. performed AFM measurements, S.S. and M.K.-V. performed AFM confocal micrsoscopy, S.S. and P.F. performed confocal microscopy, S.S., M.t.L. and J.F. performed Electron microscopy, S.S., B.L. and L.B. performed Surface Plasmon Resonance spectroscopy, A.J.M., U.M., and R.M. generated β1 integrin deficient MEFs, S.K. generated ß1/ß3 integrin KD MV3 cells. S.S. and P.F. wrote the manuscipt and all authors discussed the results and commented on the manuscript.

Author information

Correspondence should be addressed to P.F. (Peter.Friedl@radboudumc.nl).

Supplementary Information is linked to the online version of Nature at **www.nature.com/nature**.

Supplemental Information

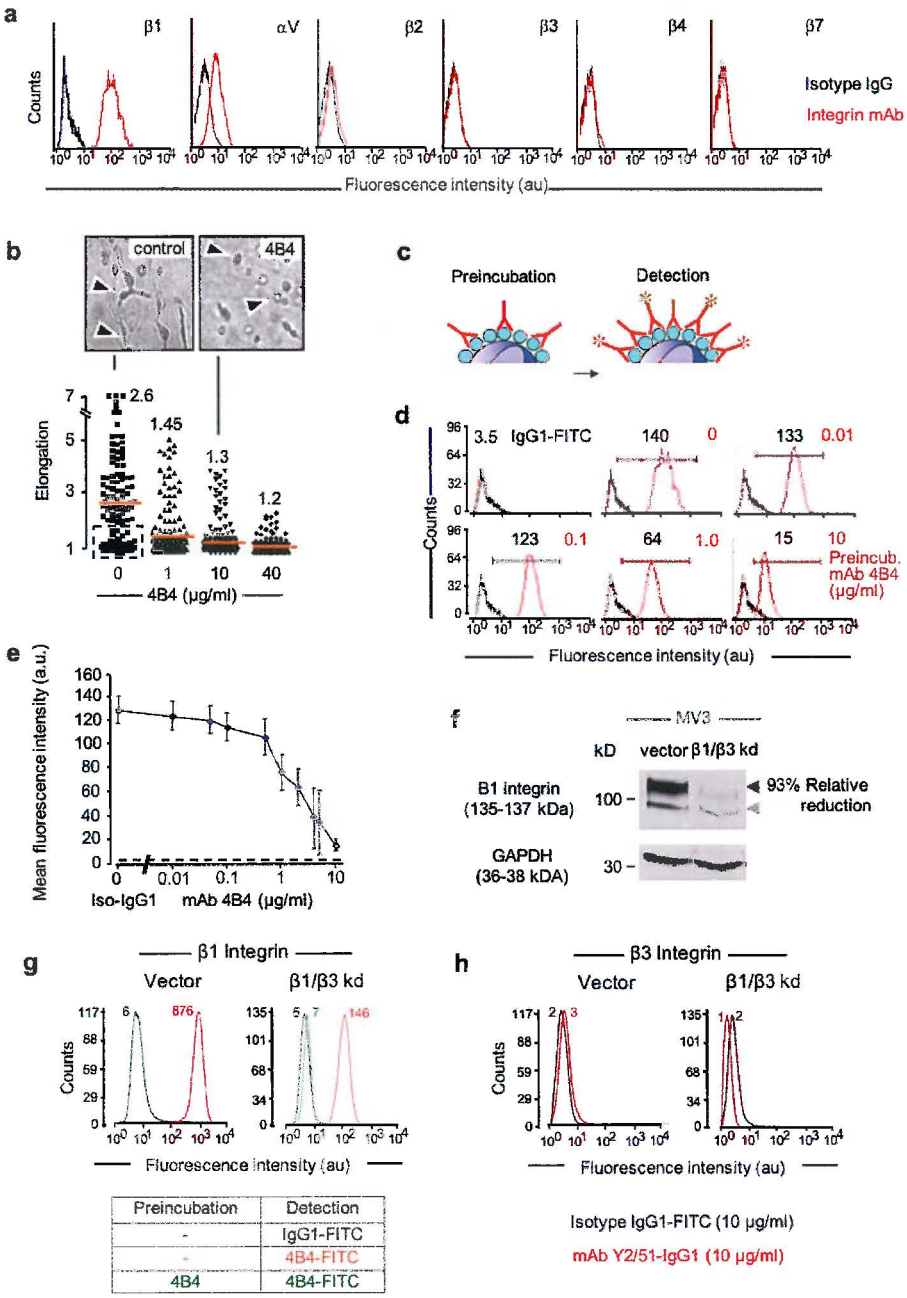

Preincubation	Detection
-	IgG1-FITC
-	4B4-FITC
4B4	4B4-FITC

Figure S1.

a) Integrin surface levels on MV3 cells after detachment from subconfluent cultures by EDTA prior to the migration experiment. Red line, anti-integrin mAb; black line, isotypic control antibody. (b) Amoeboid phenotype after interference with integrins in tumor cells. Mesenchymal-amoeboid transition in MV3 melanoma cells after interference with β1 integrin function. Spindle-shaped morphology in MV3 control cells and conversion to a rounded phenotype induced by anti-β1 mAb 4B4. Influence of increasing doses of mAb 4B4 on cell morphology. Elongation was determined as length/width for moving cells only. Red lines, medians. Dashed box, moving subset in control cells that lacks spindle-shaped elongation. (c-e) Epitope saturation by anti-β1 integrin mAb 4B4. Titration of mAb 4B4 results in up to 95 % binding inhibition of fluorescent detection antibody. (c) Principle of the detection assay. MV3 cells were incubated for 30 min with non-fluorescent mAb 4B4 at different concentrations, washed, stained with FITC-conjugated detection mAb 4B4 (10 µg/ml), and analyzed by flow cytometry. (d) Fluorescence intensities (mFI) of FITC-conjugated detection mAb after pretreatment with nonlabeled mAb 4B4 (red line) or isotypic control antibody (black line). (e) Mean fluorescence intensities +/- standard deviation with increasing doses of mAb 4B4 (n=3). Dashed line in (e), isotypic control level. (f) Knockdown β1 integrin efficiency detected by Western blot (> 90 %) and (f) flow cytometry (> 80 %). The β1 integrin of vector control cells ran at approximately 110 kD (black arrowhead) and pre-β1 at 90 kD (gray arrowhead). (g) Residual epitopes were saturated by additional incubation with anti-β1 integrin mAb 4B4 leading to a total β1 integrin interference of 97 % shown by flow cytometry. (h) Integrin β3 surface levels on MV3 vector control cells and on MV3 β1 and β3 integrin knockdown cells from subconfluent cultures prior to the migration experiment. Red line, anti-integrin β3 mAb Y2/51; black line, isotypic control antibody. In experiments residual epitopes were saturated by additional incubation with cyclic RGD peptide.

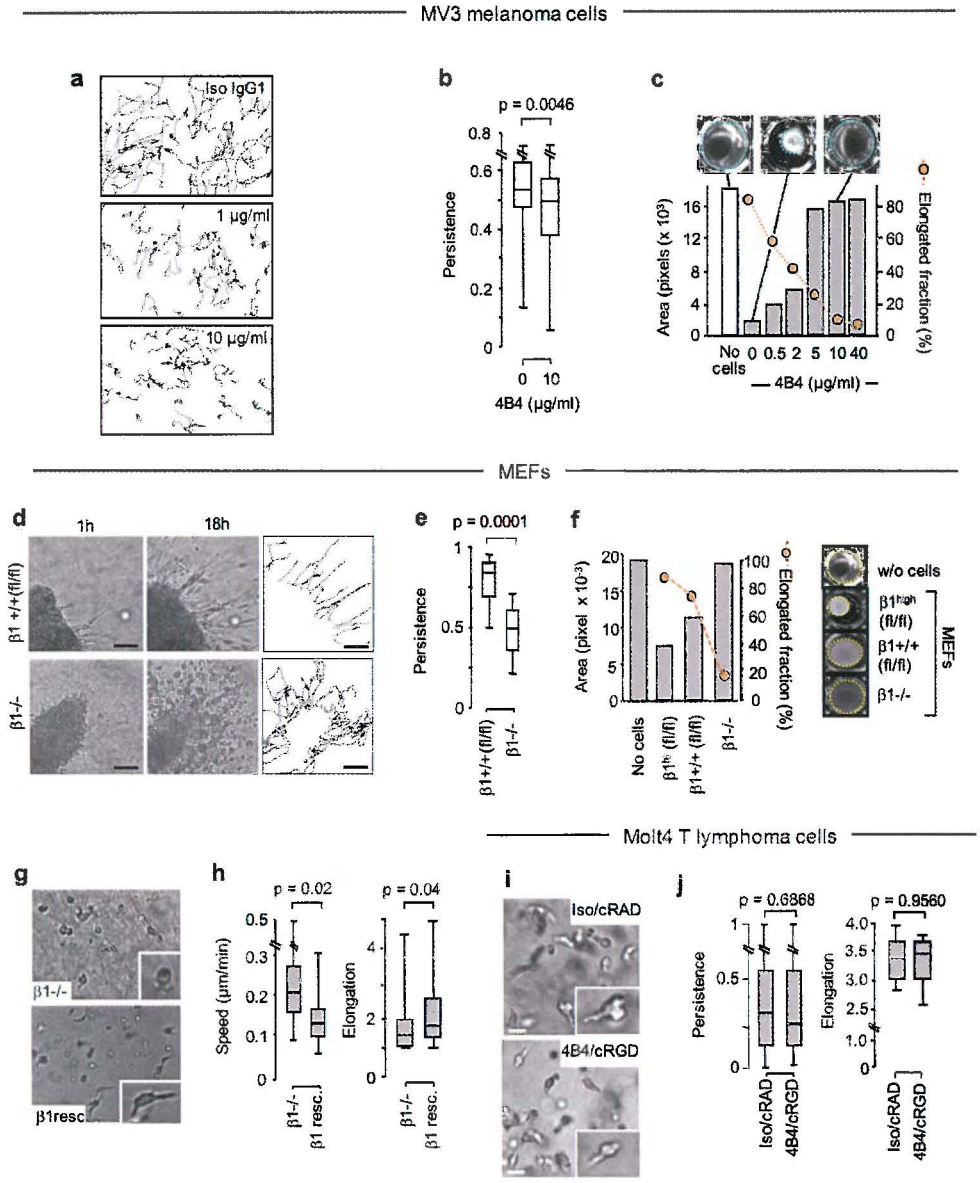
MV3 melanoma cells
a
Iso IgG1
1 µg/ml
10 µg/ml
b
p = 0.0046
Persistence
0.8
0.6
0.4
0.2
0
0 10
4B4 (µg/ml)
c
Area (pixels (x 10³)
16
12
8
4
0
Elongated fraction (%)
80
60
40
20
0
No cells
0 0.5 2 5 10 40
4B4 (µg/ml)
MEFs
d
1h
18h
β1 +/+(fl/fl)
β1-/-
e
p = 0.0001
Persistence
1
0.5
0
β1+/+(fl/fl)
β1-/-
f
Area (pixel x 10⁻³)
20
15
10
5
0
Elongated fraction (%)
100
80
60
40
20
0
No cells
β1^high (fl/fl)
β1+/+ (fl/fl)
β1-/-
w/o cells
β1^high (fl/fl)
β1+/+ (fl/fl)
β1-/-
MEFs
Molt4 T lymphoma cells
g
β1-/-
β1resc
h
p = 0.02
Speed (µm/min)
0.5
0.3
0.2
0.1
0
β1-/-
β1 resc.
p = 0.04
Elongation
4
2
0
β1-/-
β1 resc.
i
Iso/cRAD
4B4/cRGD
j
p = 0.6868
Persistence
1
0.5
0
Iso/cRAD
4B4/cRGD
p = 0.9560
Elongation
4.0
3.5
3.0
2.5
1.0
0
Iso/cRAD
4B4/cRGD

Figure S2.

(a) Amoeboid phenotype after interference with integrins in tumor cells and fibroblasts. (a-c) Mesenchymal-amoeboid transition in MV3 melanoma cells after interference with β1 integrin function. Influence of increasing doses of mAb 4B4 on (a) migratory activity shown by reduced cell paths and (b) directional persistence. (a) Data show a representative sample of path lengths obtained by 40 single cells for an 18 h observation period and (b) for 120 cells from 3 independent experiments. (c) Impaired contraction of free-floating collagen lattices by mAb 4B4 associated with impaired cell elongation (elongation fraction > 2). Bars, 10 µm. (d-h) Mesenchymal-amoeboid transition in murine embryonic fibroblasts after interference with β1 integrin function. Amoeboid migration in β1-deficient embryonic murine fibroblasts (d) Migration of β1+/+(fl/fl) and β1-/- MEFs from multicellular spheroids into the adjacent 3D collagen lattice (left) and individual cell paths (right). (e) Persistence of β1-expressing and β1-/- MEFs. (e) Bars, 10 µm (f) Collagen contraction assay with β1-/- MEFs cells, compared to β1-positive cells. Area of the collagen lattice after 24 h was quantified from digital images (right). The fraction of amoeboid cells (elongation < 2) within 3D collagen lattices was obtained from still images, thus containing mobile and nonmobile subsets. (g) Rescue of mesenchymal phenotype and (h) reduced migration speed at moderately increased elongation after re-expression of β1/GFP, compared to parental β1-/- MEFs. (i) Morphology, (j) persistence and elongation of Molt 4 cells with β1/β3 integrin blocked cells (4B4), compared with isotype control cells. (j) Bars, 20 µm.

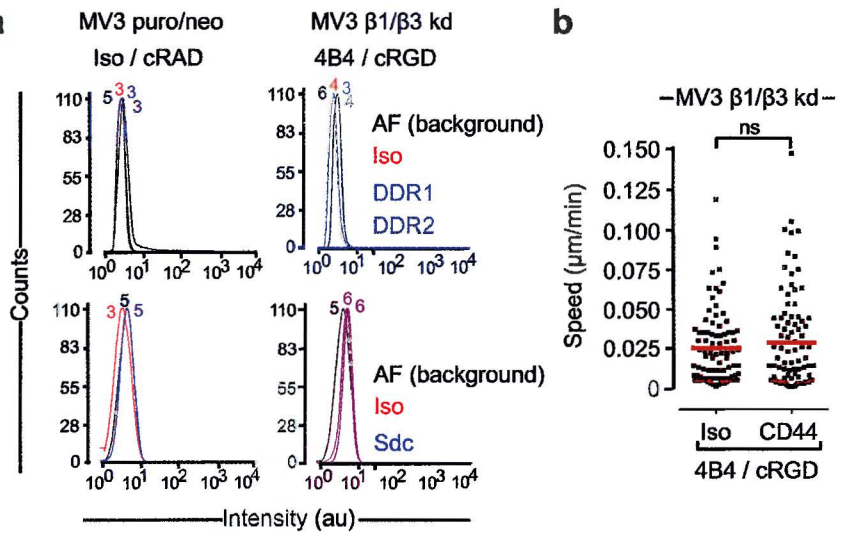

Figure S3.

(a,b) Detection and Analysis of putative compensation receptors. (a) Indicated cells were incubated with integrin-blocking 4B4 and integrin-masking cRGD for 30 min and subsequently cultured in 3D bovine collagen I in presence of 4B4 and cRGD for 9 h. Cells were enzymatically digested out of 3D collagen I using collagenase I and incubated with antibodies DDR1 and DDR2 or Sdc followed by incubation with 2nd fluorescently labelled antibodies and flow cytometry. (b) Cells were pre-treated with integrin blocking 4B4 and cRGD and Isotype or anti- CD44 blocking antibody for 30 min and embedded in 3D collagen I. Cell migration was recorded over 24 h. (c,d) Migration of Dictyostelium discoideum into 3D collagen lattices. Cells were overlaid onto a 3D collagen matrix and allowed to spontaneously immigrate. (c) Still images after 3 and 4 h of culture and migration tracks recorded within this time period are shown. (d) Speed distribution and median, obtained by single cell tracking. Bar, 10 µm.

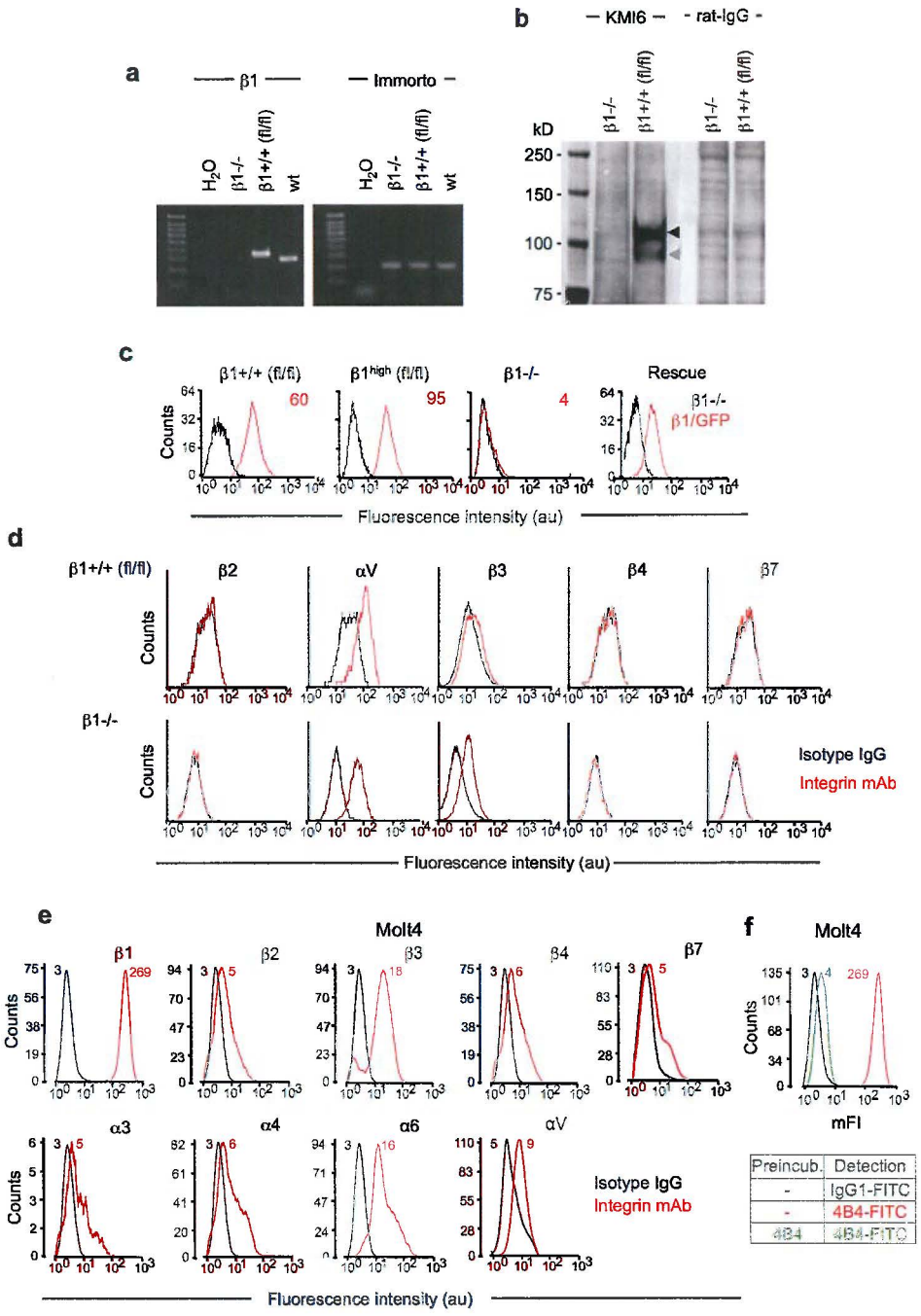
a
β1
Immorto
H2O
β1-/-
β1+/+ (fl/fl)
wt
b
KMI6
rat-IgG
kD
250
150
100
75
c
β1+/+ (fl/fl)
β1high (fl/fl)
β1-/-
Rescue
β1-/- β1/GFP
60
95
4
Counts
Fluorescence intensity (au)
d
β1+/+ (fl/fl)
β1-/-
β2
αV
β3
β4
β7
Isotype IgG
Integrin mAb
e
Molt4
β1
β2
β3
β4
β7
α3
α4
α6
αV
269
18
16
9
Isotype IgG
Integrin mAb
f
Molt4
mFI
Preincub.
Detection
IgG1-FITC
4B4-FITC

Figure S4.

Characterization of β1 integrin null MEFs and rescue after reintroduction of β1. (a) PCR analysis of β1(fl/fl), β1-/- and wild-type MEFs (cell line 7929) for β1 integrin and Immorto alleles. β1-/- cells had no detectable β1 integrin, while the floxed and the wildtype β1 integrin locus resulted in bands of 320 and 285 bp, respectively (left panel). All cell lines carried the Immorto allele (right panel). Primers for β1 were GCCGCCACAGCTTTCTGCTGTAGG (sense) and CTGATCAATCCAATCCAGGAAACC (antisense). (b) Lysates of β1(fl/fl) and β1-/- MEFs were probed with anti-β1 antibody KMI6 or rat IgG. β1-/- cells had no detectable β1 integrin. The floxed β1 integrin of the parental MEF 7929 cell line ran at approximately 110 kD (black arrowhead) and pre-β1 at 90 kD (gray arrowhead) (c) β1 integrin surface expression in MEFs cells analyzed by flow cytometry. Re-expression of β1/GFP in β1-/- MEFs, resulting in moderate expression level. (d) Surface expression of integrins on β1(fl/fl) and β1-/- MEFs after detachment from subconfluent 2D culture by EDTA. Except minor upregulation of β3 integrins, no difference was detected. (e) Integrin surface levels on Molt-4 cells from subconfluent cultures prior to the migration experiment. (f) Residual β1 integrin epitopes on Molt-4 cells were saturated by additional incubation with anti-β1 integrin mAb 4B4 leading to a total β1 integrin interference of 97 % shown by flow cytometry. Red line, anti-integrin mAb; black line, isotypic control antibody.

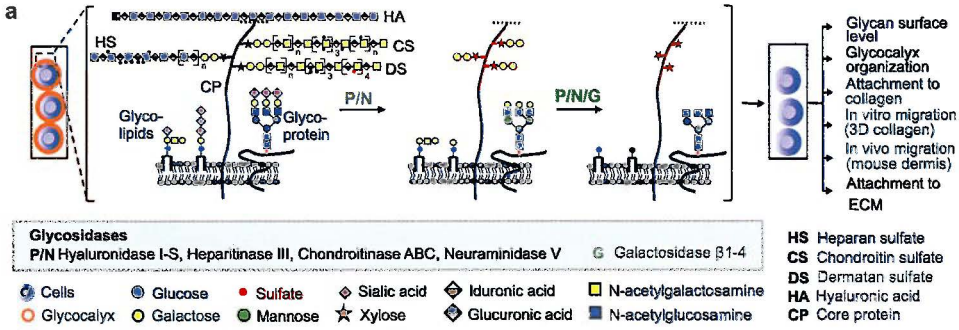

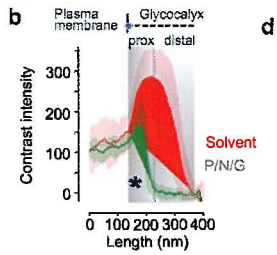

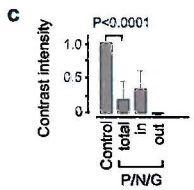

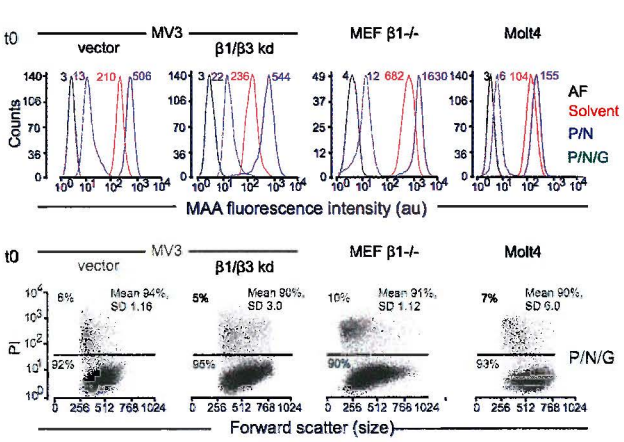

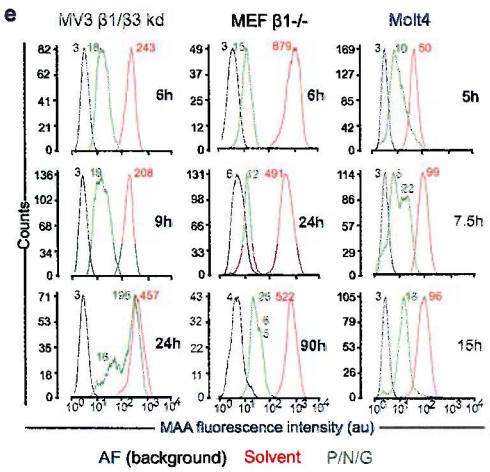

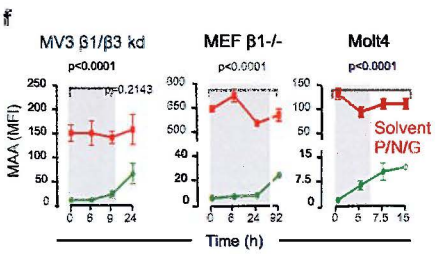

g

Reduction of epitope

Cells \ Epitope	HS	DS	CS	β1-4 Gal
MV3 β1/β3kd + P/N/G	- 97%	- 95%	- 95%	- 91%
Mef β1-/- + P/N/G	- 98%	- 98%	- 46%	- 98%
Molt 4 + P/N/G	- 71%	- 67%	- 62%	- 94%

Figure S5.

(a-d) Enzymatic removal of glycan moities on the cell surface of living cells using glycosidases for 6 h at 37 °C and 5 % CO_2. The expression of cell surface glycan structures and the efficient removal were analyzed by flow cytometry (FACS) and transmission electron microscopy (TEM). The impact of the enzymatic treatment of living cells on adhesive strength to fibrillar collagen was studied by atomic force microscopy and spectroscopy (AFM/AFS) and single cell migration in vitro and in vivo using automatic cell tracking. (b) Cumulative density of Ruthenium red staining before and after glycan removal resulting from 10 analyzed cells of 2 independent experiments (shaded areas, SD). Blue dot, position of the plasma membrane. Dashed line, cross-sections perpendicular to the plasma membrane used for image analysis. Asterisk, interpolated gradient between intracellular and extracellular background signal used for calculating the integral. (c) Data show intensities normalized to the control cells including standard deviation, calculated from the position-controlled integral to represent outer and membrane-proximal, inner zones of the glycocalyx. P values, non-paired Mann-Whitney t test for independent means. (d) Detection of glycan removal using fluorescently-labeled Maackia amurensis agglutinin and propidium iodide (PI) for cell viability in flow cytometry of MV3 integrin expressing and β1/β3 integrin knockdown and 4B4- and cRGD blocked cells, MEF β1-/- and Molt-4 cells. (e+f) Analysis of retention of the deglycosylated status of enzyme treated cells over a time span of 6-9 h (MV3), more than 90 h (MEF) and 5-6 h (Molt-4) and the step-wise recovery of β-1,4 galactose expression. Mean fluorescence intensities of Maackia amurensis agglutinin (MAA) with standard deviations of 3 independent experiments. (g) Efficiency of the glycan removal using P/N/G analyzed by FACS and presented as reduction of the epitopes heparan-, dermatan- and chondroitin sulfate (HS, DS, CS) and β-1,4 Galactose (β-1,4 Gal) after treatment compared to untreated control cells. Results are based on 3 independent experiments.

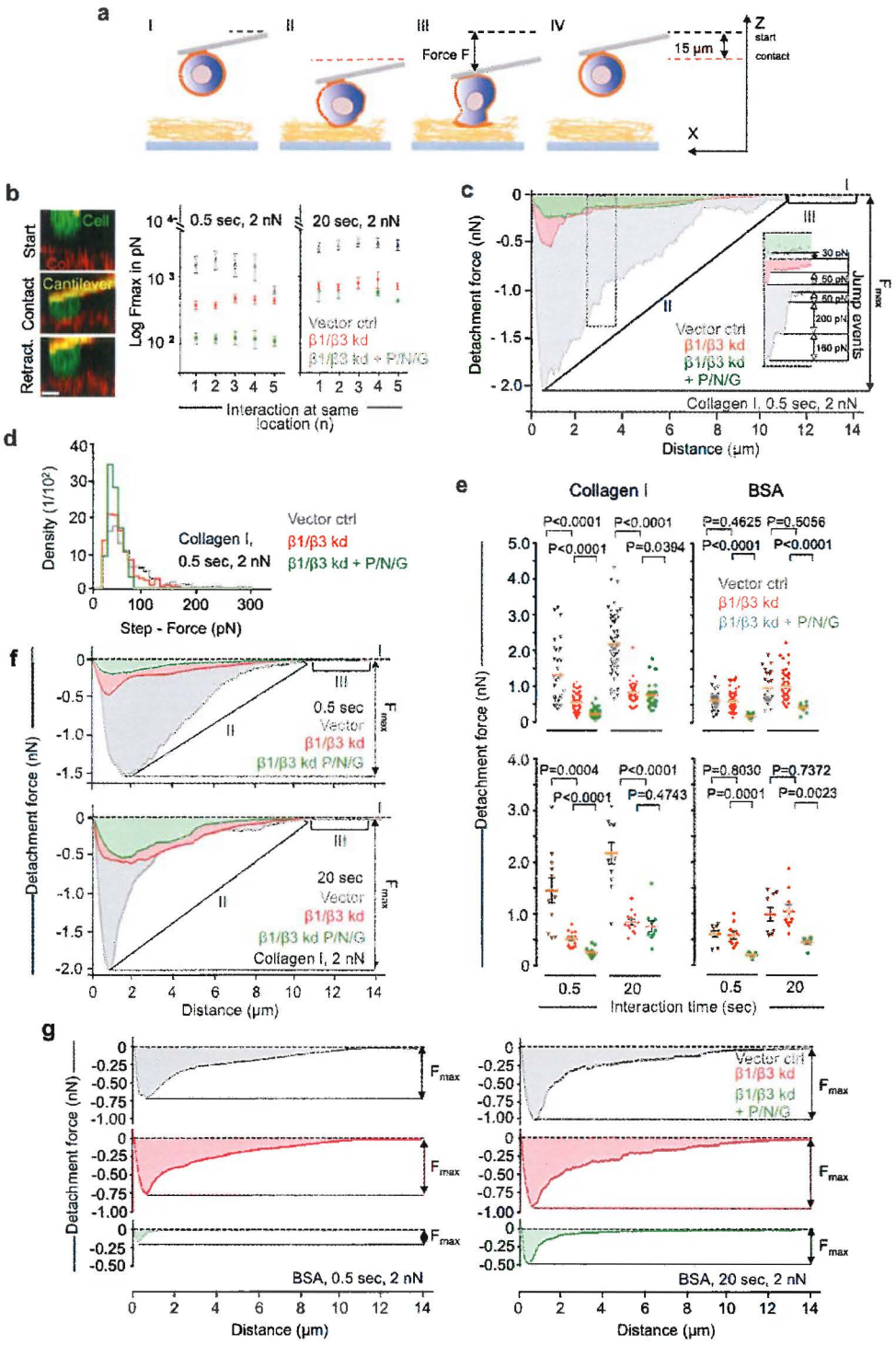
a
I
II
III
IV
Force F
15 µm
Z
start
contact
X
b
Start
Contact
Retract.
Cell
Cantilever
0.5 sec, 2 nN
20 sec, 2 nN
Log Fmax in pN
Vector ctrl
β1/β3 kd
β1/β3 kd + P/N/G
Interaction at same location (n)
c
Detachment force (nN)
Distance (µm)
Vector ctrl
β1/β3 kd
β1/β3 kd + P/N/G
Collagen I, 0.5 sec, 2 nN
Jump events
30 pN
50 pN
60 pN
200 pN
160 pN
Fmax
d
Density (1/10²)
Collagen I, 0.5 sec, 2 nN
Vector ctrl
β1/β3 kd
β1/β3 kd + P/N/G
Step - Force (pN)
e
Collagen I
BSA
P<0.0001
P=0.0394
P=0.4625
P=0.5056
P=0.0004
P=0.4743
P=0.8030
P=0.7372
P=0.0023
Vector ctrl
β1/β3 kd
β1/β3 kd + P/N/G
Detachment force (nN)
0.5
20
Interaction time (sec)
f
0.5 sec
20 sec
Vector
β1/β3 kd
β1/β3 kd P/N/G
Collagen I, 2 nN
Detachment force (nN)
Distance (µm)
g
Detachment force (nN)
BSA, 0.5 sec, 2 nN
BSA, 20 sec, 2 nN
Vector ctrl
β1/β3 kd
β1/β3 kd + P/N/G
Distance (µm)

Figure S6.

(a-d) Force spectroscopy of cell-surface glycan-binding to collagen fibres using atomic force life cell microscopy. Cell surface glycan-mediated interaction forces to collagen fibres. (a) Coupling of a single cell to a Concanavalin A coated AFM cantilever to probe the force required for cell detachment F [max] from a 3D fibrillar collagen surface. (b) Confocal microscopy of a single force measurement cycle between MV3 vector control and KD cells and collagen I surface, including start position, contact acquisition to the fibre and retraction. Life cell AFM single-cell force spectroscopy for 0.5 s and 20 s interaction time between MV3 cells and collagen I. Repeated cell – matrix interaction on the same collagen spot (47 cells, 3 independent experiments). (c) Force-distance curve of a single force measurement cycle between MV3 cell and collagen surface, including start position (I), retraction (II), and detachment phase (III). The maximum detachment force exerted on the cantilever F_{max} was calculated from the peak to background level. (c, inset) Representation of unbinding events and determination of the step sizes (single rupture / jump events) occuring during the detachment phase (III). (d) Histograms of jump event forces at short contact times (0.5 s contact time). (e) Life cell atomic force spectroscopy for 0.5 s and 20 s interaction time between MV3 cells and collagen I and BSA. Pooled values of F_{max} for all cells (upper panel) and merged values to a mean value for each cell (lower panel) from 3 independent experiments. (f) Averaged retraction curves of MV3 vector control cells (grey, 22 curves), β1/β3 integrin knockdown cells (red, 49 curves) and β1/β3 integrin knockdown cells with glycan removal (green, 50 curves) of 3 independent experiments. (g) Averaged control values for cell to bovine serum albumin (BSA) coated surface. MV3 vector control (0.5 s, 2nN: grey, 28 curves; 20 s, 2nN: grey, 42 curves), β1/β3 integrin knockdown cells (0.5 s, 2nN: red, 45 curves; 20 s, 2nN: red, 33 curves) and cells additionally treated with enzyme cocktail (P/N/G) (0.5 s, 2nN: green, 34 curves; 20 s, 2nN: green, 33 curves). Data sets were compared using ANOVA followed by a Bonferroni test.

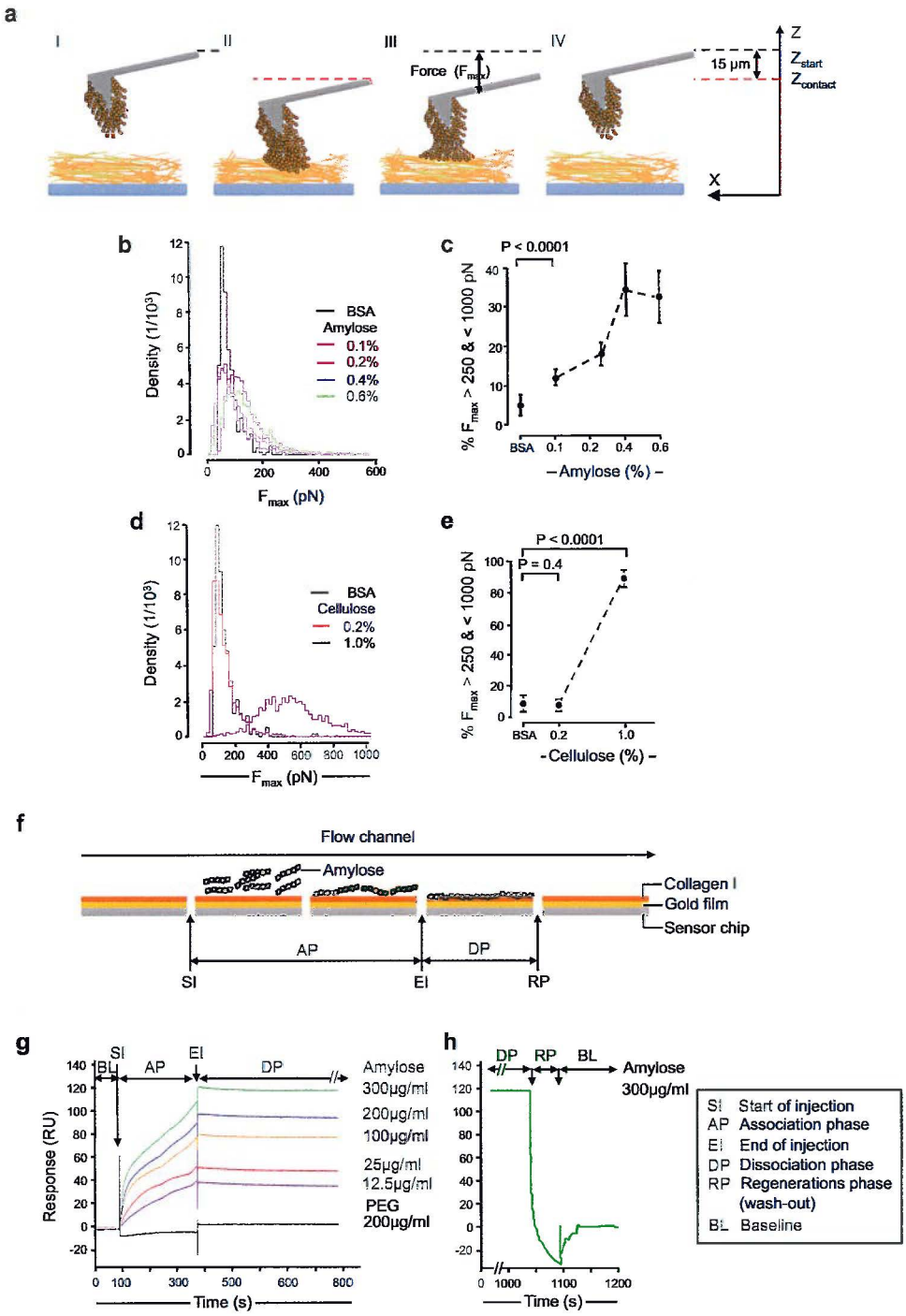
a
I
II
III
IV
Force (F_{max})
15 µm
Z
Z_{start}
$Z_{contact}$
X
b
Density ($1/10^3$)
BSA
Amylose
0.1%
0.2%
0.4%
0.6%
F_{max} (pN)
c
P < 0.0001
% F_{max} > 250 & < 1000 pN
BSA 0.1 0.2 0.4 0.6
– Amylose (%) –
d
Density ($1/10^3$)
BSA
Cellulose
0.2%
1.0%
F_{max} (pN)
e
P < 0.0001
P = 0.4
% F_{max} > 250 & < 1000 pN
BSA 0.2 1.0
- Cellulose (%) –
f
Flow channel
Amylose
Collagen I
Gold film
Sensor chip
AP
DP
SI
EI
RP
g
SI
EI
BL
AP
DP
Response (RU)
Amylose
300µg/ml
200µg/ml
100µg/ml
25µg/ml
12.5µg/ml
PEG
200µg/ml
Time (s)
h
DP
RP
BL
Amylose
300µg/ml
Time (s)
SI Start of injection
AP Association phase
EI End of injection
DP Dissociation phase
RP Regenerations phase (wash-out)
BL Baseline

Figure S7.

Force spectroscopy of glycan-binding to collagen fibers using atomic force microscopy. (a) Covalent coupling of multimeric polysaccharide chains to the surface of the cantilever tip to probe the force (F) required for cantilever detachment from a 3D fibrillar collagen surface. (b) Determination of F [max] with increased amylose coating of the cantilever, compared to background binding (BSA). $P < 0.0001$ for amylose coating 0.2 % and higher, compared to BSA (unpaired two-tailed Mann Whitney test). (c) Representation of 'high-force' interactions above 250 pN with increased coating concentration of amylose. (d-e) Force distribution for low- and high-concentration of cellulose ($p < 0.0001$ compared to BSA control, unpaired two-tailed T test). (f-h) Glycan-mediated binding affinities to collagen fibres monitored by surface plasmon resonance (SPR). (f) Immobilization of bovine collagen I (orange layer) to a carboxymethyldextran-modified gold surface (yellow layer) of a CM5 sensor chip (grey layer) for biospecific interaction analysis in a surface plasmon resonance sensor. Amylose (orange squares) solution is injected as an analyte (SI) and binds to the stationary collagen I ligand during the association phase (AP) followed by the dissociation phase (DP) sustained by buffer flow and finally regeneration phase (RP). (g) Overlay of amylose-collagen I affinity sensorgrams obtained by measurements of changes in the SPR response of increased amylose concentrations. (h) Representation of amylose binding to collagen I after the regeneration phase (RP) obtained with a short pulse of 100mM NaOH at the End of the experiment (wash-out), shown for the sample with the highest amylose concentration (300µg/ml).

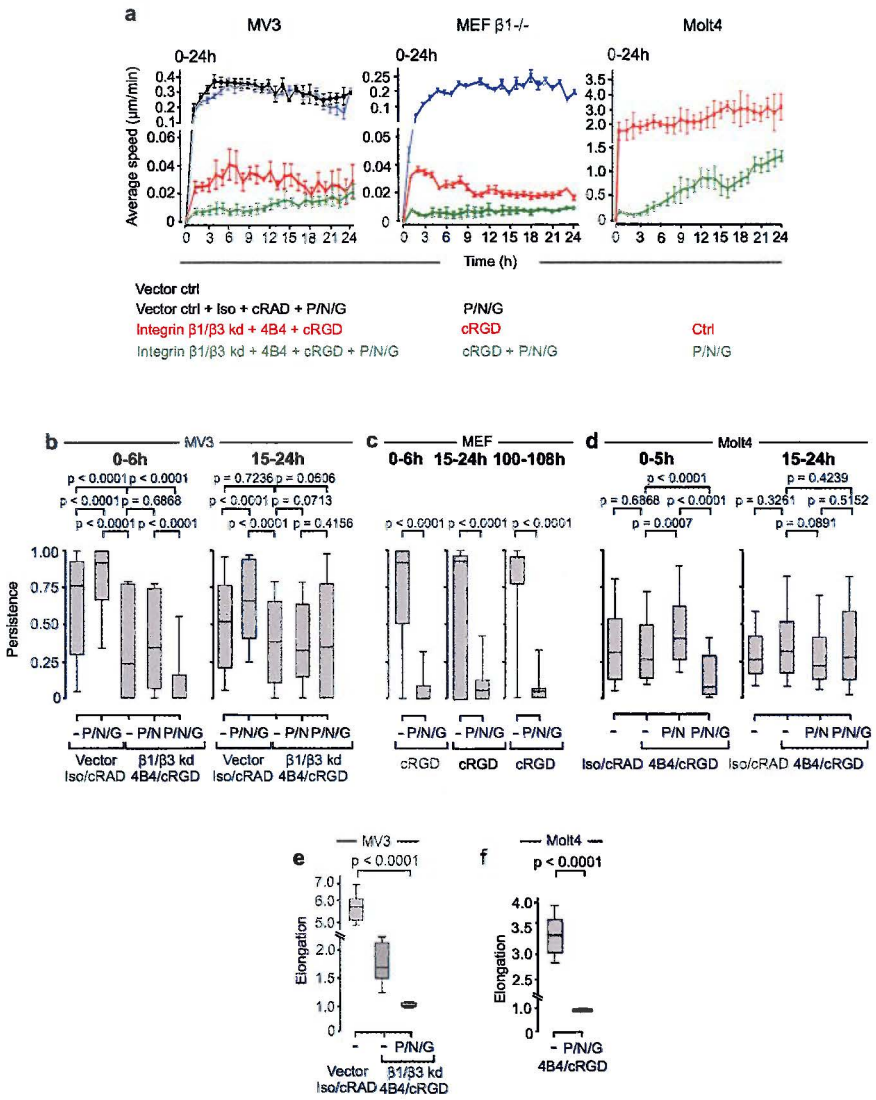

Figure S8.

(a-d) Impact of glycan removal on migration of (a) MV3, MEF and Molt-4 cells and (b-d) migration persistence over 24 h. Black line, average speed of cells without integrin and glycan interference, (blue line) with glycan interference, (red line) after β1/3 integrin knockdown and treatment with mAb 4B4 and cRGD and (green line) with additional glycan removal. Mean average speeds with SEM of 3 independent experiments. (e, f) Impact of glycan removal on morphology of (e) MV3 and (f) Molt-4 cells. Elongation was determined as length/width of cells embedded in 3D collagen I in 3 different experiments. Statistical analysis was obtained by the non-paired Kruskal-Wallis test for independent samples including Bonferoni adjustment (b-d) or including Dunn's multiple comparison test (e, f).

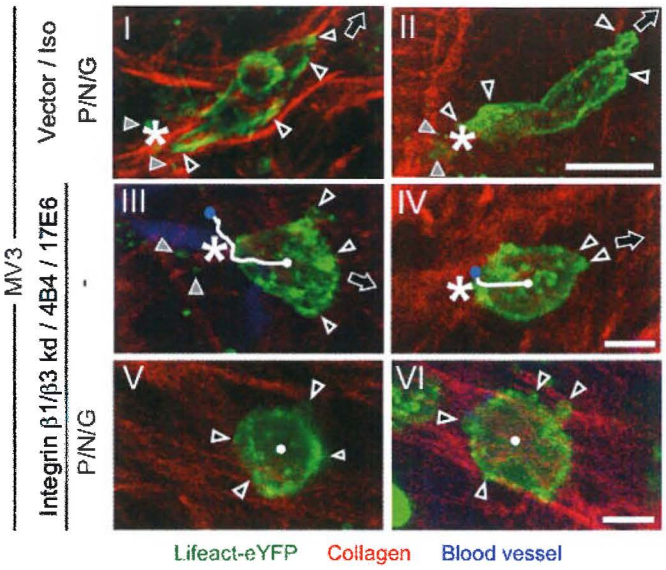

Figure S9.

Re-onset of elongated phenotype of lifeact-expressing MV3 vector control cells and amoeboid migration of MV3 β1/β3 integrin knockdown cells without and with surface glycan removal (P/N/G) after intradermal injection in vivo. ROIs of the imaging field of the dorsal skinfold chamber showing cells with typical morphological phenotypes within 3D collagen of the mouse deep dermis. White lines represent migration paths. Blue dots, startpoints. Arrows, direction of migration, based on retraction fibres and microparticles (I-III, grey-filled arrowheads) released from the cell rear (asterisks). Black-filled arrowheads, focal cell-collagen interaction sites (I, II), polarized (III, IV) and difused (V, VI) distribution of actin-filled membrane blebs. Asterisks, cell rear. (I-II) Bar, 20 µm, (III-VI) Bar, 10µm.

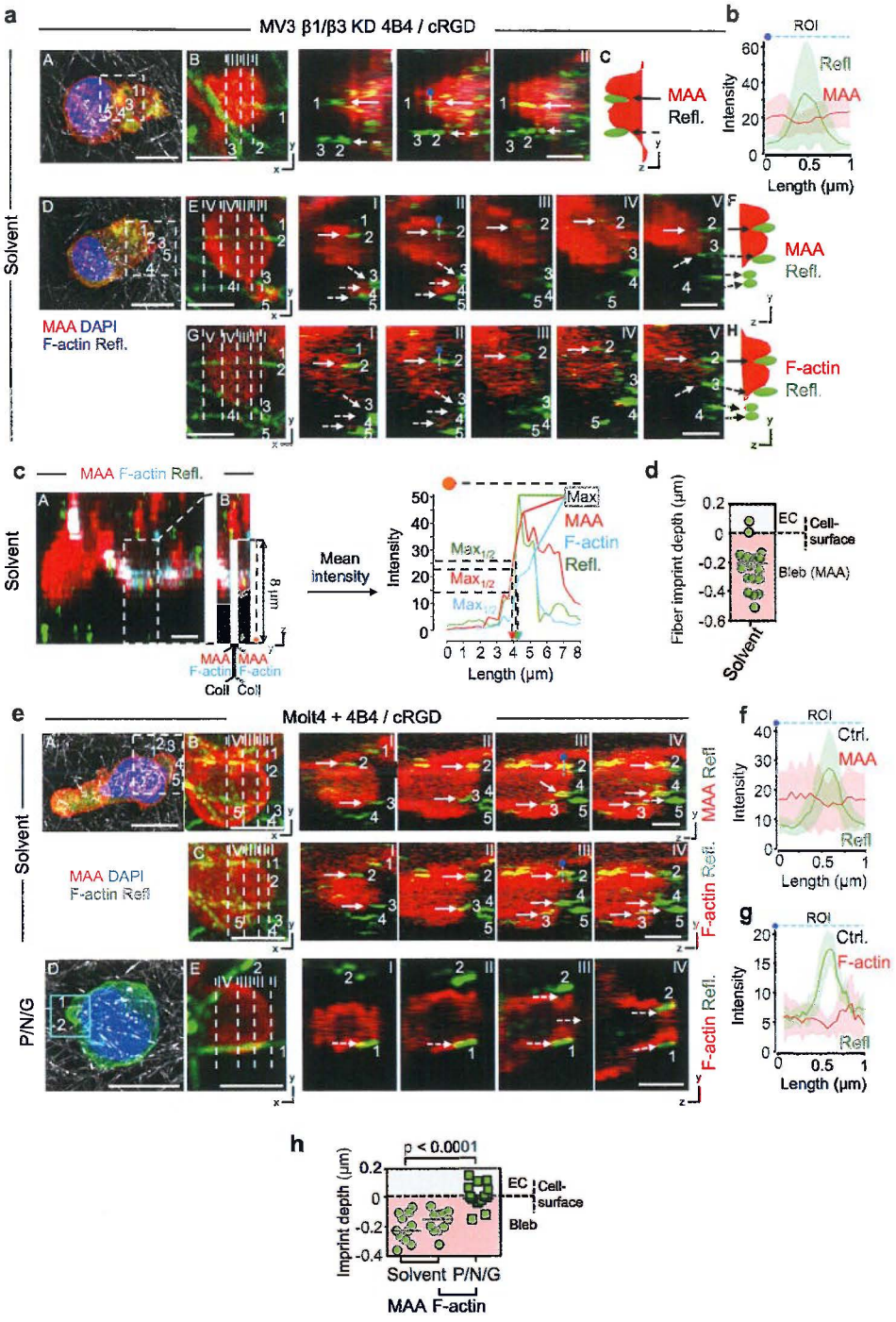
a
MV3 β1/β3 KD 4B4 / cRGD
Solvent
MAA DAPI
F-actin Refl.
MAA
Refl.
F-actin
Refl.
b
ROI
Refl
MAA
Intensity
Length (µm)
c
MAA F-actin Refl.
Solvent
8 µm
MAA F-actin
Coll
Mean intensity
Max
MAA
F-actin
Refl.
Intensity
Length (µm)
d
Fiber imprint depth (µm)
EC
Cell-surface
Bleb (MAA)
Solvent
e
Molt4 + 4B4 / cRGD
Solvent
MAA DAPI
F-actin Refl
P/N/G
MAA Refl.
F-actin Refl.
f
ROI
Ctrl.
MAA
Refl
Intensity
Length (µm)
g
ROI
Ctrl.
F-actin
Refl
Intensity
Length (µm)
h
p < 0.0001
Imprint depth (µm)
EC
Cell-surface
Bleb
Solvent P/N/G
MAA F-actin

Figure S10.

(a: A, D; e: A, D) Maackia amurensis agglutinin (MAA) staining of cell surface β1-4 galactose residues (red signal), F-actin (green signal), collagen I (reflection) and nucleus (DAPI), (a: B; e: B) MAA (red signal), collagen I (green reflection) and (a: E, G; e: C, E) F-actin (red signal), collagen I (green reflection). (a) In 3D collagen I embedded and fixed amoeboid ellipsoid-shaped MV3 cells with β1/β3 integrin interference. Schematic representation of the YZ projections shown in I-III (a: C) and I-V (a: F, H). Arrows, collagen fibers, dipped into the glycan-enriched blebs. Dashed arrows, collagen fibers lateral intercalating in blebs. Numbers indicate collagen fibers. (b) Mean densitometry curves with standard deviation of bleb cross sections (21 curves) with β1-4 galactose residues (red) and collagen I (green). (c) Determination of the imprint depth of Collagen fibers into membrane blebs of MV3 KD cells. (c: A, B) YZ projection of a MAA (red) and F-actin (cyan) positive membrane bleb. Dashed box, region of interest showing MAA signal for β1-4 galactose (c: B, red) and Phalloidin signal for F-actin (c: B, cyan) next to the reflection for collagen I (c: A, B green) signal. White traces indicate the measuring lines with a constant length of 8 µm and a width of 5 pixels. (c: C) Overlay of averaged intensity curves for MAA (red), F-actin (cyan) and collagen I (green) including points of maximal (Max) and half-maximal ($Max_{1/2}$) intensities. (d) Calculation of the fiber imprint depth based on 21 bleb cross sections of MV3 KD cells without glycan removal from 3 independent experiments. (e: A, D) Fixed polarized Molt-4 cell in 3D collagen I with amoeboid shape (e, A) which is completely abrogated after glycan removal (e: D). Cross sections of the ROI (e: B, C, D) shown as YZ projections (I-IV). Arrows, position of collagen I fibers (green). Numbers indicate collagen fibers. (f) Mean densitometry curves of a bleb cross section with β1-4 galactose residues (red, 32 curves) and collagen I (green, 32 curves) and (g) with F-actin (red, 15 curves) and collagen I (green, 15 curves). (h) Calculation of the fiber imprint depth for collagen I fibers in MAA based on 11 cross sections and in F-actin based on 10 cross sections of cell blebs without and 17 bleb cross sections of cells with glycan removal from 3 independent experiments. Molt-4 Bars, 10 µm (a: A, D; e: A, D), 2µm (a: B, E, G; c: A; e: B, C, E). Statistical analysis was obtained for MV3 cells by the non-paired, nonparametric Mann-Whitney t-test.

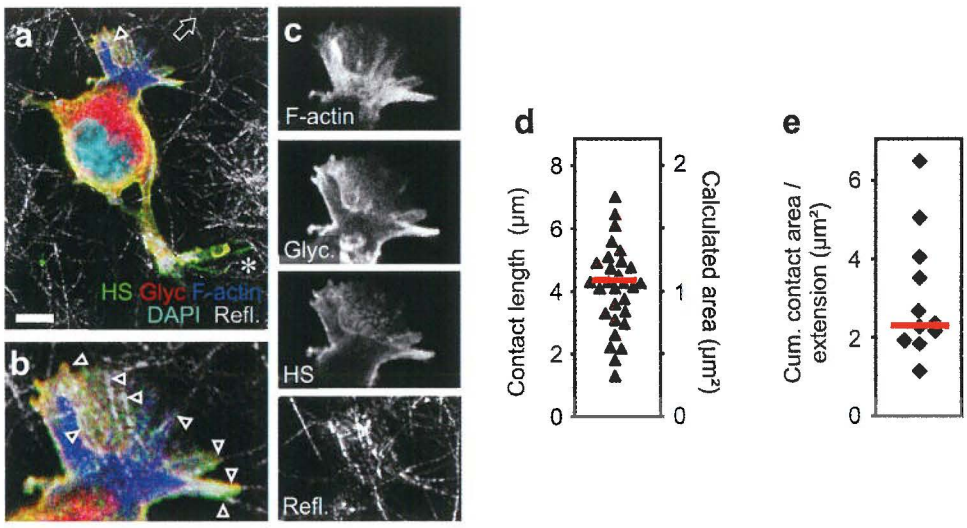

Figure S10.2.

Structure and molecular composition of cellular interactions with collagen fibres. Reconstructions from b1-/- MEF after fixation after 6-h-culture in collagen lattices. (a-c) Non-focalized distribution of heparan sulfate (HS) and glycans (stained by concanavalin A) at the surface of actin-rich filopodia extending along collagen fibres. (d) Length and calculated area of the interface between filopodia and collagen fibres and (e) cumulative contact area of all filopodia originating from the same protrusion (11 cells). The area of contacts was calculated by multiplying contact length by the mean fibre diameter (300 nm). Arrowheads, location of collagen fibres, based on the single-channel reflection images. Arrows, direction of migration, based on retraction fibres or small particles released from the cell rear (asterisks). Bars, 5 µm.

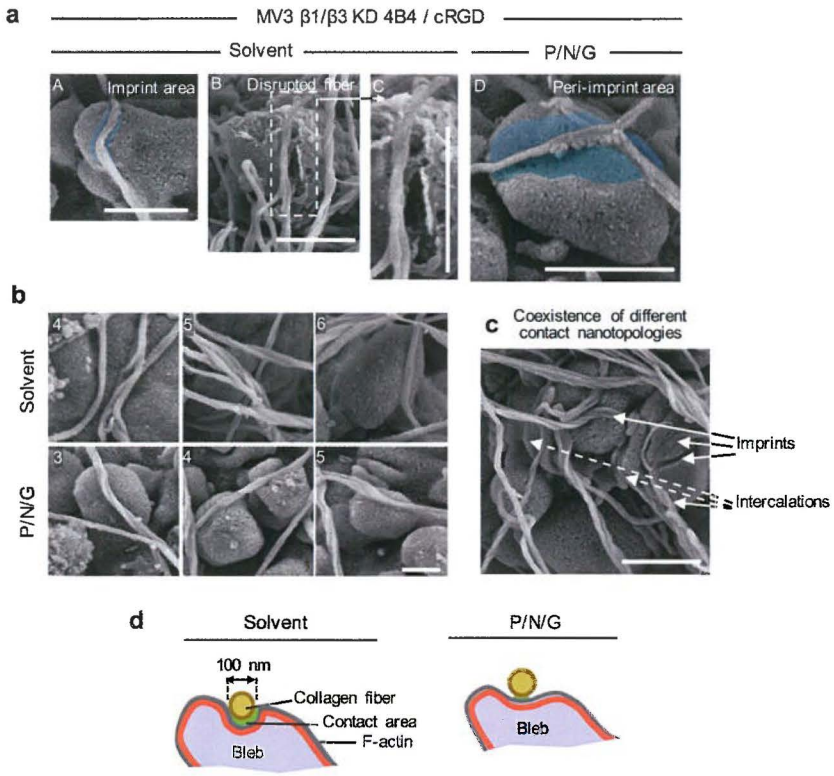

Figure S11.

(a-c) Scanning electron microscopy of MV3 KD cells before and after glycan removal with P/N/G glycosidase cocktail. MV3 cells were fixed after 2h of culture in 3D collagen lattices. ROIs showing collagen fibers which form deep imprints into membrane blebs of MV3 KD cells (a: A-C, b: 4-6) which are absent in cells after P/N/G glycosidase digestion (a: D, b: 3-5). (c) Representative ROI showing coexistence of imprints and intercalations in MV3 KD cells without glycan removal. (d) Schematic representation of the imprint formation between a membrane bleb and a collagen fiber for cells without glycan removal and its loss after interference with cell surface glycosylation. Bars, 0.5µm (a, b), 1 µm (c). Statistical analysis was obtained for MV3 cells by the non-paired, nonparametric Mann-Whitney t-test.

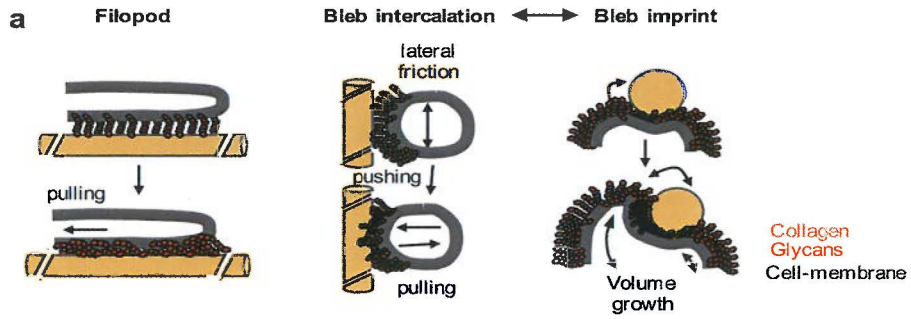

Migration mode	Immobile	Amoeboid		Mesenchymal
		Blebby	Filopodal	

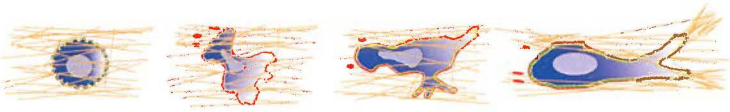

Mechanism of cell-ECM interaction	Passive	Interacalating	Surface glycans	Integrins
Contact organization	Random, loose (detached)	Rigid cell cortex, nonfocalized	Elongated extensions, fan-shaped	Focalized adhesion contacts
Actin organization	Cortical, smooth	Cortical, blebs	Focalized, fibrillar	Focalized
Force generation	None	Propulsive elbowing	Weak pulling	Strong pulling

Figure S12.

Glycans serve as multivalent and universal adhesion scaffold. (a) Glycocalyx- mediated adhesion strategies developed by cells after interference with β1/β3 integrin expression and function. (b) Distinct cell-matrix interactions govern transitions in cell migration strategy. Mesenchymal movement can interconvert into two types of amoeboid migration. The filopodal migration mode is strictly glycocalyx-dependent and reminiscent of Rac/Cdc42 phenotypes, whereas blebby migration is only in part glycan-dependent and mimics the Rho/ROCK phenotype. With decreasing adhesion strength, integrins, surface glycans and blebs provide overlapping cell-matrix interaction systems with decreasing adhesion strength and, concomitantly, reduced migration rates until reaching near-complete cell detachment, loss of polarity, and immobilization.

REFERENCES

1 Ridley, A. J. *et al.* Cell migration: integrating signals from front to back. *Science* **302**, 1704-1709, doi:10.1126/science.1092053 (2003).

2 Palecek, S. P., Loftus, J. C., Ginsberg, M. H., Lauffenburger, D. A. & Horwitz, A. F. Integrin-ligand binding properties govern cell migration speed through cell-substratum adhesiveness. *Nature* **385**, 537-540, doi:10.1038/385537a0 (1997).

3 Paluch, E. K., Aspalter, I. M. & Sixt, M. Focal Adhesion-Independent Cell Migration. *Annual review of cell and developmental biology*, doi:10.1146/annurev-cellbio-111315-125341 (2016).

4 Bergert, M. *et al.* Force transmission during adhesion-independent migration. *Nat Cell Biol* **17**, 524-529, doi:10.1038/ncb3134 (2015).

5 Liu, Y. J. *et al.* Confinement and low adhesion induce fast amoeboid migration of slow mesenchymal cells. *Cell* **160**, 659-672, doi:10.1016/j.cell.2015.01.007 (2015).

6 Lammermann, T. *et al.* Rapid leukocyte migration by integrin-independent flowing and squeezing. *Nature.* **453**, 51-55 (2008).

7 Cukierman, E., Pankov, R., Stevens, D. R. & Yamada, K. M. Taking cell-matrix adhesions to the third dimension. *Science.* **294**, 1708-1712 (2001).

8 Hood, J. D. & Cheresh, D. A. Role of integrins in cell invasion and migration. *Nat.Rev.Cancer.* **2**, 91-100 (2002).

9 Maaser, K. *et al.* Functional hierarchy of simultaneously expressed adhesion receptors: integrin alpha2beta1 but not CD44 mediates MV3 melanoma cell migration and matrix reorganization within three-dimensional hyaluronan-containing collagen matrices. *Mol.Biol. Cell.* **10**, 3067-3079 (1999).

10 Stupack, D. G., Puente, X. S., Boutsaboualoy, S., Storgard, C. M. & Cheresh, D. A. Apoptosis of adherent cells by recruitment of caspase-8 to unligated integrins. *J Cell Biol* **155**, 459-470, doi:10.1083/jcb.200106070 (2001).

11 Keely, P. J., Westwick, J. K., Whitehead, I. P., Der, C. J. & Parise, L. V. Cdc42 and Rac1 induce integrin-mediated cell motility and invasiveness through PI(3)K. *Nature* **390**, 632-636, doi:10.1038/37656 (1997).

12 Friedl, P. & Wolf, K. Tumour-cell invasion and migration: diversity and escape mechanisms. *Nat.Rev.Cancer.* **3**, 362-374 (2003).

13 Brockbank, E. C., Bridges, J., Marshall, C. J. & Sahai, E. Integrin beta1 is required for the invasive behaviour but not proliferation of squamous cell carcinoma cells in vivo. *Br J Cancer* **92**, 102-112, doi:10.1038/sj.bjc.6602255 (2005).

14 Friedl, P., Entschladen, F., Conrad, C., Niggemann, B. & Zanker, K. S. CD4+ T lymphocytes migrating in three-dimensional collagen lattices lack focal adhesions and utilize beta1 integrin-independent strategies for polarization, interaction with collagen fibers and locomotion. *Eur.J.Immunol.* **28**, 2331-2343 (1998).

15 Hegerfeldt, Y., Tusch, M., Brocker, E. B. & Friedl, P. Collective cell movement in primary melanoma explants: plasticity of cell-cell interaction, beta1-integrin function, and migration strategies. *Cancer Res.* **62**, 2125-2130 (2002).

16 Carragher, N. O. *et al.* Calpain 2 and Src dependence distinguishes mesenchymal and amoeboid modes of tumour cell invasion: a link to integrin function. *Oncogene.* **25**, 5726-5740 (2006).

17 Zaman, M. H. *et al.* Migration of tumor cells in 3D matrices is governed by matrix stiffness along with cell-matrix adhesion and proteolysis. *Proc.Natl.Acad.Sci.U.S.A.* **103**, 10889-10894 (2006).

18 Takada, Y., Wayner, E. A., Carter, W. G. & Hemler, M. E. Extracellular matrix receptors, ECMRII and ECMRI, for collagen and fibronectin correspond to VLA-2 and VLA-3 in the VLA family of heterodimers. *J Cell Biochem* **37**, 385-393, doi:10.1002/jcb.240370406 (1988).

19 Klein, C. E. *et al.* Integrin alpha 2 beta 1 is upregulated in fibroblasts and highly aggressive melanoma cells in three-dimensional collagen lattices and mediates the reorganization of collagen I fibrils. *J Cell Biol* **115**, 1427-1436 (1991).

20 Knight, B. *et al.* Visualizing muscle cell migration in situ. *Curr Biol* **10**, 576-585 (2000).

21 Wolf, K. *et al.* Compensation mechanism in tumor cell migration: mesenchymal-amoeboid transition after blocking of pericellular proteolysis. *J Cell Biol* **160**, 267-277, doi:10.1083/jcb.200209006 (2003).

22 Sahai, E. & Marshall, C. J. Differing modes of tumour cell invasion have distinct requirements for Rho/ROCK signalling and extracellular proteolysis. *Nat.Cell Biol.* **5**, 711-719 (2003).

23 Lammermann, T. & Sixt, M. Mechanical modes of 'amoeboid' cell migration. *Curr.Opin.Cell Biol.* (2009).

24 Naor, D., Nedvetzki, S., Golan, I., Melnik, L. & Faitelson, Y. CD44 in cancer. *Crit Rev.Clin.Lab Sci.* **39**, 527-579 (2002).

25 Negi, L. M. *et al.* Role of CD44 in tumour progression and strategies for targeting. *J Drug Target* **20**, 561-573, doi:10.3109/1061186X.2012.702767 (2012).

26 Couchman, J. R. Syndecans: proteoglycan regulators of cell-surface microdomains? *Nat.Rev. Mol.Cell Biol.* **4**, 926-937 (2003).

27 Longley, R. L. *et al.* Control of morphology, cytoskeleton and migration by syndecan-4. *J.Cell Sci.* **112**, 3421-3431 (1999).

28 Chalkiadaki, G. *et al.* Fibroblast growth factor-2 modulates melanoma adhesion and migration through a syndecan-4-dependent mechanism. *Int.J.Biochem.Cell Biol.* **41**, 1323-1331 (2009).

29 Midwood, K. S., Valenick, L. V., Hsia, H. C. & Schwarzbauer, J. E. Coregulation of fibronectin signaling and matrix contraction by tenascin-C and syndecan-4. *Mol.Biol.Cell.* **15**, 5670-5677 (2004).

30 Fey, P., Stephens, S., Titus, M. A. & Chisholm, R. L. SadA, a novel adhesion receptor in Dictyostelium. *J Cell Biol* **159**, 1109-1119, doi:10.1083/jcb.200206067 (2002).

31 Eichinger, L. *et al.* The genome of the social amoeba Dictyostelium discoideum. *Nature* **435**, 43-57, doi:10.1038/nature03481 (2005).

32 Cornillon, S. *et al.* An adhesion molecule in free-living Dictyostelium amoebae with integrin beta features. *EMBO Rep* **7**, 617-621, doi:10.1038/sj.embor.7400701 (2006).

33 Sebe-Pedros, A., Roger, A. J., Lang, F. B., King, N. & Ruiz-Trillo, I. Ancient origin of the integrin-mediated adhesion and signaling machinery. *Proc Natl Acad Sci U S A* **107**, 10142-10147, doi:10.1073/pnas.1002257107 (2010).

34 Wang, Y., Slade, M. B., Gooley, A. A., Atwell, B. J. & Williams, K. L. Cellulose-binding modules from extracellular matrix proteins of Dictyostelium discoideum stalk and sheath. *Eur J Biochem* **268**, 4334-4345 (2001).

35 Faassen, A. E. *et al.* A cell surface chondroitin sulfate proteoglycan, immunologically related to CD44, is involved in type I collagen-mediated melanoma cell motility and invasion. *J Cell Biol* **116**, 521-531 (1992).

36 Zimmerman, E., Geiger, B. & Addadi, L. Initial stages of cell-matrix adhesion can be mediated and modulated by cell-surface hyaluronan. *Biophys.J.* **82**, 1848-1857 (2002).

37 Fuster, M. M. & Esko, J. D. The sweet and sour of cancer: glycans as novel therapeutic targets. *Nat Rev Cancer* **5**, 526-542, doi:10.1038/nrc1649 (2005).

38 Mandeville, J. T., Lawson, M. A. & Maxfield, F. R. Dynamic imaging of neutrophil migration in three dimensions: mechanical interactions between cells and matrix. *J.Leukoc.Biol.* **61**, 188-200 (1997).

39 Stowell, S. R., Ju, T. & Cummings, R. D. Protein glycosylation in cancer. *Annu Rev Pathol* **10**, 473-510, doi:10.1146/annurev-pathol-012414-040438 (2015).

40 Pinho, S. S. & Reis, C. A. Glycosylation in cancer: mechanisms and clinical implications. *Nat Rev Cancer* **15**, 540-555, doi:10.1038/nrc3982 (2015).

41 Koda, J. E., Rapraeger, A. & Bernfield, M. Heparan sulfate proteoglycans from mouse mammary epithelial cells. Cell surface proteoglycan as a receptor for interstitial collagens. *J.Biol.Chem.* **260**, 8157-8162 (1985).

42 Megens, R. T. *et al.* Two-photon microscopy of vital murine elastic and muscular arteries. Combined structural and functional imaging with subcellular resolution. *J Vasc Res* **44**, 87-98, doi:10.1159/000098259 (2007).

43 van Haaren, P. M., VanBavel, E., Vink, H. & Spaan, J. A. Localization of the permeability barrier to solutes in isolated arteries by confocal microscopy. *Am J Physiol Heart Circ Physiol* **285**, H2848-2856, doi:10.1152/ajpheart.00117.2003 (2003).

44 Ito, S. Structure and function of the glycocalyx. *Federation proceedings* **28**, 12-25 (1969).

45 Martins Mde, F. & Bairos, V. A. Glycocalyx of lung epithelial cells. *International review of cytology* **216**, 131-173 (2002).

46 Daniels, M. A., Hogquist, K. A. & Jameson, S. C. Sweet 'n' sour: the impact of differential glycosylation on T cell responses. *Nat Immunol* **3**, 903-910, doi:10.1038/ni1002-903 (2002).

47 Bi, S. & Baum, L. G. Sialic acids in T cell development and function. *Biochim Biophys Acta* **1790**, 1599-1610, doi:10.1016/j.bbagen.2009.07.027 (2009).

48 Jacobelli, J. *et al.* Confinement-optimized three-dimensional T cell amoeboid motility is modulated via myosin IIA-regulated adhesions. *Nat Immunol* **11**, 953-961, doi:10.1038/ni.1936 (2010).

49 Evans, E. A. & Calderwood, D. A. Forces and bond dynamics in cell adhesion. *Science* **316**, 1148-1153, doi:10.1126/science.1137592 (2007).

50 Helenius, J., Heisenberg, C. P., Gaub, H. E. & Muller, D. J. Single-cell force spectroscopy. *J Cell Sci* **121**, 1785-1791, doi:10.1242/jcs.030999 (2008).

51 Laukaitis, C. M., Webb, D. J., Donais, K. & Horwitz, A. F. Differential dynamics of alpha 5 integrin, paxillin, and alpha-actinin during formation and disassembly of adhesions in migrating cells. *J Cell Biol* **153**, 1427-1440 (2001).

52 Taubenberger, A. *et al.* Revealing early steps of alpha2beta1 integrin-mediated adhesion to collagen type I by using single-cell force spectroscopy. *Mol Biol Cell* **18**, 1634-1644, doi:10.1091/mbc.E06-09-0777 (2007).

53 Paluch, E., Sykes, C., Prost, J. & Bornens, M. Dynamic modes of the cortical actomyosin gel during cell locomotion and division. *Trends Cell Biol* **16**, 5-10, doi:10.1016/j.tcb.2005.11.003 (2006).

54 van Kuppevelt, T. H., Dennissen, M. A., van Venrooij, W. J., Hoet, R. M. & Veerkamp, J. H. Generation and application of type-specific anti-heparan sulfate antibodies using phage display technology. Further evidence for heparan sulfate heterogeneity in the kidney. *The Journal of biological chemistry* **273**, 12960-12966 (1998).

55 Smits, N. C. *et al.* Phage display-derived human antibodies against specific glycosaminoglycan epitopes. *Methods Enzymol* **416**, 61-87, doi:10.1016/S0076-6879(06)16005-X (2006).

56 Lensen, J. F. *et al.* Selection and characterization of a unique phage display-derived antibody against dermatan sulfate. *Matrix Biol* **25**, 457-461, doi:10.1016/j.matbio.2006.06.003 (2006).

57 Smetsers, T. F. *et al.* Human single-chain antibodies reactive with native chondroitin sulfate detect chondroitin sulfate alterations in melanoma and psoriasis. *J Invest Dermatol* **122**, 707-716, doi:10.1111/j.0022-202X.2004.22316.x (2004).

58 Kissler, S. *et al.* In vivo RNA interference demonstrates a role for Nramp1 in modifying susceptibility to type 1 diabetes. *Nat Genet* **38**, 479-483, doi:10.1038/ng1766 (2006).

59 Venter, G. *et al.* Glucose controls morphodynamics of LPS-stimulated macrophages. *PLoS One* **9**, e96786, doi:10.1371/journal.pone.0096786 (2014).

60 Jat, P. S. *et al.* Direct derivation of conditionally immortal cell lines from an H-2Kb-tsA58 transgenic mouse. *Proc Natl Acad Sci U S A* **88**, 5096-5100 (1991).

61 Graus-Porta, D. *et al.* Beta1-class integrins regulate the development of laminae and folia in the cerebral and cerebellar cortex. *Neuron* **31**, 367-379 (2001).

62 Caswell, P. T. *et al.* Rab25 associates with alpha5beta1 integrin to promote invasive migration in 3D microenvironments. *Developmental cell* **13**, 496-510, doi:10.1016/j.devcel.2007.08.012 (2007).

63 Friedl, P. & Brocker, E. B. Reconstructing leukocyte migration in 3D extracellular matrix by time-lapse videomicroscopy and computer-assisted tracking. *Methods Mol Biol* **239**, 77-90 (2004).

64 Wolf, K. *et al.* Multi-step pericellular proteolysis controls the transition from individual to collective cancer cell invasion. *Nat.Cell Biol.* **9**, 893-904 (2007).

65 Cox, S. M., Baur, P. S. & Haenelt, B. Retention of the glycocalyx after cell detachment by EGTA. *J Histochem Cytochem* **25**, 1368-1372 (1977).

66 Benoit, M., Gabriel, D., Gerisch, G. & Gaub, H. E. Discrete interactions in cell adhesion measured by single-molecule force spectroscopy. *Nat Cell Biol* **2**, 313-317, doi:10.1038/35014000 (2000).

67 Puech, P. H., Poole, K., Knebel, D. & Muller, D. J. A new technical approach to quantify cell-cell adhesion forces by AFM. *Ultramicroscopy* **106**, 637-644, doi:10.1016/j.ultramic.2005.08.003 (2006).

68 Te Riet, J. *et al.* Dynamic coupling of ALCAM to the actin cortex strengthens cell adhesion to CD6. *J Cell Sci* **127**, 1595-1606, doi:10.1242/jcs.141077 (2014).

69 Friedrichs, J., Helenius, J. & Muller, D. J. Quantifying cellular adhesion to extracellular matrix components by single-cell force spectroscopy. *Nat Protoc* **5**, 1353-1361, doi:10.1038/nprot.2010.89 (2010).

70 te Riet, J. *et al.* Interlaboratory round robin on cantilever calibration for AFM force spectroscopy. *Ultramicroscopy* **111**, 1659-1669, doi:10.1016/j.ultramic.2011.09.012 (2011).

71 Janovjak, H., Struckmeier, J. & Muller, D. J. Hydrodynamic effects in fast AFM single-molecule force measurements. *Eur Biophys J* **34**, 91-96, doi:10.1007/s00249-004-0430-3 (2005).

72 Thevenaz, P., Ruttimann, U. E. & Unser, M. A pyramid approach to subpixel registration based on intensity. *IEEE Trans Image Process* **7**, 27-41, doi:10.1109/83.650848 (1998).

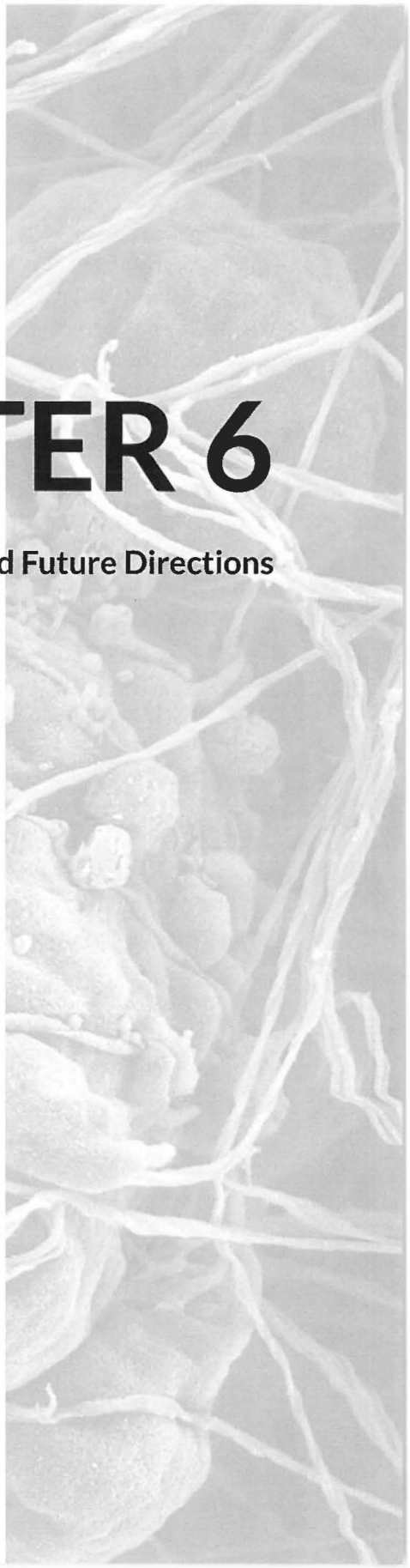

CHAPTER 6

Summary, Conclusion and Future Directions

Summary

This thesis provides a first evidence for a direct relation between glycocalyx polarity and integrin-independent cell adhesion and migration. To prove this relationship, novel approaches were established, including glycan detection and glycan digestion, or adapted to study glycan-mediated adhesion, force generation and cell migration *in vitro* and *in vivo*. The new insights and further molecular characterization will contribute to a better understanding of the glycocalyx in distinct modes of cell migration and invasion and may have predictive value in targeting tumor progression and metastasis.

Cancer is one of the leading causes of death worldwide with 14 million new cases and 8.2 million cancer-related deaths in 2012 (World Health Organization 2016). During and after their transformation into neoplasm cancer cells make use of the intrinsic capacity of normally resident tissue cells to migrate upon activation, a process typically employed by cells during morphogenesis, immune response and wound healing.

Important steps to initiate tumor dissemination and metastasis formation are the penetration and degradation of the basement membrane, the detachment of tumor cells from the primary tumor, and invasion into the extracellular matrix (ECM)- rich connective tissue for further dissemination.[1] The common process underlying cell migration through ECM is polarized actin polymerization-mediated protrusion, actomyosin-driven contraction, and resulting shape change and forward locomotion of the cell body[2]. To establish contact with and transmit actomyosin-driven forces to the surrounding ECM, the cell either develops protrusions that form adhesion sites to the tissue through adhesion receptors, e.g. integrins or alternative receptors[3]; or on the other hand, cells may use poorly adhesive intercalation or propulsion into ECM-free clefts, or friction against confining ECM fibers.[4] The role of integrins in cell migration has been conclusively described over the last decades, but how alternative adhesion-systems are involved in adhesion and de-adhesion processes is still challenging and remains largely unclear.

The motivation to study the contribution of the glycocalyx to tumor cell adhesion and migration was due to the fact that cells, despite inhibition of β1 integrin, the dominant adhesion receptor to fibrillar collagen I, maintained the ability to migrate in three-dimensional fibrillar collagen.[5] Following integrin inhibition, MV3 human melanoma cells and murine embryonic fibroblasts (MEFs) underwent a morphological and migratory transition from a mesenchymal to an amoeboid filopodal or amoeboid blebbing phenotype and maintained substrate contact and migration with lower speeds (Chapter 5). Human T-leukemia cells, on the opposite, maintained adhesion and migration at constant speeds after integrin interference in 3D fibrillar collagen, corresponding to a natural amoeboid

morphology and migration mode by integrin-independent mechanisms [6, 4d, 5b, 7]. Based on these findings, the alternative mechanisms used by cells to compensate for their loss of integrin-mediated adhesion and migration were the focus of this thesis.

Alternative adhesion mechanisms in cell adhesion and migration

As summarized in **Chapter 2**, next to the integrin superfamily of adhesion receptors, a collection of alternative cell surface receptors was attributed to contribute to cell anchoring and migration. The expression of a set of putative collagen receptors was measured in MV3 melanoma cells, including proteoglycans CD44, syndecan-4 (SDC-4), and receptor tyrosine kinase discoidin domain receptors (DDR) 1 and 2. Whereas CD44 was consistently expressed, no expression of DDR-1 and -2 or SDC-4 was detected (Chapter 5). CD44 perturbing antibody did not affect the migration of MV3 cells in 3D fibrillar collagen.[8] This was confirmed independently here for cells after interference with β1 and β3 integrins as CD44 blockage showed no effect on the residual amoeboid cell migration. Consequently no indication for CD44 as a potential compensation receptor in these cells was obtained. Because every cell carries a strongly polar outer layer, the glycocalyx, the work in this thesis focused on the role of the glycocalyx in mediating residual adhesion and migration of cells. The here presented new insights identify the sticky property of the glycocalyx as adhesion mechanism through which cells can generate adhesion forces to collagen in the piconewton range and support integrin-independent adhesion and migration *in vitro* and *in vivo*. In summary, a novel adhesion mechanism is identified which mediates cell substrate interaction to solid-state ligands, which may be relevant when integrin-mediated attachment is restricted or even impossible, e.g. due to integrin receptor downregulation and / or limited accessibility of ligands.

Detection and enzymatic degradation of the glycocalyx on live cells

In **Chapter 3**, Bicyclo [6.1.0] nonyne (BCN) was introduced as a novel probe for biorthogonal labeling, which provides an appropriate staining tool for visualization of glycans including sialic acids in living cells. There is a strong need for staining tools that allow the detection of glycan moieties in living cells since reporter techniques, e.g. GFP fluorescent fusion proteins are not applicable for glycan imaging. Further, glycan-binding proteins (lectins) influence cell function by crosslinking surface receptors, and antibodies recognizing small glycan structures are rare. Cells incubated with BCN retained morphological integrity and viability allowing subsequent functional studies, e.g. cell migration assays.

In **Chapter 4**, to investigate the influence of the glycocalyx as polar layer in cell adhesion, a protocol was developed that allows a gradual enzymatic degradation of carbohydrate chains while maintaining optimal viability. The efficient digestion of the bulk glycocalyx was shown using conventional staining with antibodies for glycosaminoglycans (GAGs) and lectin for β-1,4 galactose (Gal), but also bioorthogonal labeling of sialic acids (SAs). Lectins recognize their epitopes with a certain carbohydrate binding specificity. In contrast, bioorthogonal labeling enables the detection of "global" sialic acid residues and their enzymatic degradation in one step regardless of the orientation of the glycosidic bonds. The results identify differences in the composition of the glycocalyx between the analyzed cell types. MV3 human melanoma cells and murine embryonic fibroblasts (MEFs) showed high expression patterns for glycosaminoglycans (GAGs), sialic acids (SAs) and galactoses (Gal), whereas Molt-4 immune cells expressed only small amounts of GAGs, but similar amounts of SAs and Gal.

In order to retain identical glycan digestion conditions for all cells and enable direct cell-to-cell comparison, Molt-4 cells were treated equally to MV3 cells and MEFs. The digestion procedure combines a yet unprecedented number and type of high-purity glycosidases in a two-step procedure to remove first the outer layer of the glycocalyx followed by quantitative removal of the bulk of most glycocalyx layers, while – importantly – retaining cell viability. This digestion strategy was instrumental to probe cell functions, including adhesion, migration and formation of contact structures to complex-shaped interaction with fibrillar collagen and identify specific functions of the glycocalyx in cell-matrix interactions.

Digestion of the glycocalyx to study its role in migration *in vitro* and *in vivo*

To study the influence of the glycocalyx on cell migration, the glycan digestion protocol (Chapter 4) was combined with integrin interference strategies in **Chapter 5** to perform cell migration analysis *in vitro* and *in vivo*. The results show that digestion of the glycosaminoglycans (GAGs), including heparan sulfate (HS), chondroitin sulfate (CS), dermatan sulfate (DS), and sialic acids (SAs) were insufficient to impair migration. Additional removal of β-1,4 galactose (Gal) caused a transient loss of migration in integrin inhibited cells, that were either embedded in 3D collagen I gel *in vitro* or in the collagen-rich mouse dermis *in vivo*. This was accompanied by a transition from the amoeboid-polarized to a complete roundish phenotype. The disabled migration and round morphology lasted for 7 to 10 hours, depending on the used cell line, and was followed by a step-wise recovery of the amoeboid migration phenotype, which occurred concurrently with re-expression of endogenous surface glycans. These results indicate that glycan-matrix interactions are not exclusively reserved for negatively charged glycan chains or

residues[9], but rather require additional contribution of less complex carbohydrates such as β 1-4 galactoses. Thus, besides negative cell surface charge mediated by GAGs and sialic acids, bipolar interactions mediated by β-1,4 galactose are essential to facilitate contact to collagen I fibers and thereby enable integrin-independent adhesion and migration. The ability of cells to generate non-specific weak molecular interactions to ECM, independent of predicted epitopes, facilitates a more rapid adaptation to steadily changing environments that are abundant in biological systems and would usually require a realignment of receptor expression.

Adhesion forces mediated by the glycocalyx *in vitro*

To explore whether the glycocalyx functions as direct adhesion scaffold that mediates integrin-independent migration, glycan-mediated adhesion strength was quantified in Chapter 5. Single-cell force spectroscopy (SCFS) was used to study the dynamic formation of cellular adhesion to a fibrillar collagen surface. SCFS allows for controlled and accurate screening of cell-substrate interactions even for short contact times, a prerequisite for early measurements of glycan-mediated integrin-independent adhesion events[10] with piconewton accuracy.[11] The results summarized in Chapter 5 show substantial interaction forces between the glycocalyx of MV3 human melanoma cells and collagen after integrin interference. This interaction force was lost after enzymatic glycan removal. Measured binding forces rapidly exceeded 500 pN at short interaction times (0.5 sec). This indicates that integrin- and glycan-mediated adhesion occur concurrently, however interference with integrins was required to accurately detect the mediated adhesion by the glycocalyx. Future work will be required to identify the mechanisms of glycan-collagen binding, such as electrostatic bonds, hydrogen bonds and van der Waals forces.[12]

Glycocalyx-mediated adhesion develops different contact nanotopologies to fibrillar collagen

As summarized in Chapter 5, diffraction-limited 3D confocal microscopy combined with 3D scanning electron microscopy of MV3 melanoma control and enzyme-treated cells revealed that glycan-dependent cell interactions to collagen fibers consisted of actin-rich cell filopodal or bleb-like protrusions engaging with collagen fibers. In dependence on glycan availability, these cell protrusions form morphologically diverse interfaces. They contain focalized galactosyl residues, include single blebs forming grip-like structures that generate a complex-shaped, "grasp-like" interphase to collagen fibers. Additional interaction types, which appeared independent of glycan availability, included collagen

fiber intercalation lateral to blebs with deep imprints across the cell body in high-density ECM regions. This identifies the glycocalyx as mediator for complex-shaped membrane topologies that provide 3D interactions to complex-shaped extracellular topologies. By mediating adhesion through adaptive interfaces, novel adhesion mechanisms beyond integrin-mediated mechanocoupling were identified. These findings will contribute to a better understanding of the broad range of adaptations cells might acquire to facilitate and maintain adhesion and migration in response to the heterogeneous environmental demands found in the body.

Conclusion and future directions

Over the past decades, insight has been gained into the role of the glycocalyx in various biological processes, including tumor cell adhesion, migration and invasion. Transformation of normal cells into cancer cells results in significant changes in glycosylation[1, 13], indicating a role of the glycocalyx in tumor formation and metastasis.[14] As consensus strategy, previous research focussed on proteoglycans and glycoproteins as specific glycan chains presented by corresponding protein cores that bridge the cell membrane and induce intracellular signal transduction. In this thesis, an alternative concept on glycan chains forming a sticky coat for cell-substrate interaction and amoeboid migration was established. The results indicate that the glycocalyx is indispensable for cell adhesion and migration when integrin functions are disabled. The introduced findings present the sticky glycocalyx as an active mediator for integrin-independent cell adhesion and migration and provide a strong potential for further studies that investigate the cytoskeletal steps underlie the revealed complex topology. It would be interesting to find out whether cells can adopt diverse topologies or whether specific shapes are preferred. Can glycocalyx-interfered cells recover membrane topologies under certain circumstances or conditions such as higher compression found e.g. in more confined tissues? Are these glycan adhesions relevant to all cells under all circumstances or only during specific, low-adhesion conditions?

In terms of glycan mediated adhesion there is a strong need for the understanding, which signals are generated by glycan adhesions. Following bleb adhesion subsequent molecular steps are required to stabilize the bleb-matrix contact, generate actin polymerization and myosin-mediated contraction[15], but how does glycan adhesion enable downstream signaling events that ultimately lead to migration? One should note, also integrins comprise over 20 potential N-glycosylation binding sites that have crucial functions in the regulation of integrin-mediated migration[16], but further studies are needed to understand how glycan-mediated adhesions cooperate with integrin-mediated interactions. In this thesis, collagen I, the main structural protein in the extracellular

space[17], was exclusively used for adhesion and migration assays. Further studies should also implement matrices others than collagen I to define the glycocalyx- mediated adhesion as a general mechanism in the heterogeneous system of the body. Fibronectin e.g. was found to comprise highly basic triple helical domains including disaccharide acceptor sites[9a, 9b, 18] as specific binding sites for negatively charged glycosaminoglycans, indicating a pro-adhesive function for glycans, similar to fibrillar collagen. The results will provide significant contribution to the understanding of processes underlying cell adhesion and migration in steadily changing environments, which require dynamic adaptations diverse sets of adhesion strategies to deal with complex substrate topologies and molecular composition and maintain mobility.

Studies related to glycomics are generally cost-intensive. A combination of experimental approaches by e.g. implementing computer simulations or molecular dynamics (MD) simulations might contribute to the understanding of glycocalyx-mediated functions and mechanisms in these processes prior to *in vitro* or even *in vivo* experiments. Current *in situ* approaches such as MD provide the technical requirements for a detailed and dynamic representation and simulation of biological mechanisms, that are recently accurately described for the glycocalyx.[19] The ability to witness such changes in the context of living organisms would augment our understanding of systems biology and provide new clinical tools for disease diagnosis.

References

[1] M. M. Fuster, J. D. Esko, *Nat Rev Cancer* 2005, ***5***, 526-542.

[2] aA. J. Ridley, M. A. Schwartz, K. Burridge, R. A. Firtel, M. H. Ginsberg, G. Borisy, J. T. Parsons, A. R. Horwitz, *Science* **2003**, *302*, 1704-1709; bS. P. Palecek, C. E. Schmidt, D. A. Lauffenburger, A. F. Horwitz, *J Cell Sci* **1996**, *109 (Pt 5)*, 941-952.

[3] H. Maekawa, Y. Oike, S. Kanda, Y. Ito, Y. Yamada, H. Kurihara, R. Nagai, T. Suda, *Arterioscler Thromb Vasc Biol* **2003**, *23*, 2008-2014.

[4] aE. Paluch, C. Sykes, J. Prost, M. Bornens, *Trends Cell Biol* **2006**, *16*, 5-10; bO. T. Fackler, R. Grosse, *J.Cell Biol.* **2008**, *181*, 879-884; cV. Sanz-Moreno, C. J. Marshall, *Cell Cycle* **2009**, *8*, 1484-1487; dT. Lammermann, B. L. Bader, S. J. Monkley, T. Worbs, R. Wedlich-Soldner, K. Hirsch, M. Keller, R. Forster, D. R. Critchley, R. Fassler, M. Sixt, *Nature.* **2008**, *453*, 51-55.

[5] aP. Friedl, *Curr.Opin.Cell Biol.* **2004**, *16*, 14-23; bN. O. Carragher, S. M. Walker, L. A. Scott Carragher, F. Harris, T. K. Sawyer, V. G. Brunton, B. W. Ozanne, M. C. Frame, *Oncogene.* **2006**, *25*, 5726-5740.

[6] P. Friedl, K. S. Zanker, E. B. Brocker, *Microsc.Res.Tech.* **1998**, *43*, 369-378

[7] aM. H. Zaman, L. M. Trapani, A. L. Sieminski, D. Mackellar, H. Gong, R. D. Kamm, A. Wells, D. A. Lauffenburger, P. Matsudaira, *Proc.Natl.Acad.Sci.U.S.A.* **2006**, *103*, 10889-10894; bT. Lammermann, M. Sixt, *Curr.Opin.Cell Biol.* **2009**; cP. Friedl, F. Entschladen, C. Conrad, B. Niggemann, K. S. Zanker, *Eur.J.Immunol.* **1998**, *28*, 2331-2343.

[8] K. Maaser, K. Wolf, C. E. Klein, B. Niggemann, K. S. Zanker, E. B. Brocker, P. Friedl, *Mol.Biol. Cell.* **1999**, *10*, 3067-3079.

[9] aW. T. Butler, L. W. Cunningham, *J Biol Chem* **1965**, *240*, Pc3449-3450; bW. T. Butler, L. W. Cunningham, *J Biol Chem* **1966**, *241*, 3882-3888; cJ. D. San Antonio, A. D. Lander, M. J. Karnovsky, H. S. Slayter, *J Cell Biol* **1994**, *125*, 1179-1188.

[10] aD. Boettiger, B. Wehrle-Haller, *J Phys Condens Matter* **2010**, *22*, 194101; bJ. Friedrichs, J. Helenius, D. J. Muller, *Nat Protoc* **2010**, *5*, 1353-1361; cJ. Friedrichs, A. Manninen, D. J. Muller, J. Helenius, *J Biol Chem* **2008**, *283*, 32264-32272; dJ. Friedrichs, J. M. Torkko, J. Helenius, T. P. Teravainen, J. Fullekrug, D. J. Muller, K. Simons, A. Manninen, *J Biol Chem* **2007**, *282*, 29375-29383.

[11] aJ. Helenius, C. P. Heisenberg, H. E. Gaub, D. J. Muller, *J Cell Sci* **2008**, *121*, 1785-1791; bP. H. Puech, A. Taubenberger, F. Ulrich, M. Krieg, D. J. Muller, C. P. Heisenberg, *J.Cell Sci.* **2005**, *118*, 4199-4206.

[12] S. Nir, M. Andersen, *J Membr Biol* **1977**, *31*, 1-18.

[13] aS. Hakomori, *Adv Cancer Res* **1989**, *52*, 257-331; bK. Ohtsubo, J. D. Marth, *Cell* **2006**, *126*, 855-867.

[14] aK. S. Lau, J. W. Dennis, *Glycobiology* **2008**, *18*, 750-760; bM. N. Christiansen, J. Chik, L. Lee, M. Anugraham, J. L. Abrahams, N. H. Packer, *Proteomics* **2014**, *14*, 525-546; cD. H. Dube, C. R. Bertozzi, *Nat Rev Drug Discov* **2005**, *4*, 477-488.

[15] S. Nourshargh, P. L. Hordijk, M. Sixt, *Nat Rev Mol Cell Biol* **2010**, *11*, 366-378.

[16] M. E. Janik, A. Litynska, P. Vereecken, *Biochim Biophys Acta* **2010**, *1800*, 545-555.
[17] G. A. Di Lullo, S. M. Sweeney, J. Korkko, L. Ala-Kokko, J. D. San Antonio, *J Biol Chem* **2002**, *277*, 4223-4231.
[18] A. Sharma, J. A. Askari, M. J. Humphries, E. Y. Jones, D. I. Stuart, *Embo J* **1999**, *18*, 1468-1479.
[19] E. R. Cruz-Chu, A. Malafeev, T. Pajarskas, I. V. Pivkin, P. Koumoutsakos, *Biophys J* **2014**, *106*, 232-243.

Samenvatting

Dit proefschrift biedt een eerste bewijs van een directe relatie tussen de polariteit van de glycocalyx en integrine-onafhankelijke celadhesie en migratie. Om deze relatie te bewijzen zijn nieuwe methoden opgezet, waaronder glycaan detectie en digestie, of aangepast, om glycaan-gemedieerde adhesie, krachten, en celmigratie *in vitro* en *in vivo* te bestuderen. Deze nieuwe inzichten en verdere moleculaire karakterisering zal bijdragen aan het beter begrijpen van de glycocalyx in verschillende vormen van celmigratie en invasie en hebben mogelijk voorspellende waarde in de targeting van tumor progressie en metastase.

Kanker is wereldwijd de belangrijkste doodsoorzaak, met 14 miljoen nieuwe gevallen en 8,2 miljoen kanker gerelateerde doden in 2012 (World Health Organization 2016). Tijdens en na transformatie tot neoplasie maken kankercellen gebruik van het intrinsiek vermogen van elke normale cel in het weefsel: het vermogen om te migreren na activatie, een proces dat cellen normaal gesproken gebruiken tijdens morfogenese, immuunrespons en wondgenezing.

Belangrijke beginstappen in het verspreiden van tumorcellen en metastasevorming zijn penetratie en degradatie van het basale membraan, het loslaten van tumorcellen van de primaire tumor, en invasie in het extracellulaire matrix (ECM) -rijke bindweefsel.[1] Het gemeenschappelijk onderliggende proces waarmee cellen door ECM migreren is gepolariseerde actine polymerisatie-gemedieerde protrusie en actomyosine-gedreven contractie, resulterend in verandering van vorm en voortbeweging van het cellichaam.[2] Om contact te maken met de ECM en om er actomyosine-gedreven kracht op uit te oefenen, ontwikkelt de cel protrusies die adhesie aan het weefsel biedt door integrines en alternatieve adhesiereceptoren.[3] Anderzijds kunnen cellen zich met lage adhesie en stuwkracht tussen ECM-vrije spleten voegen, of met behulp van frictie tegen nauwgelegen ECM vezels.[4] De rol van integrines in celmigratie is de laatste decennia afdoende beschreven, maar hoe alternatieve adhesie-systemen betrokken zijn in het adhesie en de-adhesie proces is nog een uitdagende vraag en blijft grotendeels onduidelijk.

De aanleiding om de bijdrage van de glycocalyx in tumorcel adhesie en migratie te bestuderen kwam door de bevinding dat cellen, ondanks inhibitie van β1 integrine (de dominante adhesiereceptor voor fibrillair collageen I), nog konden migreren in driedimensionaal fibrillair collageen.[5] Na integrine inhibitie ondergingen MV3 humane melanoomcellen en muis embryonale fibroblasten (MEFs) een overgang in morfologie en migratie, van mesenchymaal naar een "amoeboïd filopodal" of "amoeboïd blebbing" fenotype en hielden langzamere migratie en contact met het substraat in stand (Hoofdstuk 5). Humane T-leukemie cellen daarentegen, hielden na integrine inhibitie de

adhesie en migratie op constante snelheid in 3D fibrillair collageen, corresponderend met een natuurlijk amoeboïde morfologie en migratievorm door integrine-onafhankelijke mechanismen.[6, 4d, 5b, 7] De mechanismen die cellen gebruiken om te compenseren voor verlies van integrine-gemedieerde adhesie en migratie, werden mede door deze bevindingen de focus van dit proefschrift.

Alternatieve adhesie mechanismen in celadhesie en -migratie

Zoals samengevat in **Hoofdstuk 2**, is er behalve de integrine superfamilie van adhesiereceptoren nog een verzameling van alternatieve celoppervlakte-receptoren die bijdragen aan cel verankering en migratie. De expressie van een set van vermeende collageen receptoren werd gemeten in MV3 melanoomcellen, waaronder de proteoglycanen CD44, syndecan-4 (SDC-4), en receptor tyrosine kinase discoidin domein receptoren (DDR) 1 en 2. Terwijl CD44 consistent tot expressie kwam, werd geen expressie van DDR-1 en -2 of SDC-4 gedetecteerd (Hoofdstuk 5). Toevoeging van een CD44 verstorend antilichaam had geen invloed op de migratie van MV3 cellen in 3D fibrillair collageen.[8] Dit werd hier onafhankelijk bevestigd met cellen na inhibitie van β1 en β3 integrines, want de CD44 blokkade had geen effect op de overgebleven amoeboïde celmigratie. Er was dus geen indicatie dat CD44 een compensatierol speelde als receptor in deze cellen. Omdat elke cel een sterk polaire buitenlaag heeft, de glycocalyx, werd de focus voor dit proefschrift de rol van de glycocalyx in het mediëren van de overgebleven adhesie en migratie van cellen. De gepresenteerde nieuwe inzichten identificeren de plakkerige eigenschap van de glycocalyx als adhesiemechanisme waarmee cellen adhesiekracht aan collageen genereren (in de orde van grootte van piconewtons), en ondersteunen integrine-onafhankelijke adhesie en migratie *in vitro* en *in vivo*. Samengevat, is een nieuw adhesiemechanisme geïdentificeerd dat cel-substraat interacties medieert met "solid-state" liganden, welke relevant kunnen zijn wanneer integrine-gemedieerde verbindingen beperkt of onmogelijk zijn, bijvoorbeeld door integrine receptor downregulatie en/of beperkte toegang tot liganden.

Detectie en enzymatische degradatie van de glycocalyx op levende cellen

In **Hoofdstuk 3** werd Bicyclo [6.1.0] nonyne (BCN) geïntroduceerd als een nieuwe probe voor bio-orthogonale labeling, een geschikt hulpmiddel voor het visualiseren van glycanen, waaronder siaalzuur, in levende cellen. Er is grote behoefte aan hulpmiddelen die de detectie van glycanen mogelijk maakt, omdat reporter technieken zoals fluorescente fusie-proteïnen niet toepasbaar zijn voor beeldvormend onderzoek naar glycanen. Verder beïnvloeden glycaan-bindende proteïnen (lectines) de celfunctie omdat

ze celoppervlakte receptoren crosslinken, en antilichamen die de kleine glycaanstructuur herkennen zijn zeldzaam. Cellen geïncubeerd met BCN behielden hun morfologische integriteit en levensvatbaarheid, waardoor functionele studies (zoals analyse van celmigratie) mogelijk werden.

Hoofdstuk 4 beschrijft de ontwikkeling van een protocol waarmee op geleidelijke wijze de koolhydraatketens van de glycocalyx enzymatisch worden gedegradeerd, om daarmee de invloed van de glycocalyx als polaire laag in celmigratie te onderzoeken. Met dit protocol blijven de cellen optimaal levensvatbaar. De efficiënte digestie van de bulk glycocalyx werd aangetoond met gangbare antilichamen tegen glycosaminoglycanen (GAGs) en lectine voor β-1,4 galactose (Gal), maar ook met bio-orthogonale labeling van siaalzuren (SAs). Lectines herkennen hun epitopen met een bepaalde koolhydraat specificiteit. Bio-orthogonale labeling daarentegen kan gebruikt worden voor detectie van "globale" residuen van siaalzuur en hun enzymatische degradatie in één stap, onafhankelijk van de oriëntatie van de glucosebinding. Het resultaat identificeerde verschillen in de samenstelling van de glycocalyx tussen de geanalyseerde celtypen. MV3 humane melanoomcellen en muis embryonale fibroblasten (MEFs) hadden hoge expressie van GAGs, Sas en Gal, terwijl Molt-4 immuuncellen lage expressie van GAGs hadden, maar vergelijkbare hoeveelheden Sas en Gal.

Door de staat van glycaandigestie identiek te houden voor alle cellen konden ze direct met elkaar vergeleken worden. Molt-4 cellen werden dus op dezelfde manier behandeld als MV3 cellen en MEFs. De digestieprocedure combineert een ongeëvenaard aantal en type glucosidasen van hoge zuiverheid in een twee-staps procedure waarbij eerst de buitenste laag van de glycocalyx wordt verwijderd, gevolgd door een kwantitatieve verwijdering de bulk van de meeste glycocalyx lagen, terwijl – belangrijk – de levensvatbaarheid van de cel behouden blijft. Deze digestiestrategie was cruciaal in de studie naar cellulaire functies zoals adhesie, migratie en formatie van contactstructuren met complex gevormd fibrillair collageen, en om specifieke functies van de glycocalyx in cel-matrix interacties te identificeren.

Digestie van de glycaclyx om zijn rol celmigratie *in vitro* en *in vivo* te bestuderen

Om de invloed van de glycocalyx op celmigratie te bestuderen werd het digestieprotocol (Hoofdstuk 4) gecombineerd met de integrine interferentie strategie uit **Hoofdstuk 5** om celmigratie analyses *in vitro* en *in vivo* uit te voeren. Digestie van de GAGs, inclusief heparansulfaat (HS), chondroïtinesulfaat (CS), dermatansulfaat (DS) en siaalzuren (Sas), was onvoldoende om de migratie negatief te beïnvloeden. Aanvullende digestie van β-1,4 galactose (Gal) veroorzaakte een tijdelijk verlies van migratie in integrine-geïnhibeerde

cellen ingebed in een 3D collageen I gel *in vitro*, of in de collageen-rijke dermis van de muis *in vivo*. Daarbij werd een overgang waargenomen van de amoeboïd-gepolariseerde naar een compleet rondachtig fenotype. De ronde morfologie en het verlies van migratie hielden 7 tot 10 uur aan, afhankelijk van de gebruikte cellijn, en werd gevolgd door een stapsgewijs herstel van het amoeboïde migratie fenotype, welke tegelijk plaatsvond met her-expressie van endogene oppervlakte glycanen. Deze resultaten geven de indicatie dat glycaan-matrix interacties niet exclusief gereserveerd zijn voor negatief geladen glycaanketens of residuen[9], maar eerder dat aanvullende bijdragen van minder complexe koolhydraten zoals β-1,4 galactoses. Dus, behalve negatieve celoppervlakte lading gemedieerd door GAGs en siaalzuren, zijn bipolaire interacties gemedieerd door β-1,4 galactose essentieel om het contact met collageen I-fibers te faciliteren, en zodoende gelegenheid geven voor integrine-onafhankelijke adhesie en migratie. Het vermogen van cellen om aspecifieke zwakke moleculaire interacties met de ECM te genereren, onafhankelijk van voorspelde epitopen, geeft een sneller aanpassingsvermogen aan een gestaag veranderende omgeving (die overvloedig zijn in biologische systemen) waarbij normaal gesproken een herschikking in receptor expressie vereist zou zijn.

Glycocalyx-gemedieerde adhesiekrachten *in vitro*

Om te onderzoeken of de glycocalyx als een directe adhesie "steiger" (scaffold) dient om integrine-onafhankelijke migratie te mediëren, werd de glycaan-gemedieerde kracht gekwantificeerd in Hoofdstuk 5. Single-cell force spectroscopy (SCFS) werd gebruikt om de dynamische vorming van cellulaire adhesie aan een fibrillair collageen oppervlak te bestuderen. Met SCFS kan gecontroleerd en nauwkeurig een screening van cel-substraat interacties worden gedaan, zelfs voor korte contacttijden, een vereiste voor vroege metingen van glycaan-gemedieerde integrine-onafhankelijke adhesie,[10] met piconewton nauwkeurigheid.[11] De resultaten die samengevat zijn in Hoofdstuk 5 laten substantiële interactiekrachten zien tussen de glycocalyx van MV3 humane melanoomcellen en collageen na integrine interferentie. Na enzymatische verwijdering van glycanen was deze interactiekracht verdwenen. De gemeten bindingskrachten kwamen al snel boven 500pN bij korte interactietijden (0,5 sec). Dit gaf de indicatie dat integrine- en glycaan-gemedieerde adhesie gelijktijdig plaatsvinden, maar interferentie van integrines was nodig om de glycocalyx gemedieerde adhesie nauwkeurig te meten. Toekomstig werk zal nodig zijn om de mechanismen van glycaan-collageen binding (zoals elektrostatische bindingen, waterstofbruggen en vanderwaalskrachten)[12] te identificeren.

Glycocalyx-gemedieerde adhesie ontwikkelt verschillende contact nanotopologieën

In Hoofdstuk 5 werd buigingsbegrensde 3D confocale microscopie gecombineerd met 3D scannende elektronenmicroscopie. Dit werd toegepast op MV3 controle en enzym-behandelde cellen om te demonstreren dat glycaan-afhankelijke celinteracties met collageen fibers bestaan uit actine-rijke cell "filopodal" of "bleb-achtige" protrusies. Omdat ze afhankelijk zijn van glycaan beschikbaarheid, vormen de protrusies morfologisch diverse raakvlakken. Ze bevatten gefocaliseerde galactosylresiduen, inclusief enkele blebs die grip-achtige structuren vormen, die een complex gevormd "grasp-like" raakvlak met de collageen fibers maakt. Tussenvoegingen van laterale blebs in collageen fibers met diepe afdrukken in het cellichaam waren bijkomstige interactiesoorten die onafhankelijk van glycaan beschikbaarheid verschenen in ECM-regio's van hoge dichtheid. Dit identificeert de glycocalyx als mediator voor complex gevormde membraan topologieën. Glycocalyx-gemedieerde adhesie door adaptieve raakvlakken gaf de aanwijzing voor identificatie van nieuwe adhesie mechanismen buiten integrine-gemedieerde mechanotransductie. Deze bevindingen zullen bijdragen aan een beter begrip van het brede scala van adaptaties die cellen kunnen verkrijgen om adhesie en migratie, in reactie op de heterogene omgeving in het lichaam-, te faciliteren en behouden.

Referenties

[1] M. M. Fuster, J. D. Esko, *Nat Rev Cancer* **2005**, *5*, 526-542.

[2] aA. J. Ridley, M. A. Schwartz, K. Burridge, R. A. Firtel, M. H. Ginsberg, G. Borisy, J. T. Parsons, A. R. Horwitz, *Science* **2003**, *302*, 1704-1709; bS. P. Palecek, C. E. Schmidt, D. A. Lauffenburger, A. F. Horwitz, *J Cell Sci* **1996**, *109 (Pt 5)*, 941-952.

[3] H. Maekawa, Y. Oike, S. Kanda, Y. Ito, Y. Yamada, H. Kurihara, R. Nagai, T. Suda, *Arterioscler Thromb Vasc Biol* **2003**, *23*, 2008-2014.

[4] aE. Paluch, C. Sykes, J. Prost, M. Bornens, *Trends Cell Biol* **2006**, *16*, 5-10; bO. T. Fackler, R. Grosse, *J.Cell Biol.* **2008**, *181*, 879-884; cV. Sanz-Moreno, C. J. Marshall, *Cell Cycle* **2009**, *8*, 1484-1487; dT. Lammermann, B. L. Bader, S. J. Monkley, T. Worbs, R. Wedlich-Soldner, K. Hirsch, M. Keller, R. Forster, D. R. Critchley, R. Fassler, M. Sixt, *Nature.* **2008**, *453*, 51-55.

[5] aP. Friedl, *Curr.Opin.Cell Biol.* **2004**, *16*, 14-23; bN. O. Carragher, S. M. Walker, L. A. Scott Carragher, F. Harris, T. K. Sawyer, V. G. Brunton, B. W. Ozanne, M. C. Frame, *Oncogene.* **2006**, *25*, 5726-5740.

[6] P. Friedl, K. S. Zanker, E. B. Brocker, *Microsc.Res.Tech.* **1998**, *43*, 369-378

[7] aM. H. Zaman, L. M. Trapani, A. L. Sieminski, D. Mackellar, H. Gong, R. D. Kamm, A. Wells, D. A. Lauffenburger, P. Matsudaira, *Proc.Natl.Acad.Sci.U.S.A.* **2006**, *103*, 10889-10894; bT. Lammermann, M. Sixt, *Curr.Opin.Cell Biol.* **2009**; cP. Friedl, F. Entschladen, C. Conrad, B. Niggemann, K. S. Zanker, *Eur.J.Immunol.* **1998**, *28*, 2331-2343.

[8] K. Maaser, K. Wolf, C. E. Klein, B. Niggemann, K. S. Zanker, E. B. Brocker, P. Friedl, *Mol.Biol. Cell.* **1999**, *10*, 3067-3079.

[9] aW. T. Butler, L. W. Cunningham, *J Biol Chem* **1965**, *240*, Pc3449-3450; bW. T. Butler, L. W. Cunningham, *J Biol Chem* **1966**, *241*, 3882-3888; cJ. D. San Antonio, A. D. Lander, M. J. Karnovsky, H. S. Slayter, *J Cell Biol* **1994**, *125*, 1179-1188.

[10] aD. Boettiger, B. Wehrle-Haller, *J Phys Condens Matter* **2010**, *22*, 194101; bJ. Friedrichs, J. Helenius, D. J. Muller, *Nat Protoc* **2010**, *5*, 1353-1361; cJ. Friedrichs, A. Manninen, D. J. Muller, J. Helenius, *J Biol Chem* **2008**, *283*, 32264-32272; dJ. Friedrichs, J. M. Torkko, J. Helenius, T. P. Teravainen, J. Fullekrug, D. J. Muller, K. Simons, A. Manninen, *J Biol Chem* **2007**, *282*, 29375-29383.

[11] aJ. Helenius, C. P. Heisenberg, H. E. Gaub, D. J. Muller, *J Cell Sci* **2008**, *121*, 1785-1791; bP. H. Puech, A. Taubenberger, F. Ulrich, M. Krieg, D. J. Muller, C. P. Heisenberg, *J.Cell Sci.* **2005**, *118*, 4199-4206.

[12] S. Nir, M. Andersen, *J Membr Biol* **1977**, *31*, 1-18.

Acknowledgements

I would like to take the opportunity to thank all the people who have accompanied and supported me over the last years. Finishing the PhD would not have been possible without them.

First, I would like to thank my promotor. **Peter**, I can still remember our meeting in which you told me something about an experiment that still needs to be done and will not take more than 3 weeks. I immediately went to work with the goal to get it in time. Without success. Fortunately, because it was precisely the experiment that aroused my interest in glycobiology and was seminal for my future research career. Thus, a small experiment resulted in a full project and countless subprojects and made me a scientist who is said to be a "sugar addict". ☺ I want to thank you for giving me the opportunity to find this way. With your support and your trust, I have been able to become the glycobiology scientist I am today. I greatly appreciate this!

Dirk, my co-promoter and collaborator, thank you very much for your support over the last years. Immediately after my move to Nijmegen I contacted you as I was inspired by the research direction of your group. Over the years, a strong and productive cooperation has developed, which always motivates me anew. But I would also like to thank you for your personal support and your open ear, especially in the last months during the completion of the PhD thesis and finding new opportunities. All this has helped me to successfully complete this work and to develop further ideas and concepts. I look forward to further joint projects in the future.

Kata, my second Co-promotor, I would like to thank you for your support especially in the final phase of the thesis but also for the helpful conversations about science and everyday life. If there are any problems regarding your computer equipment or if you just want to chat, don't hesitate to contact me. ☺ You are always welcome.

Bettina, where should I start. We met 9 years ago in Würzburg, where we started quite early with late night experiments. Having arrived in Nijmegen, we quickly found our places in the 1st unit, which became our second home. Here, at any time, we were able to retreat and plan uncountable *in-vivo* experiments and pore over the results obtained. Ok, we have to admit that we discussed other topics and ideas sometimes, that were not necessarily related to work. ☺ But whatever it was, it was enriching and motivating. One or the other project, e.g. "Labkids", didn't work out unfortunately, but much has been achieved. Our projects like many others were not always easy, but constructive cooperation with you always gave me a boost. The late-night experiments, the delicious sushi and the one or the other good film in the coffee room in PRIME I will never forget.

It was not only the work, but also a friendship that has bound us together. I will miss the evenings with pizza, cocktails and football together with Claudius and Robert. I would like to thank you for your openness, your willingness to help and your reliance and yes, your sense of aesthetics, which can be found in each of your *in vivo* pictures and will finally be part of our publication.

Olga, you are also one of the "founding members" of the Cell Dynamics group in Nijmegen and have built up the lab and the infrastructure. Together we have experienced a lot, confocal sessions in the lab, dinner on the roof during long-term experiments (always with an unreliable pizza-service), or on our search for planets with my old Telescope under the night sky at the periphery of Nijmegen. I'm still not sure wheater we really saw the Saturn rings or whether it was a bottle of beer too much, but it was definitely fun. What always fascinates me is your endeavor to discover something new and to push your limits. On some trips, I was even able to participate. You have both, a great foresight and a careful eye for the tiny things. Keep this. It makes you an interesting and indispensable conversation partner and friend.

Pavel, even though you came later to the Fried! group, you still somehow belong to the "first guard". From initial reservation, a close friendly relationship developed very quickly. Thank you for your support in finding answers to scientific and philosophical questions. With your constant interest in Glycobiology, you have, of course, quickly inspired me. Conversations with you have always shown me how important it is to have a biochemist around you. Thank you for that.

Marina, we have lived in Kleve over years, shared the car and actively practiced sports as I have never done before (and to be honest, never done again). ☺ I remember the time when we were jogging through the Klever forest to release our frustration about a failed experiment or simply to enjoy nature. And there were the countless cooking and movie events. They will remain unforgotten. One thing is really important to me: Thank you for your patience, when I wasn't able to finish my experiment in time and you had to wait for me. And yes, thank you very much for your help with proofreading. Many small mistakes I would have overlooked without your accurate corrections.

Joost, I would like to thank you for your contribution and help during our AFM measurements but also for your intensive feedback especially in the final phase of the manuscript and my thesis. It was a great experience to work with you.

Mariska, who would have thought that you will eventually find the way to Glycobiology. ☺ Thank you for your help and patience in the laboratory and during the SEM experiments. Your cooperation has finally provided the crucial insights that have been missing for the

description of the mechanism of migration. I also feel deeply honored to have you as my paranymph. Thank you!

Sjoerd, thank you for being my professional Dutch translator. Although it was very short-term you immediately offered your help. I really appreciate it. But thank you also for the interesting and helpful discussions about the atomic force microscopy.

Cornelia, thanks for the interesting conversations about science and music. It was great for me to join the concerts. The Requiems from Brahms and Fauré were fulminant. Thank you also for the yearly "Feuerzangenbowle" event at your place. I have enjoyed it.

Julia, thanks for the nice cooking events and the concerts of the great Nijmeegs Studenten Koor.

Esther, I would like to thank you for your great work in the lab. Although working to full capacity you offer help at any time which is remarkable. Thank you!

Yvette, Patpong, Jonathan and **Annette**, you were my students during the PhD time and I would like to thank you for your contribution to my uncountable projects. You worked pretty hard without losing patience and I really appreciate it.

I would like to thank my collaborators **Floris, Dirk, Toin, Joost, Barbara, Lorenz, Kay, Monique, Xander, Rinske** and **Myrtille** for the intensive and fruitful discussions and your feedback.

The Nijmegen lab members, **Olga, Antoine, Cindy, Bettina, Anna, Gert-Jan, Esther, Mirjam, Kata, Linda, Cornelia, Sarah, Marina, Manon, Pavel, Julia, Jan-Hendrik, Sjoerd** and **Lianne**, thank you for your support, the refreshing atmosphere in the lab and the inspiring conversations and discussions during the meetings or social gatherings. I really enjoyed it.

The former and current lab members in Houston, especially **Steffi, Steve** and **Veronica,** thank you for your input and helpful discussions over the last years.

Moni, Margit, Ute, Martina, Angelika, Eva, Steffi and **Markus**, with you I started my scientific work in Wurzburg and I would like to thank you all for the wonderful time. Back then the real glycan project started and I really appreciate your outstanding contribution. I will never forget you and look forward to our traditional yearly x-mas dinner.

In 2008, we joined the Department of Cell Biology and thanks to all colleagues we were warmly welcomed and integrated immediately. **Bé,** thank you for your helpful advice and contribution. **Huib**, thank you for helping me anytime. If there was a problem at the microscopes it was a great relief to know that there is someone who can definitively cope with that. **Mietske,** thanks to your contribution it was possible for me to perform EM experiments in Nijmegen. It was great to work with you and I want to thank you for your help and feedback. **Wiljan and Jan,** I am sure our *in vivo* experiments wouldn't be performed without you up to now. It was your outstanding commitment to provide expertise and equipment for the generation of new Life-act expressing cells. Thank you so much! **Jack and Marieke**, thank you for all the help around microscopes and for the interesting discussions.

Since 2013 I am working in the Department of Biochemistry and I would like to thank all the people for the impressive time.

Roland, I want to thank you for providing me the great opportunity to work in your group and also for giving me the chance to finish my "old" project even though it took much longer than expected. It was a tough and challenging time and I want to thank you for your patience, helpful discussions, advice and openness. I will never forget this.

Rike, you were my neighbour at home, in the lab and even in the car over years. Apparently, we couldn't get enough from each other. ☺ I want to thank you for the great time we had, the uncountable experiments, that eventually found their places in several publications, but also the cooking and movie events together with Jan and Robert. And due to the fact, that besides Marina it also affected you, I would like to thank you for your patience when I had to finish my experiment and you had to wait for me. It is great to have a friend like you.

Robin, thank you for your critical view and the helpful discussions. The book cover wouldn't be so impressive without your contribution.

I would like to thank all the other current and former BIS colleagues, **Merel, Jenny, Petra, Christiane, Lisanne, Wouter, Robin, Judith, Lisette, Alokta, Giel, Jürgen, Marco, Sander, Dirk, Omar** and **Joames** for the great and refreshing atmosphere in the lab and during our social activities.

The Nijmegen Glycobiology Platform (NGP): When I started my PhD project in Nijmegen in 2008, I was still a newcomer in the glycomics field, but the Glycobiology Platform gave me very fast access to other interesting people working in this (still young) scientific field. The discussions at the glycobiology meetings and conferences were always

very enriching and constructive and have decisively contributed to the development and outcomes of my projects. Thank you!

I would like to thank my **family** and **friends**. Especially my **Mom, Dad** and my brother **Michael** but also **Evi**, **Helmut**, **Ulrike**, **Haru**, **Heike**, **Alexander**, **Grit** and **Sarah**, thank you for your support.

Robert, thank you for being with me for so long. Your support, your contribution and endless patience make it possible to tackle any problem. I wouldn't stand here without you. Thank you for all that.

Curriculum Vitae

Samuel Schmidt was born on October 23rd, 1978 in Magdeburg, Germany. He studied in Leipzig, Germany and performed his diploma in Medical Biochemistry in 2007. Thereafter he started his PhD studies at the clinic for Dermatology at the University of Würzburg, Germany in the group of Prof. Dr. Peter Friedl. Together with the lab he moved to the Radboud University Nijmegen, The Netherlands, in 2008 and joined the Department of Cell Biology in the Radboud Institute for Molecular Life Sciences where he completed his experimental PhD thesis work with the title "Impact of Cell Surface Glycosylation on Tumor Cell Migration: Glycans as multivalent and universal adhesion scaffold". Following the PhD project, in 2012 he continued as Postdoc in the same department, concentrating on the validation of the role of surface glycosylation in mediating cell migration and invasion *in vivo* using multiphoton microscopy and visualization of the complex nanotopography between the cell membranes and collagen fibers using confocal and scanning electron microscopy. His work was presented on numerous national and international conferences. In 2013 he received the prestigious Roche Postdoc Fellowship (RPF) and joined the group of Prof. Dr. Roland Brock at the Department of Biochemistry where he developed a GFP complementation assay to study the transport of functional cell-penetrating peptides from the cell surface to the cytosol with focus on endosomal release. Furthermore, he studied the influence of cell surface glycosylation on the uptake of cell-penetrating peptides (CPPs).

List of Publications

Schmidt, S., and Friedl, P. (2010) Interstitial cell migration: integrin-dependent and alternative adhesion mechanisms, Cell Tissue Res 339, 83-92.

Dommerholt, J.*, **Schmidt, S.***, Temming, R., Hendriks, L. J. A., Rutjes, F. P. J. T., van Hest, J. C. M., Lefeber, D. J., Friedl, P., and van Delft, F. L. (2010) Readily Accessible Bicyclononynes for Bioorthogonal Labeling and Three-Dimensional Imaging of Living Cells, Angewandte Chemie-International Edition 49, 9422-9425. *(*shared 1st authors)*

Mohamed, M., Ashikov, A., Guillard, M., Robben, J. H., **Schmidt, S.**, van den Heuvel, B., de Brouwer, A. P., Gerardy-Schahn, R., Deen, P. M., Wevers, R. A., Lefeber, D. J., and Morava, E. (2013) Intellectual disability and bleeding diathesis due to deficient CMP-sialic acid transport, Neurology.

Verdurmen, W. P., Wallbrecher, R., **Schmidt, S.**, Eilander, J., Bovee-Geurts, P., Fanghanel, S., Burck, J., Wadhwani, P., Ulrich, A. S., and Brock, R. (2013) Cell surface clustering of heparan sulfate proteoglycans by amphipathic cell-penetrating peptides does not contribute to uptake, Journal of controlled release: Official Journal of the Controlled Release Society.

Wallbrecher, R., Verdurmen, W. P., **Schmidt, S.**, Bovee-Geurts, P. H., Broecker, F., Reinhardt, A., van Kuppevelt, T. H., Seeberger, P. H., and Brock, R. (2013) The stoichiometry of peptide-heparan sulfate binding as a determinant of uptake efficiency of cell-penetrating peptides, Cell Mol Life Sci.

Vallen, M. J., **Schmidt, S.**, Oosterhof, A., Bulten, J., Massuger, L. F., and van Kuppevelt, T. H. (2014) Primary ovarian carcinomas and abdominal metastasis contain 4,6-disulfated chondroitin sulfate rich regions, which provide adhesive properties to tumour cells, PLoS One 9, e111806.

Favretto, M. E., Wallbrecher, R., **Schmidt, S.**, van de Putte, R., and Brock, R. (2014) Glycosaminoglycans in the cellular uptake of drug delivery vectors - Bystanders or active players?, Journal of controlled release : official journal of the Controlled Release Society.

Schmidt, S., Adjobo-Hermans, M. J., Wallbrecher, R., Verdurmen, W. P., Bovee-Geurts, P. H., van Oostrum, J., Milletti, F., Enderle, T., and Brock, R. (2015) Detecting Cytosolic Peptide Delivery with the GFP Complementation Assay in the Low Micromolar Range, Angew Chem Int Ed Engl.

Schmidt, S., Wallbrecher, R., van Kuppevelt, T. H., and Brock, R. (2015) Methods to Study the Role of the Glycocalyx in the Uptake of Cell-Penetrating Peptides, Methods Mol Biol 1324, 123-131.

Schmidt, S., Adjobo-Hermans, M.J.W., Kohze, R., Enderle, T., Brock, R., Milletti, F. (2016) Identification of short hydrophobic CPPs for cytosolic peptide delivery by rational design, Bioconj Chemistry

Last author publication:

Kohze, R., Dieteren, C., Koopman, W.J., Brock, R., **Schmidt, S.**, Frapbot: an interactive open-source application for qualitative and quantitative FRAP-data analysis. Oxford Journal of Cytometry A *(submitted)*

In revision, in submission or in preparation:

Schmidt, S., Weigelin, B., te Riet, J., Daryab, N., te-Lindert, M., Lelli, B., Rognoni, L., Krause-Vortmeyer, M., Gottschalk, K.E., Kissler, S., Fransen, J., Humphries, M.J., Friedl, P., Glycocalyx-Mediated Integrin-Independent Amoeboid Cell Migration, Nature *(in revision)*

Zuconelli, C., **Schmidt, S.**, Adjobo-Hermans, Manipulation of Orai1 by cationic peptides mediates their direct cytosolic uptake *(in preparation)*

Schmidt, S., Friedl, P., Quantitative removal of multiple glycan species from live cells. *(in preparation)*

Marco J. Klein, **Samuel Schmidt**, Parvesh Wadhwani, Jochen Bürck, Johannes Reichert, Sergii Afonin, Marina Berditsch, Tim Schober, Roland Brock, Manfred Kansy and Anne S. Ulrich, Lactam-Stapled Cell-Penetrating Peptides: Cell Uptake and Membrane Binding Properties *(in preparation)*